CASCADING LOGIC GATES USING ION SIGNALS GENERATED BY PHOTOLABILE CAGED COMPOUNDS

A DISSERTATION SUBMITTED TO
MATERIALS SCIENCE AND NANOTECHNOLOGY PROGRAM
OF THE GRADUATE SCHOOL OF ENGINEERING AND SCIENCE
OF BILKENT UNIVERSITY
IN PARTIAL FULFILLMENT OF THE REQUIREMENTS
FOR THE DEGREE OF
MASTER OF SCIENCE

By
AHMET ATILGAN
May, 2013

I certify that I have read this thesis and that in my opinion it is fully adequate, in scope and in quality, as a thesis of the degree of Doctor of Philosophy.

…….

Prof. Dr. Engin U. Akkaya (Principal Advisor)

I certify that I have read this thesis and that in my opinion it is fully adequate, in scope and in quality, as a thesis of the degree of Doctor of Philosophy.

…….

Assoc. Prof. Dr. Tamer Uyar

I certify that I have read this thesis and that in my opinion it is fully adequate, in scope and in quality, as a thesis of the degree of Doctor of Philosophy.

…….

Assist. Prof. Dr. Emren Nalbant-Esenktürk

Approved for the Institute of Engineering and Science:

…….

Prof. Dr. Levent Onural

Director of the Graduate School

ABSTRACT

CASCADING LOGIC GATES USING ION SIGNALS GENERATED BY PHOTOLABILE CAGED COMPOUNDS

Ahmet Atılgan
M.S. in Materials Science and Nanotechnology
Supervisor: Prof. Dr. Engin Umut Akkaya
May, 2013

Caged compounds have attracted great attention due to their use in the elucidation of numerous biochemical processes. Photolabile caged compounds release covalently bound moieties upon exposure of ultraviolet light. Releasing the active species in such a controlled manner enables concentration of the molecules to be manipulated in spatiotemporal way.

Getting inspired from the knowledge of cellular information transfer through second messenger systems which Ca and Zn ions play important role, we synthesized a photolabile caged Zn(II) compound so that we benefit from its controlled ion release feature, so as to integrate two molecular logic gates physically. For that reason, a molecular logic operation was designed and the released ion was used as information carrier from one logic gate to other. After proving its practicality, we tested same principle for higher molecular logic systems. To do that, photolabile caged Zn(II) compound and previously proved supermolecule with coupled AND logic gates were physically integrated. Results proved that photolabile caged Zn(II) compounds is a useful way to combine two separate logic gates by means of free zinc ions. From this point of view, the approach physical integration of molecular logic gates through a metal ion or compound might be a solution for building more complex molecular logic systems.

Keywords: Photolabile caged compounds, zinc, molecular logic gates, BODIPY

ÖZET

FOTOLABİL KAFESLENMİŞ BİLEŞİKLER TARAFINDAN ÜRETİLEN İYON SİNYALLERİ İLE MANTIK KAPILARININ BAĞLANMASI

Ahmet Atılgan
Malzeme Bilimi ve Nanoteknoloji, Yüksek Lisans
Tez Yöneticisi: Prof. Dr. Engin Umut Akkaya
Mayıs, 2013

Kafeslenmiş bileşikler canlılardaki biyokimyasal süreci aydınlatmada önemli rol oynadıkları için oldukça ilgi çekmektedirler. Fotolabil kafes bileşikler kendisine kimyasal bağla bağlanmış olan grubu, ultraviyole ışık sayesinde salabilmektedirler. Biyoaktif moleküllerin bu şekildeki kontrollü salınışları onların zamansal ve mekânsal olarak yönetimine imkân sağlıyor.

Ca ve Zn iyonlarının önemli rol oynadığı ikinci mesajcı sistemler vasıtasıyla yapılan hücresel bilgi transferlerinden esinlenerek, fotolabil kafeslenmiş çinko iyonu bileşiklerin kontrollü çinko salınım özelliğinin iki ayrı moleküler mantık kapısını fiziksel olarak birleştirebileceğini düşündük. Bu yüzden fotoaktif kafeslenmiş bileşik sentezledik. Bu bileşikten ışık vasıtasıyla salınmış çinko iyonlarının bilgi taşıyıcı olarak görev yaptığı ve 510 nm'de ışık çıktısı veren INH-AND moleküler mantık işlemi gerçekleştirdik. Sonrasında aynı temel prensibin daha karmaşık yapılarda da çalıştığını gösterebilmek için daha önceden ispatlanmış birleşik iki AND mantık kapısına sahip bir süpermolekül kullandık. Yapılan çalışmalar fotolabil kafeslenmiş Zn(II) bileşiklerinin iki ayrı mantık kapısını birleştirmek için etkili bir yöntem olduğunu göstermiştir. Bu açıdan baktığımızda, moleküler mantık kapılarını metal iyonuyla fiziksel olarak birleştirme fikri daha karmaşık moleküler mantık kapılarının yapımına çözüm olabilir.

Anahtar Kelimeler: Fotolabil kafeslenmiş bileşikler, çinko, moleküler mantık kapıları, BODIPY

Dedicated to my family

ACKNOWLEDGEMENT

I would like to express my immense gratitude and sincere thanks to my master Prof. Dr. Engin Umut Akkaya for giving me the opportunity to join his group and introducing me to this interesting scope of research. It was great privilege and honor to learn how to become a scientist from him. I am very proud of being student of such a great person and scientist.

I would like to express my sincere thanks to Dr. Esra Tanriverdi for her invaluable guidance, help, support and experience. She was not only an outstanding collaborator but also a great person. We owe this study to her patience.

I owe a special thank to my brother Bilal Uyar for his everlasting friendship, help and support. We put signature to many academic studies together. I hope we do much more in future. It is very big chance to have such a friend with great personality and wisdom.

I am sincerely grateful to Dr. Ruslan Guliyev for his invaluable guidance, and everlasting help and support. Whenever I had a question, the first address I applied to was him. I benefited from his knowledge and personality very much.

I sincerely thank assist. Prof. Dr. Ayşegül Gümüş for her important contribution to this study and for her invaluable experience and knowledge.

One of my special thanks goes to my close friend Captain Bilal Kılıç. To meet with him was big fortune for me. He always supported my success with his famous photocopies and by ordering me delicious foods. He was always a great collaborator, friend and brother for me. I am very proud to be called as Löwe Ahmet by him.

I am grateful to Onur Büyükçakır, Dr. Yusuf Çakmak and his wife Dr. Sündüs Erbaş-Çakmak. They were always like a member of my family and they will. I have learned many things from our nice conversations.

One of my special thanks is belong to group EPFL, Ziya Köstereli, Ahmet Bekdemir, Elif Ertem for their close friendship, help and support. It was very joyful to be with them and share the same environment during our master studies.

My special thanks also extending to Dr. Murat Işık, Dr. Fazlı Sözmen, Safacan Kölemen, İlke Turan Şimşek, Tuğba Özdemir Kütük, Nisa Yeşilgül, Şeyma Öztürk, Yiğit Altay, Tuba Yaşar, Tuğçe Durgut, Hale Atılgan, Özge Yılmaz, Dr. Seda Demirel, Hatice Turgut, Gizem Çeltek, Fatma Pir Çakmak, Hande Boyacı Selçuk, Ahmet Selim Han, Ulvi Karaca, and Muhammed Büyüktemiz for their valuable friendship and support. It was definitely a great pleasure working with them shoulder to shoulder.

I would like to thank all members of UNAM family for providing a multidisciplinary research atmosphere and for joyful friendships. I thank especially Zeynep Erdoğan for her kind help for mass spectrometer analysis. In addition to UNAM, I also would like to express my gratitude and appreciation to TUBİTAK for financial support.

I owe the biggest thank you to my family because I owe everything to their care, affection, support and trust. Words are not enough to express my gratitude to them. I will always need their endless love, and prayers and they will always be in my heart. Now, it is indefinable pleasure to bestow this thesis on my family.

LIST OF ABBREVIATIONS

AcOH	:	Acetic Acid
Bodipy	:	Boradiazaindacene
$CHCl_3$	:	Chloroform
DDQ	:	Dichlorodicyanoquinone
DMF	:	Dimethylformamide
ET	:	Energy Transfer
Et_3N	:	Triethylamine
FRET	:	Förster Resonance Energy Transfer
HOMO	:	Highest Occupied Molecular Orbital
ICT	:	Internal Charge Transfer
LUMO	:	Lowest Unoccupied Molecular Orbital
MALDI	:	Matrix-Assisted Laser Desorption/Ionization
MS	:	Mass Spectroscopy
NMR	:	Nuclear Magnetic Resonance
PET	:	Photoinduced Electron Transfer
TFA	:	Trifluoroacetic Acid
THF	:	Tetrahydrofuran
TLC	:	Thin Layer Chromotography
TOF	:	Time of Flight

TABLE OF CONTENTS

LIST OF FIGURES

CHAPTER 1

INTRODUCTION

Although roots of supramolecular chemistry date back to last quarter of 19th century, it drew great attention in large scale with synthesis of first crown ether by Charles J. Pedersen in 1960s.[1] This important development motivated Donald J. Cram and Jean-Marie Lehn to synthesis shape and ion selective receptors and, therefore, to establish new concepts of "host-guest" chemistry. Due to significant endeavors of these two scientists, chemistry community comprehended its generality and principal importance and ratified it as supramolecular chemistry. At these years, supramolecular chemistry was defined by Jean-Marie Lehn as "chemistry beyond molecule" and "chemistry of the intermolecular bond".[2]

Over time, supramolecular chemistry outruns its starting border with great contribution of Fraser Stoddart to the field. New concepts such as molecular machinery, complex self-assembled systems and sensors have been involved to the supramolecular chemistry. Evolution from host-guess molecules to complex systems and to more complex ones exhibits current perspective of supramolecular chemistry. Bottom-up approach will have achieved a meaningful capability to operate certain tasks successfully by this way, like combination of letters to make a word, sentence, and then a whole story as Stoddart implied.[3]

One of the subfield of supramolecular chemistry with an impressive evolution is molecular sensors. Host-guest approach of Jean-Marie Lehn inspired many to design highly selective and sensitive and reversible receptors towards certain species, from ions to molecules. Later on, photochemistry has become an important tool to complete the idea of molecular sensors. The photochemical molecular sensor includes a fluorophore part as reporter and a receptor part as sensor. In other words, as selective receptor part holds analyte, reporter part gives information by fluorescence emission about analyte-receptor interaction. This methodology enables

easy, clear, fast, selective, and sensitive detection of analytes in molecular scale. Fluorescent molecular sensors were used to be recognized just with their superior detection ability until one has changed this understanding a bit.

Father of molecular logic gates Prof. Prasanna de Silva has first time put forward the idea use of molecular sensors to do logical operations like in silicon-based logic gates which are building blocks of current computers.[4] This idea, building up molecular logic gates by bottom-up approach instead of conventional top-down approach has being attracted great attention by many scientists. Molecular logic gates imply much less space when compared to current silicon based technology. It is a big advantage of course. Regarding the fact that miniaturization concept which silicon technology relies on is estimated to end around 2020 due to quantum tunneling effect[5], molecular logic gates are potential alternative technology for post-transistor era and might fill silicon technology's shoes in next decades.

Scientists have designed successfully almost all single logic gates with supermolecules. Today, they are trying to persuade molecules to do more complicated arithmetic operations. Up to now, advanced logic systems, for example, full-adder, half-adder, half-subtractor, password protection, reset, de/multiplexer were accomplished.[6] For higher functions, molecular logic gates should be concatenated virtually and/or physically. Virtual integration means combination of inputs of each gate to process final outputs without real cascading between logic gates. It is a feasible way to make superposed logic gates and it is obvious an advantages over electronic ones. However, virtual integration method is not applicable to integrate independent logic gates. On the other hand, physical integration refers integration of independently working logic gates as it is in wiring different electronic logic gates. Straightforwardly, separate molecular logic gates have to be physically combined with simple and generic methods to work together as concatenated systems. For that reason, physical integration opens the door to rational design and advanced molecular computing. However, it is not as easy as it is in electronic circuitry. In electronic circuitry, logic gates use same type input and output, electricity. This homogeneity contributes great to cascading logic gates. On

the other hand, molecular logic gates use different sort (heterogenic) of inputs and outputs generally. Therefore, communication between different speaking molecules becomes harder. For that reason, new methodologies are required to increase intermolecular communication so as to overcome gate to gate input-output mismatch.

There are number of studies about concatenated logic gates. Many of these studies uses enzymatically integrated systems.[7] Although reintegration of enzymatic pathways is remarkable idea especially for drug delivery systems, more generic methodologies should be implemented to have potent integrated systems for computing. Another work towards integrated molecular logic gates was reported by Credi et al. Two logic gates were physically coupled through hydrogen ion transfer.[8] However, there is no clear presentation of independent and concatenated molecular logic gates. Therefore, claim of cascading of independently working molecular logic gates to function together remains unclear in this study.

One alternative solution to the current problem might be in the nature. As we know that there is important information processing, storing and gathering in living systems. One of the significant examples to signal transduction between cells is second messenger systems. Mimicking second messengers to achieve concatenated molecular logic gates might be the covetable inspiration. Zn^{2+} ion is known today to play an important role in intracellular communication.[9–14] Provided that Zn ions are controlled by the external stimuli, it can be a potential candidate to construct multi-integrated physical molecular logic gates. As we discussed in background chapter, one of the best way to control metal cations is to use photolabile-caged compound or chelators due to their potential ability to manipulate metal ions spatiotemperally by induced light.[15]

In this study, a new methodology is reported to integrate two independent molecular logic gates through ion signals by use of photolabile caged Zn^{2+} compounds. According to our knowledge, our work includes new concepts in molecular logic literature such as using photolabile caged compounds and bridging separate molecular logic gates with ion signals.

CHAPTER 2

BACKGROUND

2.1. Fluorescence

When some molecules have absorbed energy coming from electromagnetic radiation, they can emit luminescence which is called as fluorescence. To do that, molecules or particles should be irradiated by proper energy packets, photons. This energy causes electrons to jump higher energy states. The molecule at the excited state can relax its energy in several competitive ways which are internal conversion, intersystem crossing, intramolecular charge transfer and conformational change. In addition to these, excimer formation, electron, and energy transfer are also special case competing with fluorescence.

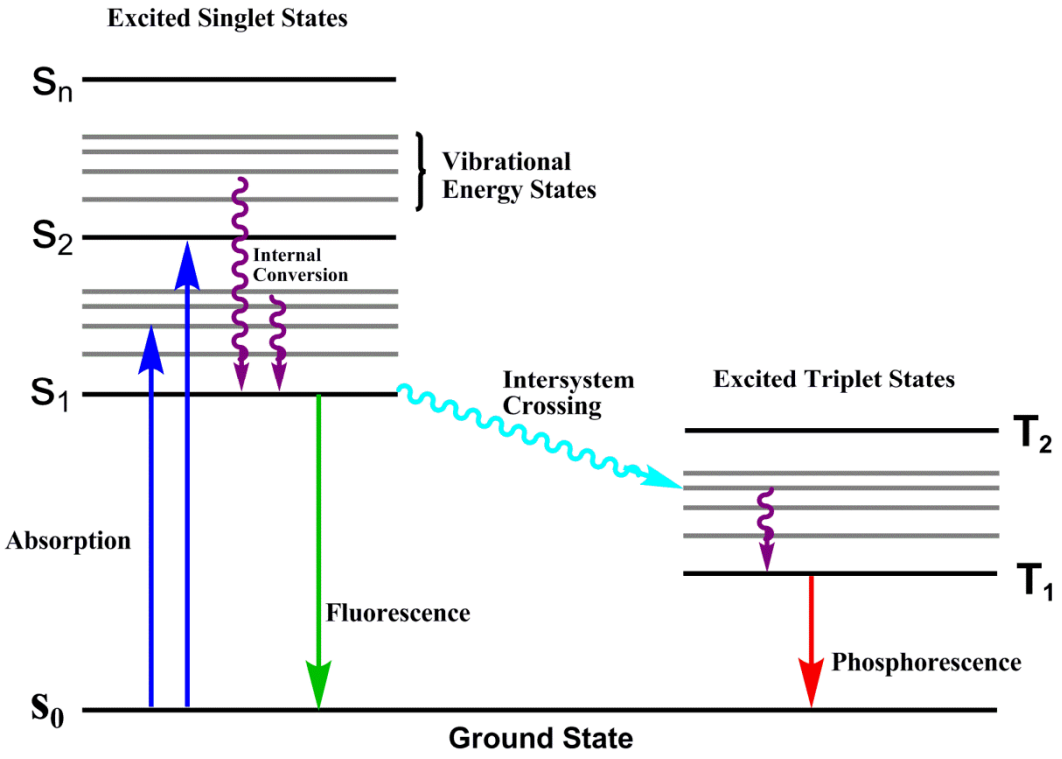

Figure 1 Jablonski Diagram

In Figure 1, Jablonski diagram demostrate the stituation of excited electron after photon absorption. S0, S1, .., Sn represents singlet electronic states and triplet electronic states are denoted by T1, T2… There are also lower energy gaps between each electronic state, which are known as vibrational levels. Absorption is presented by the vertical upward arrow which shows the electrons motion in grounds state (S0) to higher electronic states. Excited state molecule undergoes relaxation to the lowest vibration level of S1 as shown by curved arrows. This process is named as intersystem crossing. Eventually, electron in S_1 excited states returns to the ground states by releasing its energy in the form of light which is called fluorescence. One other de-excitation competing with fluorescence can occur as well. The mechanism known as intersystem crossing leads the excited electron in singlet states (S_1) to moving triplet state (T_1). Electron in T_1 state is inclined to give phosphorescence light at low temperature and appropriate conditions, however; it is common to observe non-radiative emission in solution at room temperature.

A molecule absorbed energy can relax by emitting a photon, fluorescence, as it is mentioned above. However, energy absorbed and emitted by molecule are not identical due to rapid decay of electron to the lowest vibration level of S_1 before fluorescence. The difference between the band maxima of absorption and emission spectrum of molecule is called as Stokes' shift (Figure 2). Stokes' shift distance can be changed by the factors such as solvent effect, excited state reactions, complex formation and energy transfer[16]. In contrast to Stokes' shift, energy of emitted photon may have higher energy than absorbed one. In this case, anti-Stokes' shift is observed.

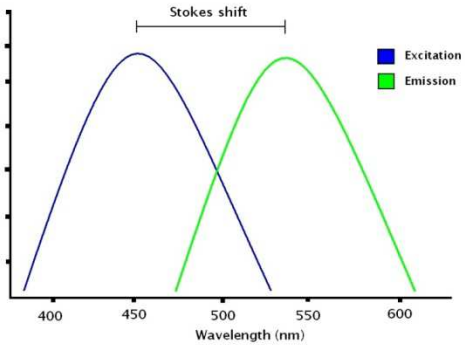

Figure 2 Stokes' shift

2.2. Fluorescent Dyes

Non-emissive objects absorb some portion of incident light by converting it into heat and reflect the rest back to environment. However, fluorescent dyes works a little bit different. Radiation coming to the fluorescent dyes is absorbed and this energy is used to form a photon in slightly different wavelength. Due to this feature of fluorescent dyes, they takes place in our life such as road signs, fluorescent vests, light bulbs etc.. Moreover, these dyes are employed intensively in genetic and medical research to understand biological process, to mark certain organelles, proteins, and antibodies, to control drug uptake and so on.

Among fluorescent dyes, ones working in UV (ultraviolet) - VIS (visible)-NIR(near infrared) region draw great atteniton due to their variety of applications ranging from solar cells, lasers to therapeutics. In Figure 3-4,[17] some of most known examples of these dyes are depicted. Tetramethyl rhodamine (TMR), carboxytetramethyl rhodamine (TAMRA), and carboxy-X-rhodamine (ROX).

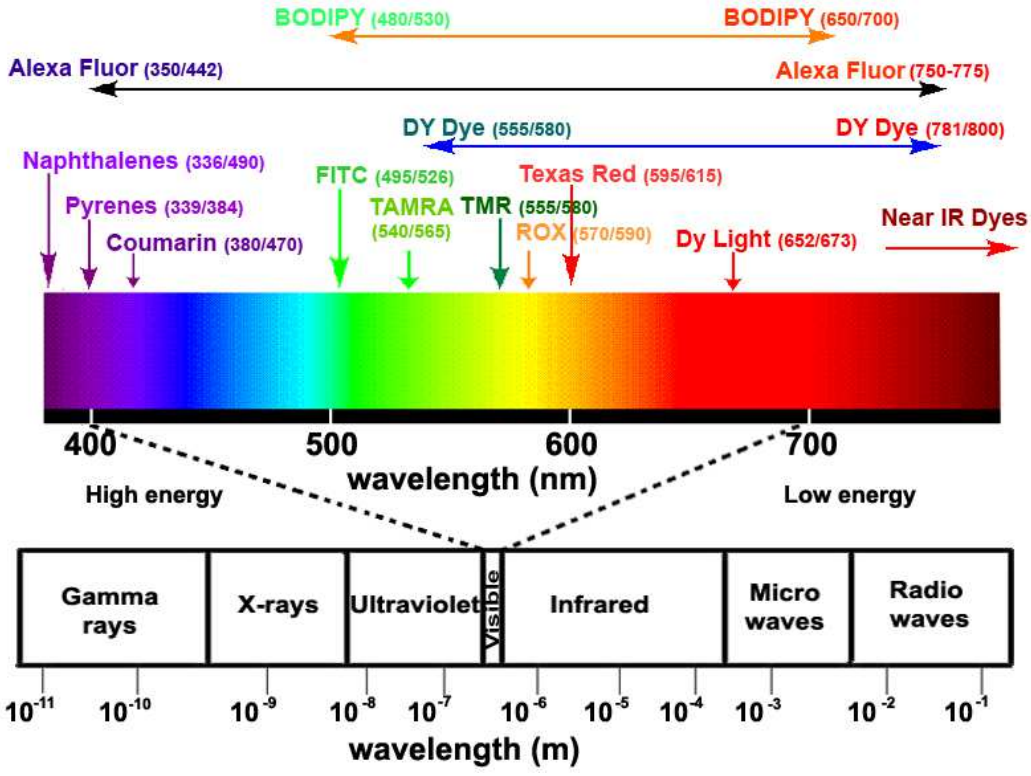

Figure 3 Fluorescent dyes in the visible region

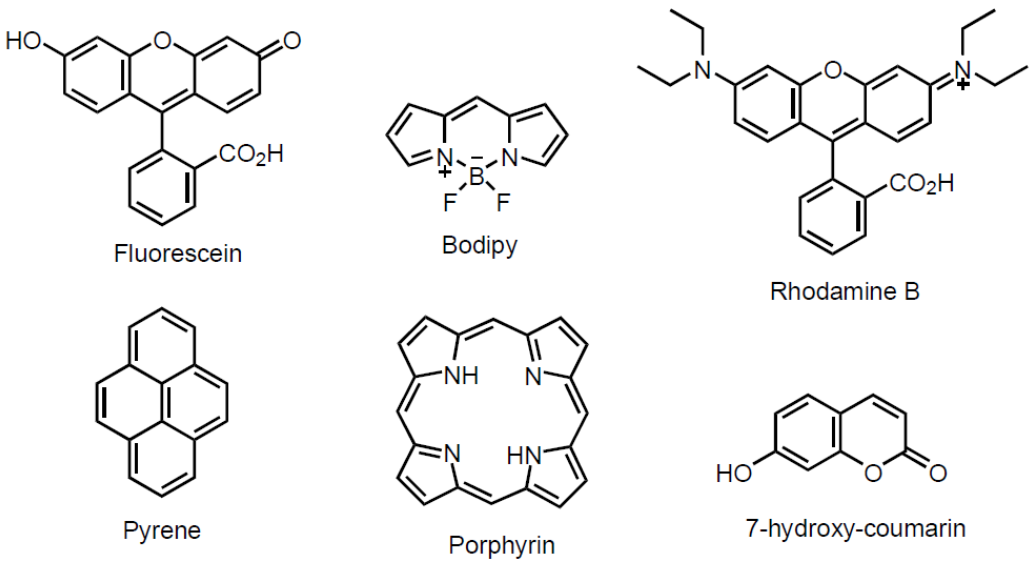

Figure 4 Chemical structures of common fluorescent dyes

Designing true fluorescent dyes is ultimate task for targetted applications. For bioimaging, for example, dyes should be biocompatible, non-toxic, chemi/photostable, water soluble, capable of working in therapeutic window (preferably in near IR region) and have high quantum yield. In addition to these properties required in bioimaging, ease, high selectivity and low detection level are also required for sensor applications[18].

2.3. Molecular Sensors

Molecular sensors, or chemosensors, are molecules which report the changes on their properties in the presence of analyte compounds. There are familiar examples of traditional chemosensors. To illustrate, bulk properties of metal oxides were used as chemosensors to detect oxidizing and reducing gases adsorbing the surface of the material by changes in conductivity[19]. In literature, there are two main classes of molecular sensors; electrochemical sensors and optical sensors. Electrochemical sensors are typically sensible to the redox active units. An electrochemical technique, such as cyclic voltametry, is employed to detect the change in the redox properties of receptor part. Although electrochemical sensors are relatively simple systems, they are restricted in lifetime and cannot be used for biological studies. As to optical

sensors, they are known as UV-VIS and fluorescence based molecular sensors. Absorption based sensor has sensibility problems compared to fluorescence ones. It is because absorption spectrum intensity is dependent on the distance that light passing through the sample. Fluorescence sensor on the other hand gives signal proportional to the substance concentration. For that reason, fluorescence method is capable of monitoring speedily changes in concentration.

There are couples of instrumentation methods including atomic absorption, inductively coupled plasma etc. to determine various analytes. Although, these methods give direct and quantitative information about analyte concentrations, they are quite expensive and destructive to biological samples. Therefore, such methods are not well-suited for biological and toxicological *in vivo* and *in vitro* studies. On the other hand, fluorescence method is nondestructive, fast, simple, cheap, highly selective and sensitive. Using fluorescent molecular sensors has an advantage of providing immediate optical feedback without requiring complex instrumentation or sample preparation[20–22].

2.4. Fluoroscent Molecular Sensors

Fluorescent chemosensors are composed of two different part; sensor and fluorophore part. Sensors part is responsible for binding to the analyte specifically, on the hand, flourophore reports current situation by sending light in different intensity and/or in different wavelength. Difference in intensity can happen as fluorescence quenching or amplification.[23] Fluorescent detectors working based on intensity change are called as turn on/off fluorescent sensors (Figure 5 (A)). For fluorescent detection of analytes, turn-on (amplification of signal) types is favorable than turn-off (fluorescence quenching) one. It is because turn-on sensors diminish the possibility of false positives and is better to use multi-sensor sensing different analytes together. Fluorescent sensors working based on intensity and wavelength change are named as ratiometric sensors (Figure 5 (B)). Ratiometric fluorescent sensors have extra advantages over formers. Ratiometric sensors give two signals at different wavelength to report changes on fluorophore with binding of analyte. This

means that ratiometric sensor are less exposed to errors and better for inhomogeneous samples, which makes analyte easy to quantify.[20]

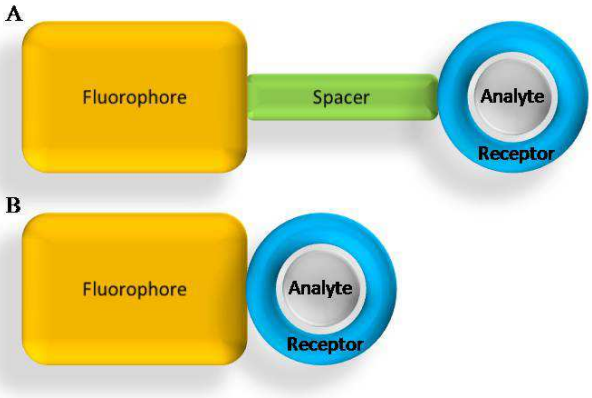

Figure 5 Schematic representations of fluoroionophores types: Fluorophore-spacer-receptor model A, integrated model B

2.4.1. Photoinduced electron transfer (PET)

As it is mentioned above, one of the working princibles of fluorescent sensors is based on fluorescent quenching and amplification. Figure 6 presents principles of PET mechanism. Receptor part includes electron rich atoms such as amino group with electron donating ability. When fluorophore is excited by a photon, one electron jumps to the lowest unoccupied molecular orbital. At the excited state, electron transfer is done from free receptor part to the fluorophore, therefore this transfer inhibits fluorescence of excited electron and compels the electron to make radiationless transition. On the other hand, if analyte binds to the receptor part, it stabilizes the free electrons on receptor part, which causes decrease in HOMO energy level. Thus, receptor part losses its electron transfer features. Consequently, relaxation of the excited electron is done by fluorescence mechanism and enhancement in fluorescence is seen.

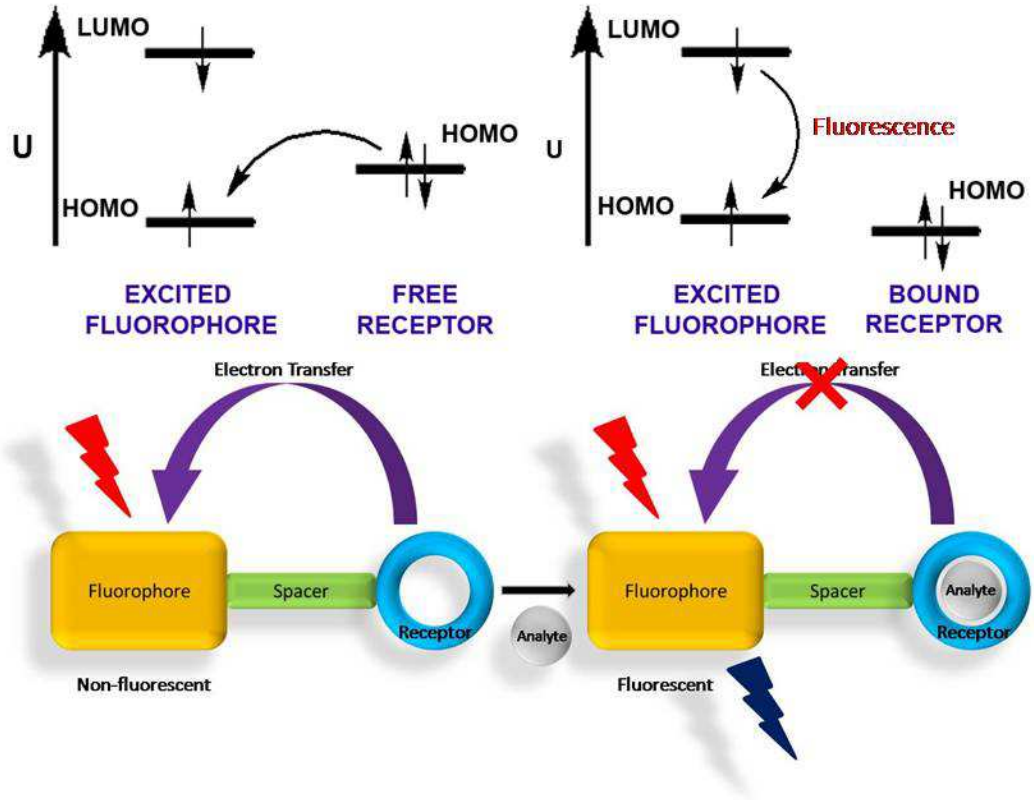

Figure 6 PET mechanism

There are many literature examples of turn-on fluorescent molecular sensors (Figure 7). In these type of sensors, binding of analyte causes fluorescence amplification by blocking the PET mechanism between receptor and fluorophore.

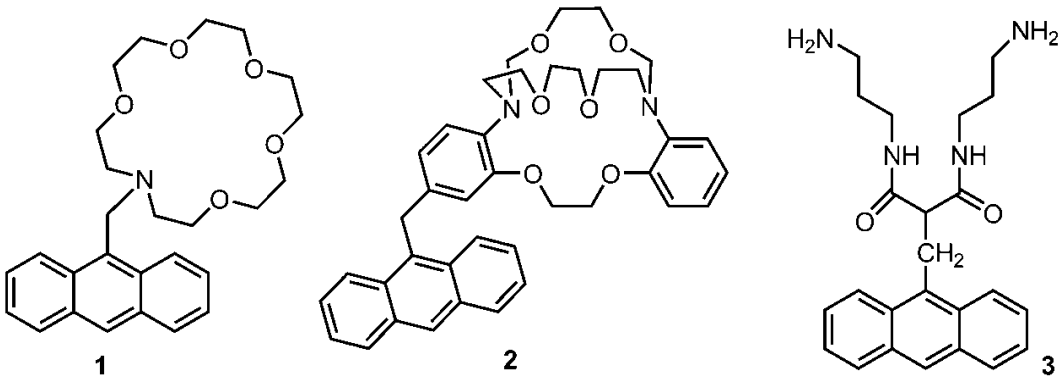

Figure 7 Examples for turn-on sensor

PET mechanism for turn-off fluorescent sensors works reversely (Figure 8). For that reason, it is called as reverse PET or oxidative PET. Unbounded molecule performs

fluorescence however, when it is bounded by analyte, LUMO of receptor become available for radiationless relaxation of excited electron. Therefore, fluorescence emission gets quenched by this way. 1,8-dianthryl derivative of the cyclam in Figure 9[24] is shown as an example of turn-off sensor.

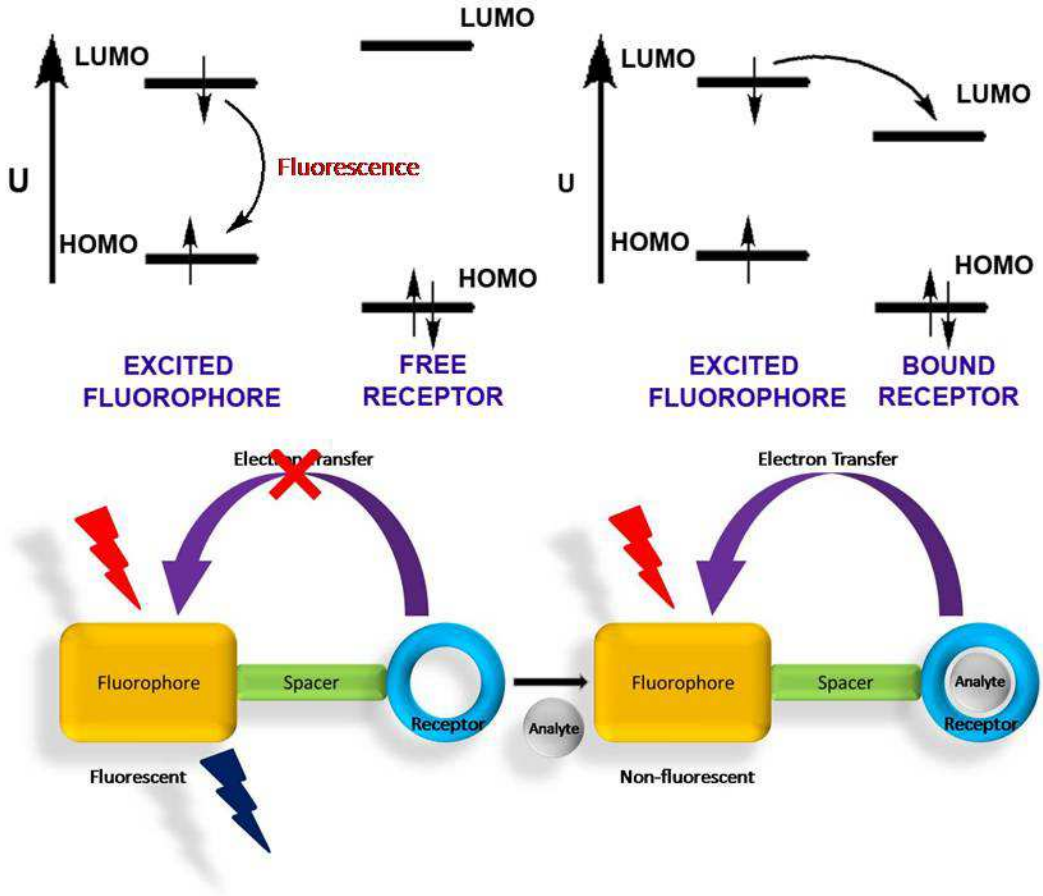

Figure 8 Reverse PET mechanism

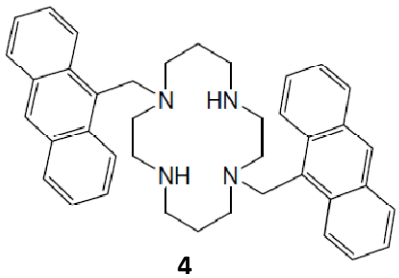

4

Figure 9 A turn-off fluorescent sensor[24]

2.4.2. Intramolecular Charge Transfer

Intramolecular charge transfer requires fluorophore and receptor to be linked in the same π electron system in which there are donor and acceptor groups. Sensors working based on ICT mechanism are known as ratiometric type fluorescent sensors. Excitation of these sensors causes electron density to redistribute on molecule, which creates a substantial dipole. New electron distribution leads intramolecular charge transfer from donor to the acceptor.

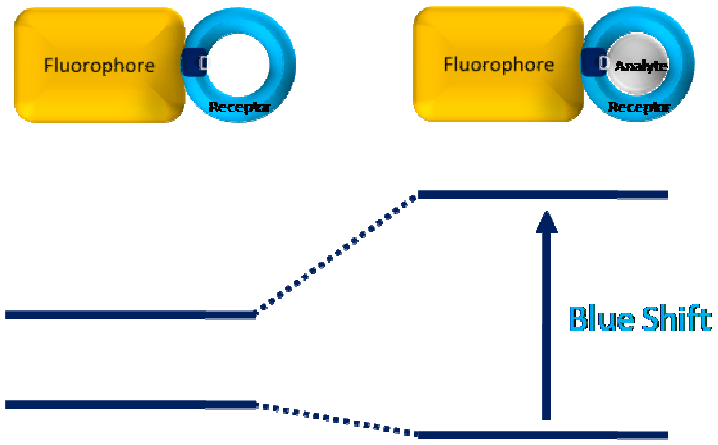

Figure 10 ICT: Interaction analyte with donor groups

Presence of analyte in receptor part interacts with excited state dipole. For example, let analyte be a cation and receptor binding unit be electron donating group like amino groups. When cation binds to receptor, it will diminish electron donating power of amino groups. Less donating amino group is present, less conjugation on fluorophore exists. This change in conjugation causes blue shift in absorption spectrum (Figure 10). Another explanation of ICT can be made by considering interaction between cation and receptor in both ground and excited state. When cation binds to receptor in ground state, the total energy will decrease, HOMO level will also decrease, due to stabilization of energy on electron donating part. In excited state, amino group will have '+' charge on it. This plus charge and cation's plus charge will destabilize each other very strongly, which will increase the LUMO energy level (energy gap between LUMO and HOMO is now bigger than free sensor molecule). Eventually, a blue shift in absorption spectrum will appear.

In contrast, if a cation binds an electron withdrawing group such as carboxylate groups, it will increase electron withdrawing power of the group(charge dipole interaction). Therefore, conjugation will increase and red-shift will be seen (Figure 11). The other explanation is that in ground state there will be a decrease in HOMO level because of charge-dipole interaction. In excited state, receptor will get a minus charge on it so the resulting interaction will be charge-charge interaction, which is stronger than charge-dipole and causes decrease in LUMO level more than HOMO. Consequently, red shift will be seen in absorption spectrum.

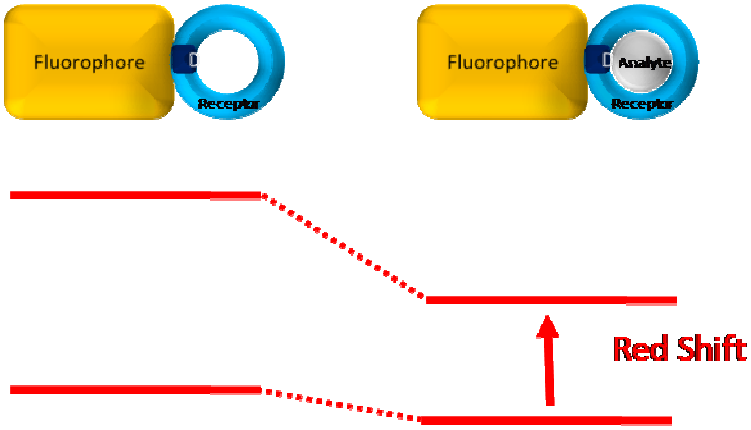

Figure 11 ICT: Interaction analyte with acceptor groups

Figure 12 shows some literature examples of fluorescent molecular sensors based on ITC. Compounds 5 and 6 demonstrate blue shift in absorption and emission spectrum in the case of cation binding.

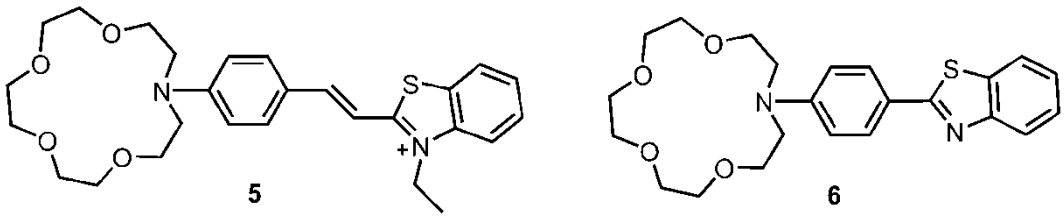

Figure 12 Ratiometric type fluorescent sensors

2.5. BODIPY

The story of BODIPY has started with Treibs and Kreuzer. Since 1968, BODIPY has drawn great attention and become chief actor in many research articles due to its

unique properties. Its applications were separated wide range of fields ranging from molecular sensors, bioimaging, photodynamic therapy, biolabeling, molecular devices to the solar cells.

4,4-Difluoro-4-bora-3a,4a-diaza-*s*-indacene dyes, abbreviated to BODIPY long more, have significant characteristics making it very popular today. They have strong absorption coefficient and quite sharp fluorescence peaks due to their high quantum yields. Polarity and solvent pH have nearly no effect on them. BODIPY dyes are stable to physiological conditions as well. Moreover, their good solubility, optical tuning (500-900), and, most importantly, ease of doing chemistry on it are main characteristics of BODIPY dyes. There are several frontier research groups working on modification of BODIPY structure to change its photophysical properties. 2nd, 3th, 5th, and 6th position of BODIPY were successfully worked to extend conjugation in order to shift spectrum to red-NIR region. 4th and 8th position of the BODIPY is also capable of being functionalized.

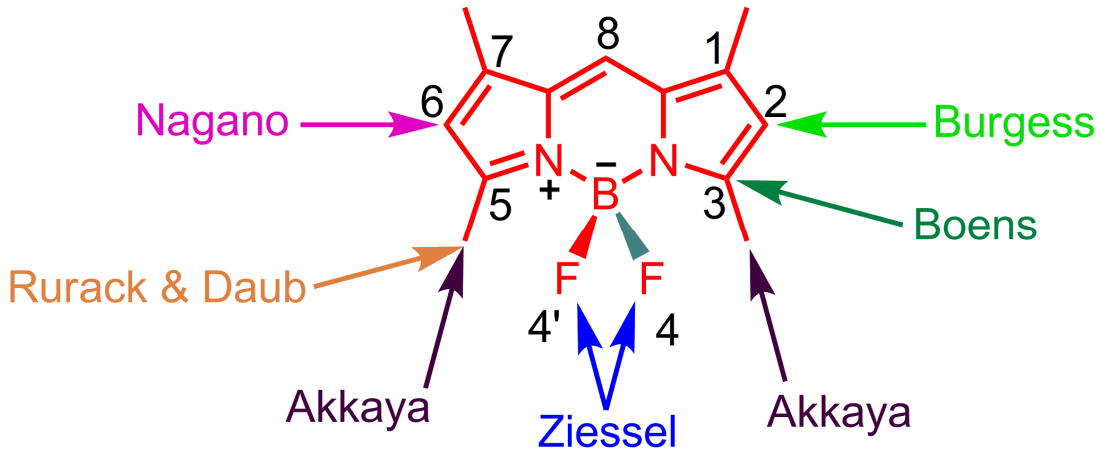

Figure 13 Research groups contributing to BODIPY chemistry

2.5.1. Application of BODIPY dyes

BODIPY dyes have taken place in many hot research area since it has useful chemical and photophysical features. (Figure 14)

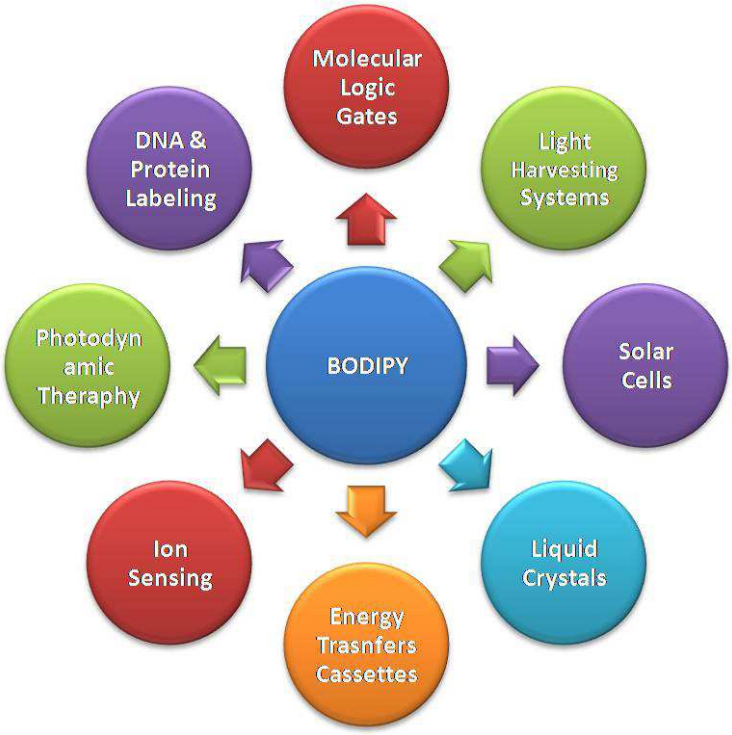

Figure 14 Application areas of BODIPY dyes

Ion sensing is one of the field in which BODIPY is quite popular. It is possible to find numerous papers about BODIPY based fluorescent sensors. It is because BODIPY can be functionalized easily for variety of analytes. Recently Akkaya et al. has published different sort of BODIPY based sensors (Figure 15). In these studies, compound 7[25] and 9[26] are good examples of energy transfer based mercury cation sensors. Compound 8[27] and 10[28] illustrates fluorescent sensors working in near IR region for metal cations. Moreover, compound 10 has also advantage of being water soluble in addition to working in NIR region.

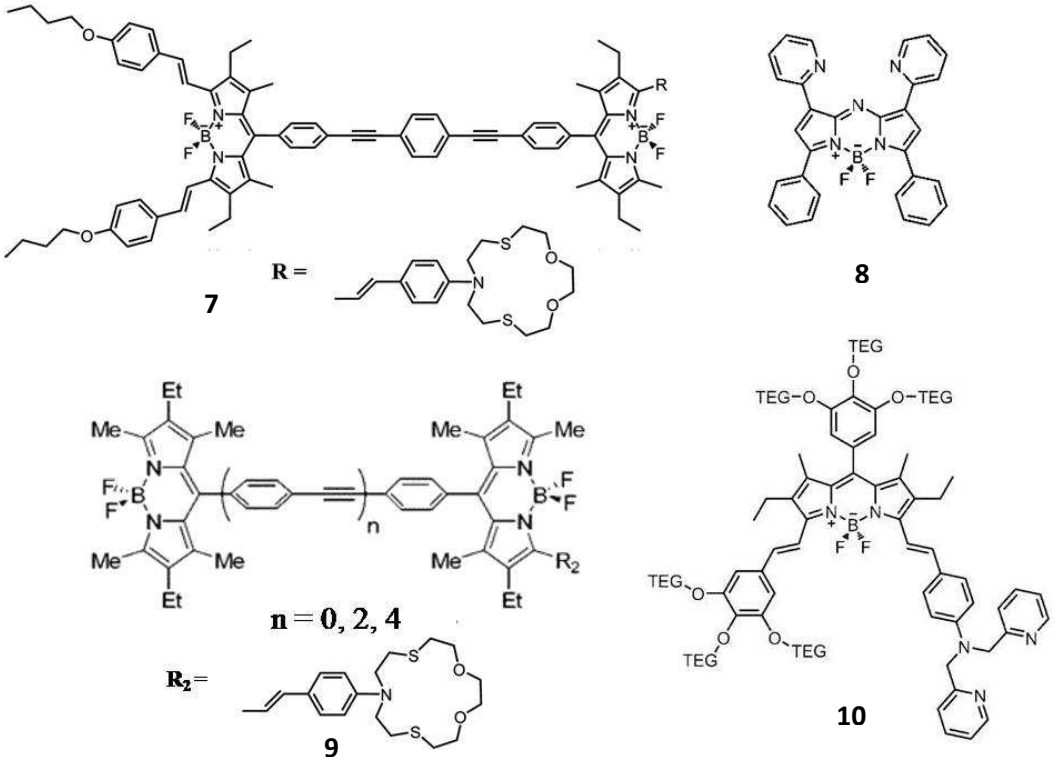

Figure 15 Some examples of BODIPY based molecular sensors

Photodynamic therapy (PDT) is also an exciting field for BODIPY dyes. Nagano et al showed that fluorescence of compound 11 decreases from 0.70 to 0.02 upon addition iodine atoms to core BODIPY and the molecule gains singlet oxygen generation feature in high efficiency[29]. Later on, Akkaya et al. synthesized orthogonal BODIPY dimers (12) to show there is no need to use harmful heavy atoms to design photosensitizer for PDT by using cell culture[30] (Figure 16).

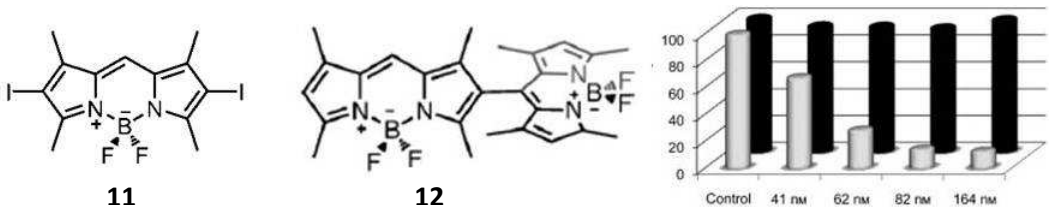

Figure 16 Photodynamic therapy agents

Dye sensitized solar cells are another field that BODIPY can be employed due to its photo stability although ruthenium based complexes seem more efficient presently. First use of BODIPY as a photosensitizer is done by Nagano et al. Compound 13 and

15 (Figure 17) showed the conversion efficiency respectively 0.16% and 0.13%. These differences arose from electron donating methoxy groups. Both of them have carboxylate group 2nd and 6th position of BODIPY in order to bind molecule to TiO_2 surface. Akkaya et al. changed position of carboxylate group and used stronger push-pull (additional cyano group) groups to increase electron conversion. The result for compound 14 is 1.66% in visible and near IR region.

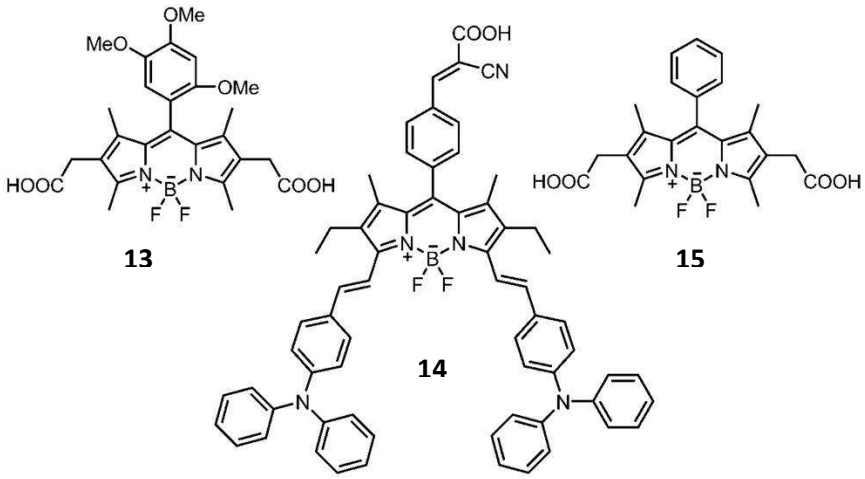

Figure 17 BODIPY based photosensitizers

Last application but not the least is newly emerging field of molecular logic gates. One of the interesting and well-presented example of it is combination of AND logic gate with PDT proposed by Akkaya et al (Figure 18). This combination will probably contribute higher selectivity to next photodynamic therapy operations[31].

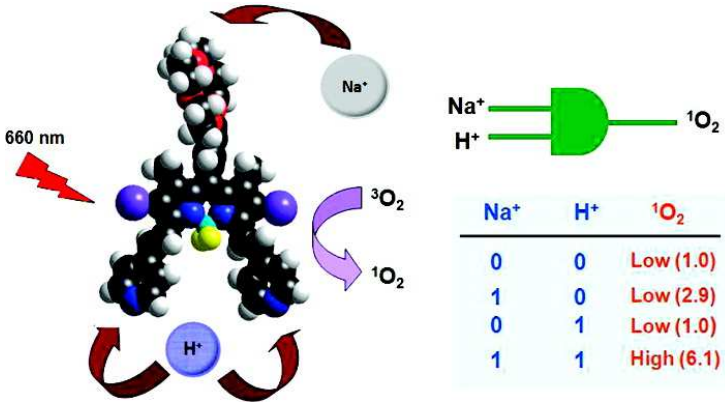

Na^+	H^+	$^1O_2$
0	0	Low (1.0)
1	0	Low (2.9)
0	1	Low (1.0)
1	1	High (6.1)

Figure 18 A BODIPY based molecular logic gate (as potential PDT agent) [31]

2.6. Energy Transfers

Fluorescent labels are supposed to be have intense and well-resolved emission peaks[32]. Today, fluorescent labels with a single excitation wavelength are used in biological studies. Many of them has an emission very close to excitation wavelength[33], [34]. The others with big Stokes' shift have intensity problems. Therefore, there is a conflict between what is desired and is done. To solve this problem, energy transfer phomenon has been employed to both increase Stokes' shift and intesity[35]. In this systems, energy is transferred donor group, which has absorption at shorter wavelength, to the acceptor one with emission at longer wavelength[32]. Energy transfer is divided in to two, Dexter type (through-bond ET) and Förster type (through-space ET).

2.6.1. Dexter type

Through bond energy transfer, Dexter type, can be performed if donor and acceptor groups are linked to each other through π conjugation. Donor and acceptor groups require their orbital to overlap for energy transfer. Overlapping can be supplied by direct bonding or by using conjugated bridge. Dexter type is known as short range ET which is smaller than 10 Aº and it is exponentially sensitive to the distance change. Unlike Forster type, there is no need to be overlapping between absorption and emission spectrum of counter groups.

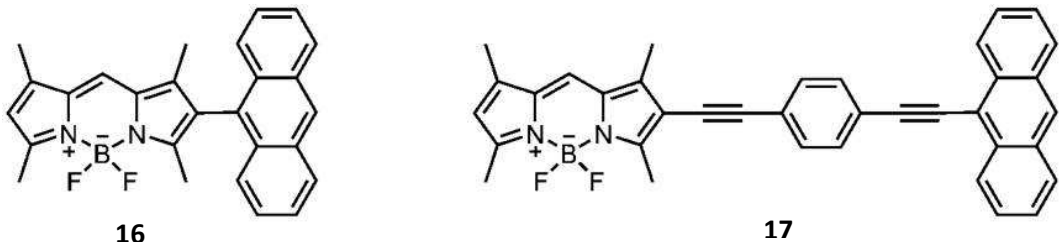

Figure 19 Examples of Dexter type energy transfer

In Figure 19, antracene-BODIPY cassettes show an example through bond electron transfer. Compound 16[36] has an internal twist distorting planarity due to steric hindrance whereas structure 17[36] has full conjugation and no internal twist. Thus,

resulting structure causes absorption band of compound 17 to be red-shifted and broaden, and eventually diminishes through bond energy transfer efficiency for 17.

2.6.2. Förster type

Fluorescent resonance energy transfer occurs through a radiationless energy transfer between donor and acceptor group in a close proximity. The proximity can be supply by chemically (non-conjugated linker) or by physically (micelles, nanoparticle etc.). Due to lack of conjugation between donor and acceptor groups, energy transfer progresses through space. Non-radiative energy transfer from donor to acceptor occurs provided by emission spectrum of donor molecule overlaps with absorption spectrum of acceptor one. Energy transfer efficiency is dependent on majorly three factors: Integration of spectral overlap, relative orientation of transition dipoles and distance between donor and acceptor molecules. Overlapping of spectra and mechanism is depicted in Figure 20.

$$\boldsymbol{E = \frac{1}{1 + (\frac{r}{R_0})^6}}$$

Equation 1 FRET quantum yield equation in terms of distance

In Equation 1, **E** represents quantum yield of energy transfer transition, **r** is distance between donor and acceptor molecules and $\mathbf{R_0}$ is the Forster distance. As can be understood from equation, quantum yield of energy transfer transition is inversely proportional to 6^{th} power of **r.** This means distance has a critical point in FRET. FRET can be done up to 10 nm distance efficiently.

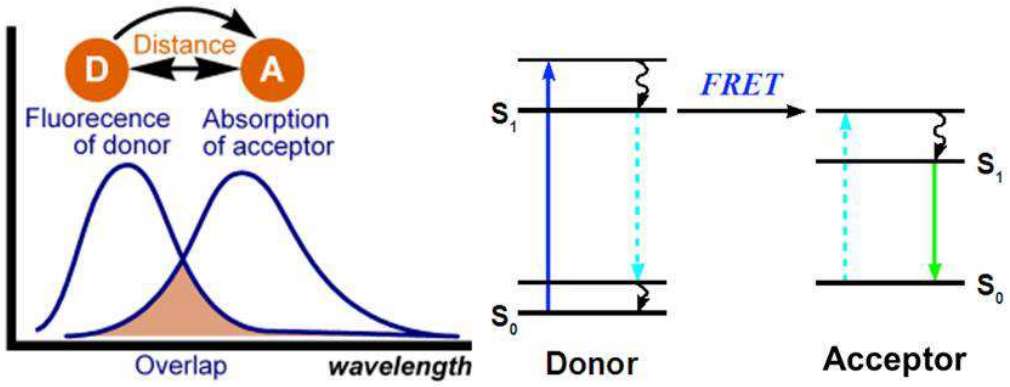

Figure 20 Overlapping of donor and acceptor spectra and FRET mechanism

In Figure 21, there is a typical example of FRET in which excitation at 520 nm causes energy transfer from edge BODIPYs to central one to make a emission at 730 nm. [37]

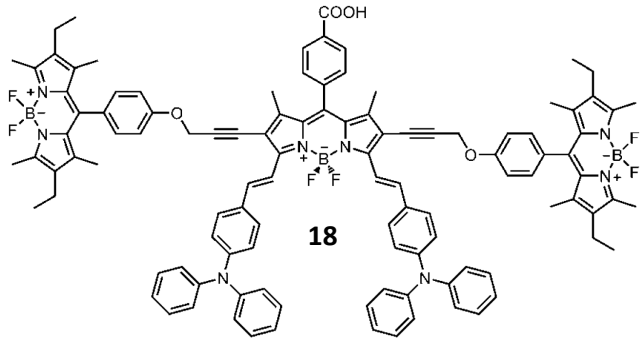

Figure 21 FRET from edge BODIPYs to the central one

FRET takes place in variety of applications. Detection of interaction and distance measurement between molecules are important applications in biology and chemistry. [38]

2.7. Caged Compounds

Once “cage” is heard, most rightfully associate with birdcage. In chemistry, however, cage describes a compound that can hold a certain species or ion and does not let it go. There are famous examples of caged compounds such as EDTA, EGTA, and DTPA. Conventional caged compounds have being found important application

areas. To illustrate, EDTA is used as drug of the chelation therapy in order for lead poisoning for many years. [39]. Textile and paper industry rely on EDTA for their production as well. With passing days, caged compounds seem to become more significant. Today, concept of caged compound has caged variety of biologically important ions, small molecules and macromolecules successfully. Current scope of research is, however, mainly on phototriggered release of caged compounds in biological environment. [40]

To understand biological function of neurotransmitters and secondary messengers which are used in intracellular signaling is an important goal. Knowing spatial and temporal data of signaling elements is the key point to comprehend what happen. Very similarly, gene expression receptors, proteins, RNA and DNA molecules are needed to be tested in spatiotemporal way to illuminate their intracellular activity. For these reasons, phototriggered release of biomolocules through caged compounds were proposed first by Kaplan et al. in 1973 as photolabile caged ATP.[41] Later on, other biomolecules were caged such as chelators, neurotransmitters, fluorescent dyes, peptides, and nucleotides.[40]

The main idea behind biological importance of caged compounds is based on photo activation of biologically active species. NPE-ATP and MNI-Glu caged compounds are shown in Figure 22. ATP and glutamate are biologically active species, thus participate physiological chemistry of living cell. However, their caged compounds are biologically inert. NPE-ATP, for example, does not undergo hydrolysis unless the compound is uncaged because caging molecule hinders enzyme to bind ATP. Similarly, MNI-Glu is not able to find its receptor with caging molecule before uncaging.[40]

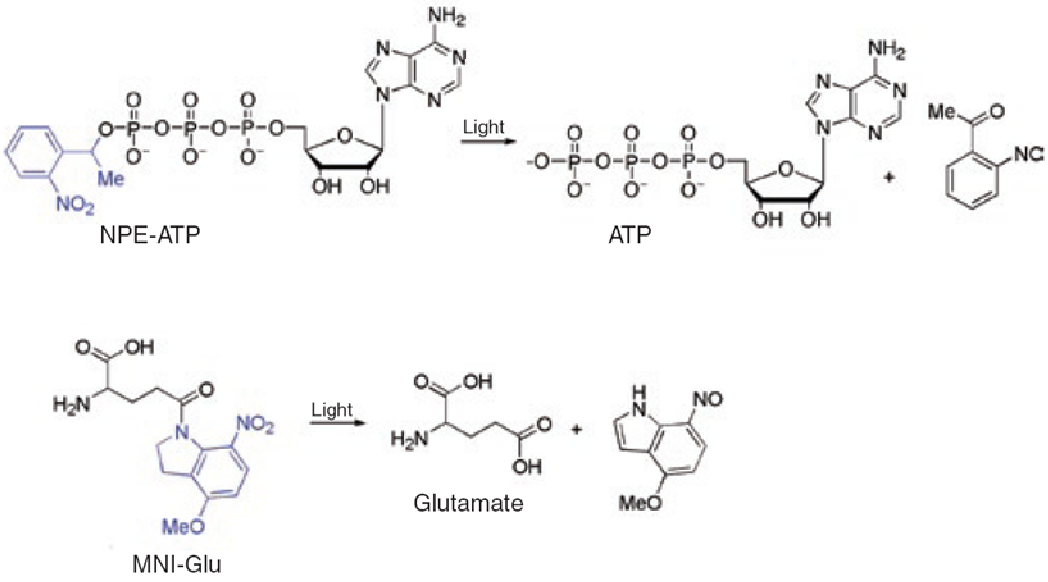

Figure 22 Examples for caging of biologically active molecules

Calcium ion is an important regulatory ion in physiological chemistry and plays role on second messenger systems in signal transduction. For that reason, there are number of proposed phototrigger molecules, however, most particular and known are nitro benzyl derivatives. Caged calcium compounds based on nitro benzyl group has been applied successfully to commercial products, for example, NP-EGTA. When NP-EGTA Ca^{2+} complex is irradiated with UV, the affinity of resulting molecule to calcium ion decreases 12,500 fold with respect to uncleaved complex. The affinity is 600,000-fold lower in the case of DMNP-EDTA (Figure 23).[42]

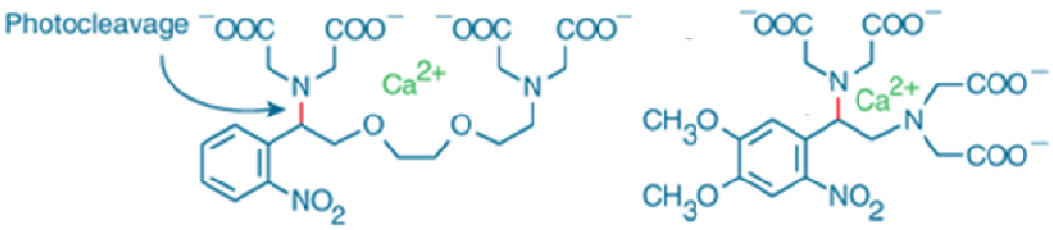

Figure 23 Commercial caged Ca(II) probes: NP-EGTA (left), DMNP-EDTA (right)

Recent developments in cell biology indicate that zinc ion also play a role as second messenger. Yamasaki et al. report that release of free zinc, in other words zinc wave, takes place in intracellular signaling by modulating length of the time and intensity of immunoglobin E receptor-based signaling, which demonstrates its role as a second

messenger.[9] Illumination of biological functions of zinc ion has prompted scientists to design caged zinc ion compounds which provide biological experiments spatiotemporal control under different physiological conditions. One of the well-presented example of them was introduced by Shawn Burdette and his coworkers.[10] In this research, photolabile nitro benzyl group was exploited as in the other caged calcium compounds such as DMNP-EDTA.

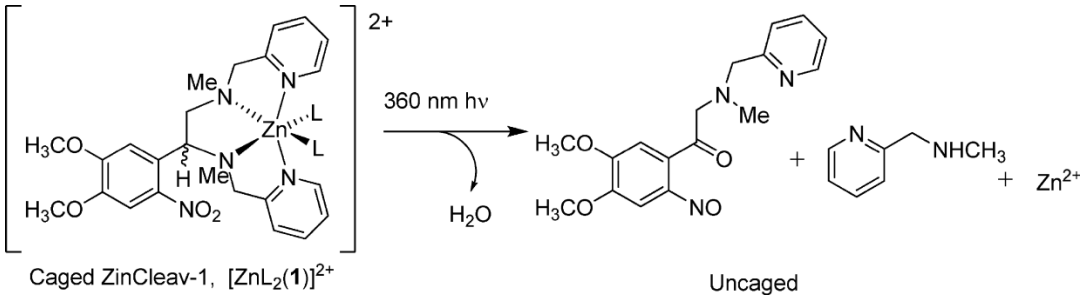

Figure 24 Photolabile caged Zn(II) ion compound ZinCleave-1

As can be seen in the Figure 24, ZinCleave-1 is broken upon irradiation of UV light and loses its chelating effect. The resultant structures have much less affinity to zinc ion, so Zn^{2+} is unleashed to the media. Reaction mechanism of the molecule can be represented as in the Figure 25.

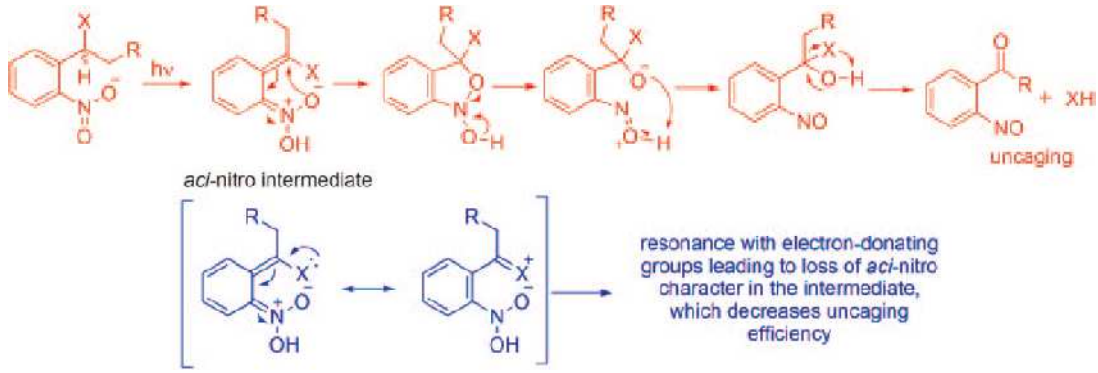

Figure 25 Photolysis mechanism of the nitrobenzyl group[43]

2.8. Logic Gates

First programmable computer has invented by Konrad Zuse about 90 years ago. Probably, Zuse would not imagine how computers doing big jobs today. Nevertheless, computers which could only do algorithmic calculations at the

beginning have become workhorses of our modern world. From social to individual, all life has been reformed by computers.

Computers are composed of integrated circuits. Logic gates that are primary building blocks of integrated circuits are designed on Boolean logic. During the process through logic gates, an output signal is formed as a result of one or more inputs. All information is encoded by zeros and ones. While (1) value represents high voltage, (0) means low voltage.

Boolean logic is composed of several functions in which AND, OR, XOR, NAND, NOR and XNOR gates are common examples as in depicted with their symbols and truth tables in Figure 26.

Truth table in Figure 26 composed of inputs and an output which are written in binary system. Inputs on each logic gates give an output regarding their logic function. In AND gate, for example, if both inputs carry value (1) at the same time, output shows (1). Otherwise, output goes to (0) meaning low voltage. In the case of OR gate, output (1) depends on inputs that at least one of them is (1). If both inputs are (0) (no input), output shows (0).

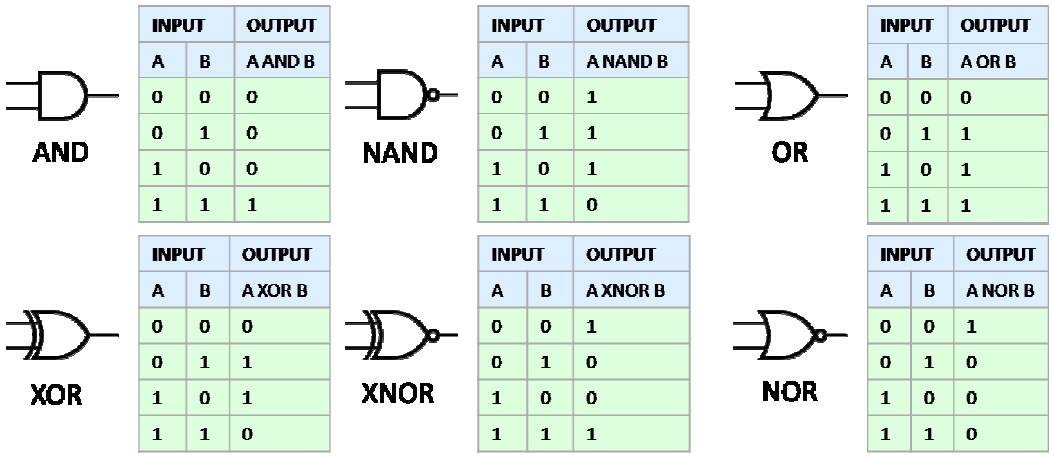

INPUT		OUTPUT
A	B	A AND B
0	0	0
0	1	0
1	0	0
1	1	1

INPUT		OUTPUT
A	B	A NAND B
0	0	1
0	1	1
1	0	1
1	1	0

INPUT		OUTPUT
A	B	A OR B
0	0	0
0	1	1
1	0	1
1	1	1

INPUT		OUTPUT
A	B	A XOR B
0	0	0
0	1	1
1	0	1
1	1	0

INPUT		OUTPUT
A	B	A XNOR B
0	0	1
0	1	0
1	0	0
1	1	1

INPUT		OUTPUT
A	B	A NOR B
0	0	1
0	1	0
1	0	0
1	1	0

Figure 26 Truth tables of different logic operations

Essential logic gates are just capable of doing simple logic operations. To form more complex digital devices doing arithmetic operations, these logic gates are required to be concatenated.

Silicon based technology relies on miniaturization concept to develop present computers since Jack Kilby's invention of integrated circuits in 1950s. Number of transistors almost doubled every year as Gordon E. Moore anticipated in 1965.[44] However, as in any life, current technology is estimated to end around 2020 with respect to miniaturization concept due to quantum tunneling effect.[5] However, molecular logic gates might be alternative technology for post-transistor era and might fill silicon technology's shoes in next decades.

2.9. Molecular Logic Gates

Father of molecular gates Prof. Prasanna de Silva has put forward the idea use of molecules, or supermolecules as he said, to do logical operations based on corresponding inputs and outputs. This idea, building up molecular logic gates by bottom-up approach instead of conventional top-down approach has being attracted great attention of many scientists. It is because current silicon technology can build a logic gate has dimensions 100 μm×100 μm×100 nm, whereas by using bottom-up approach, logic operations can be done in molecular level, pico-nanometer scale.[45]

First example of molecular logic gate was demonstrated by de Silva in 1993.[46] In this study, two-input **AND gate** was introduced (Figure 27). A fluorescent chemosensors with PeT mechanism was designed as molecular logic gate. Na^+ and H^+ ions were assigned as inputs and enhancement in fluorescence was used as output. Fluorescence output was preferred in the study as it has advantageous to get information signal in molecular scale over other methods. Photochemical mechanism of the molecule was summarized in Figure 28. PeT mechanism on the molecules is blocked by addition of both sodium ion and proton together, and then the molecule becomes fluorescent. Herein, PeT mechanism on anthracene moiety which effectively disappears in the presence of both Na^+ and H^+ ions

INPUTS		OUTPUT		
Na^+	H^+	Fluorescence Intensity	Quantum yield	Fluorescence Enhancement
0	0	0	0.011	1.0
1	0	0	0.020	1.8
0	1	0	0.013	1.2
1	1	1	0.068	6.2

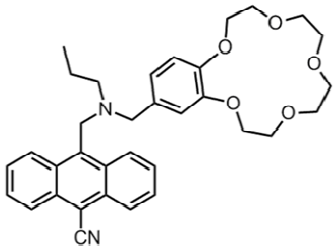

Figure 27 First AND-logic gate by de Silva et al

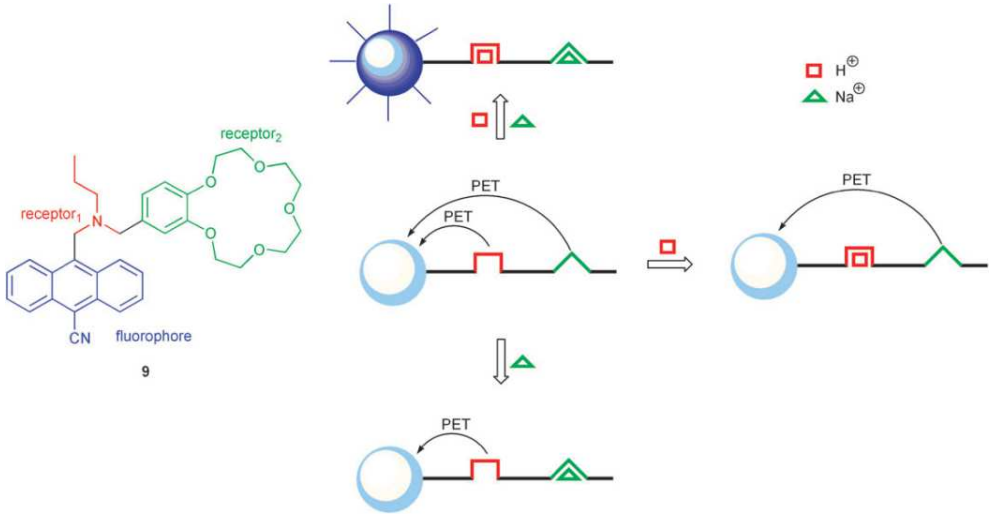

Figure 28 Working principle of de Silva's AND-logic gate [46]

Another example of molecular logic gates, **XNOR gate**, was reported by de Silva et al in Figure 29. In this study the compound has absorbance at 390 nm without any inputs. However, it undergoes red and blue shift upon the addition of proton and calcium ion respectively. It means that system does have very low absorption at 390 nm long more, that is, output goes to (0). In the case of two input is present at the same time, their total effect neutralize absorbance shift and so the molecule has absorbance maxima at 390 nm again (Output=(1)). Similar logic can be developed **XOR gates** in which output will be transmittance.

INPUTS		OUTPUT
Ca^{+}	H^{+}	Absorbance @390 nm
0	0	1
1	0	0
0	1	0
1	1	1

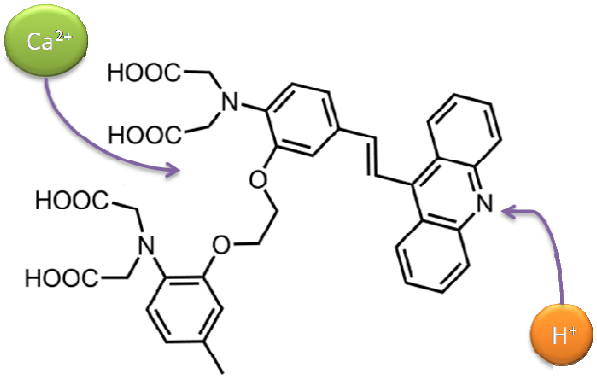

Figure 29 XNOR gate designed by de Silva et al

Molecular inhibit **(INH) gate** were accomplished as well. According to Pischel and coworkers, Eu ion with enough concentration can give luminescence through energy transfer from amino-substituted 1,8-naphthalimide as in shown in Figure 30. However, if there is O_2 in the media, low emission is observed. In short, it can be said that O_2 hinders other input to work, therefore, no emission output is obtained under O_2.[47]

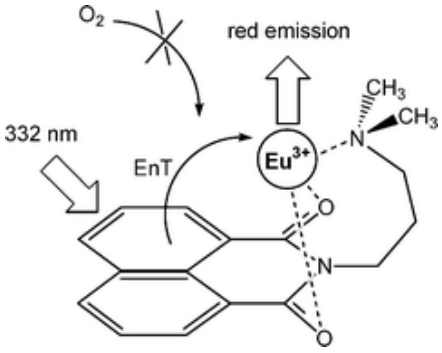

INPUTS		OUTPUT
O_2	Thereshold Conc. of Eu^{3+}	Eu^{3+} Luminescence
0	0	0
1	0	0
0	1	1
1	1	0

Figure 30 An INH gate designed by Pischel et al

OR gate is one of best logic gates for creating it by molecules, because non-selectivity towards inputs of a chromophore forms spontaneously OR logic gates. To illustrate better, one can look at the Figure 31 where tricarboxylic acid groups on the compound which is not selective towards Mg^{2+} and Ca^{2+} can bind to both of ions; therefore, fluorescence emission of the compound will enhance with each inputs[48].

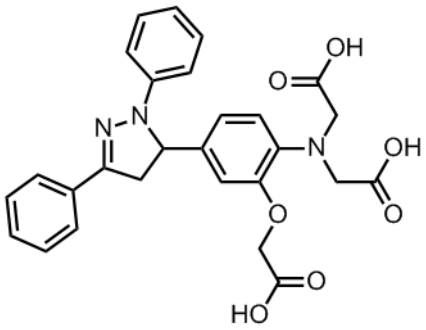

INPUTS		OUTPUT
Ca^{2+}	Mg^{+}	Fluorescence Emission
0	0	0
1	0	1
0	1	1
1	1	1

Figure 31 A typical example of OR gate

Today, scientists are trying to persuade molecules to do more complicated arithmetic operations. For higher function molecular logic gates should be concatenated physically. However, it is not as easy as it is in electronic circuitry. In silicon-based circuitry, logic gates use same type input and output, electricity. This homogeneity contributes great to concatenation of logic gates. On the other hand, molecular logic gates use different sort (heterogenic) of input-output generally. Therefore, communicating each molecule, speaking different languages, to others become harder. However, many complicated useful logic operations including half adder, half substractor, full adder, multiplexer/demultiplexer and some successive logic gates were reported successfully. Herein, some examples of molecular logic gates will be discussed.

2.9.1. Half Adder and Half Substractor

Half adder is the key element to make full adder which is used to add 2 bits of information. A half adder which contains one AND gate and one XOR gate evaluates binary data and gives two outputs as sum and carry digits.(Figure 32)

INPUTS		OUTPUTS	
A	B	AND (Carry)	XOR (Sum)
0	0	0	0
1	0	0	1
0	1	0	1
1	1	1	0

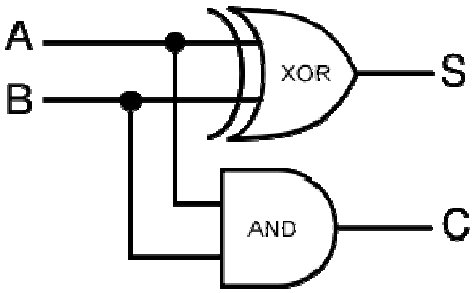

Figure 32 Presentation of truth table and symbol of half adder

First half adder designed by de Silva et al. was composed of anthracene and quinoline molecules as the reporter parts.[49] Later on, Shanzer and coworkers proposed first unimolecular half adder based on fluorescein molecule in 2005. Bozdemir et al. who carried molecular half adders one step more demonstrated a BODIPY based half adder by using easy-selective manipulation of ICT and metal ion sensing. Output for carry (AND) was assigned absorbance at 623 nm, and output for sum (XOR) was selected absorbance at 663 nm. As can be seen in the Figure 33, distyrile BODIPY molecule works well with metal inputs and supplies the summation of the number sets, 0+0=0, 0+1 or 1+0=1, 1+1=10.

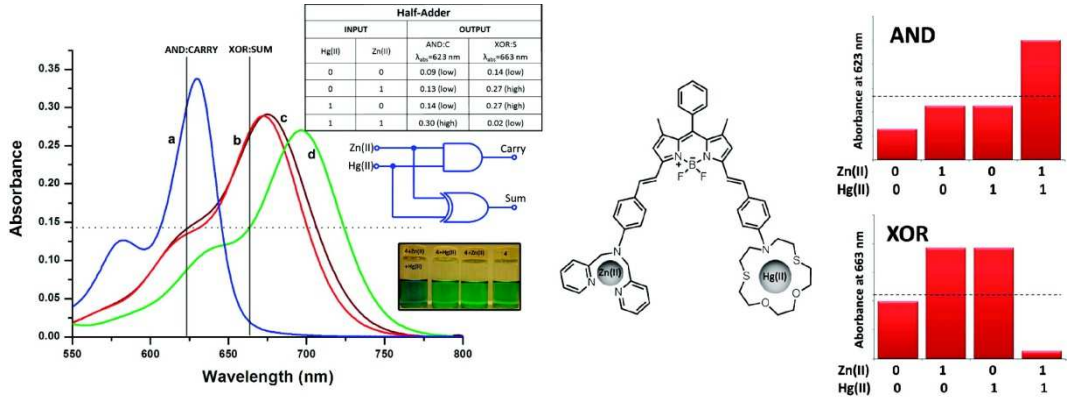

Figure 33 BODIPY based half substractor reported by Bozdemir et al[50]

Unlike half adder, **half substractor** is composed of one XOR gate and one INH gate. Outputs are named as difference for XOR gate and borrow for INH gate. Truth table and operation symbol is depicted in Figure 34.

INPUTS		OUTPUTS	
A	B	XOR (Diff)	INH (Borrow)
0	0	0	0
0	1	1	1
1	0	1	0
1	1	0	0

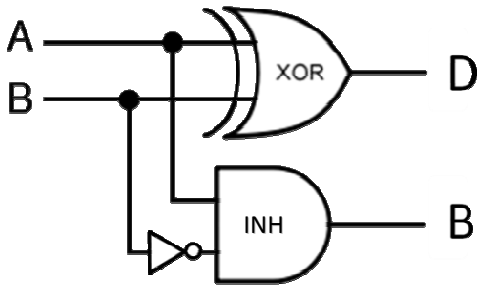

Figure 34 Presentation of truth table and symbol of half substractor

First half substrator was able to be reported 3 years after first half adder by Langford and Yann.[51] In this study tetraphenylporphyrin was used as signaling part. Inputs were selected H^+ (proton) and t-BO^- (base) that H^+ behaves as inhibitor input with respect to output of fluorescence emission at 440 nm. It is because 440 nm can be received provided that base is added. This property forms inhibit gate of the system. On the other hand, XOR gate works in the principle of transmittance of light at 417 nm. As can be understood from the truth table in the figure 35, addition of acid or base caused low absorption, or high transmittance at 417 nm due to spectral shift in absorbance to 440-450 nm.

INPUTS		OUTPUTS	
H^+	t-BuO^-	(Borrow) Flu@440nm	(Diff) T@417nm
0	0	0	0
0	1	1	1
1	0	0	1
1	1	0	0

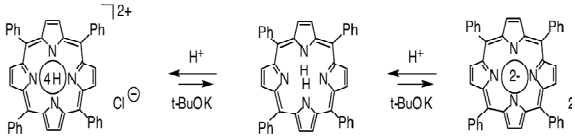

Figure 35 First example of half substractor proved by Langford et al

2.9.2. Molecular logic beyond silicon technology

Molecular logic gates mimicking silicon-based processor would mean a principle change in the conceptual framework due to its advantages on size, production and processing. Although many scientists believe one day molecular computing will be given higher value, there is lack of practical utility beyond proof of principle.

Actually, there is no need to restrict molecular logic to in the area of silicon industry. Molecules can work in many places where silicon based systems cannot operate. According to Prof. Prasanna de Silva pioneer of molecular logic, "Molecular devices will reach where silicon devices cannot easily go, whether it be inside living cells, on the surface of plastic beads or inside detergent micelles"[52]. As de Silva says, combination of molecular logic with life science would be a useful way to follow. Suriye Ozlem and Engin Akkaya has demonstrated this idea by designing an agent for photodynamic therapy working with Boolean logic.[31] AND gate-based agent starts to generate reactive singlet oxygen only if two inputs, Na^+ and H^+, are present together. (Figure 36)

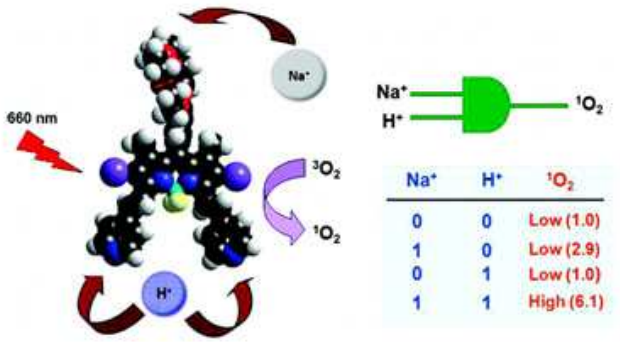

Figure 36 Super PDT agent: Application of Boolean logic to life science[31]

Uchiyama et al has demonstrated in 2005 how molecular devices can go very small spaces and operate molecular logic which silicon devices cannot. In this study, it is reported that AND logic gate-based molecule could take place in detergent micelle and work in more realistic aqueous environment by using Na^+ and H^+ as inputs and fluorescence emission as output.(Figure 37)

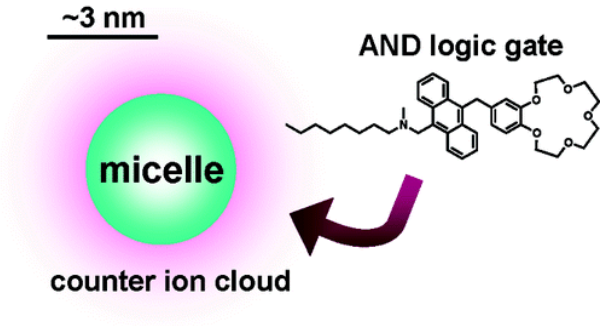

Figure 37 Molecular AND logic gates operating in micelle by Uchiyama et al[45]

Multiparameter sensing is another important area that molecular logic can show immediate utility. "Lab-on-a-molecule" idea reported by de Silva aims to show potential application of molecular logic in medical diagnostic and chemical sensing. In his paper, anthracene based reporter fluorophore can work in water and sense Zn^{2+} Na^{+} and H^{+} ions as inputs with bright fluorescence signal. Therefore, it gives information when ion concentrations are greater than pre-determined threshold.(Figure 38)

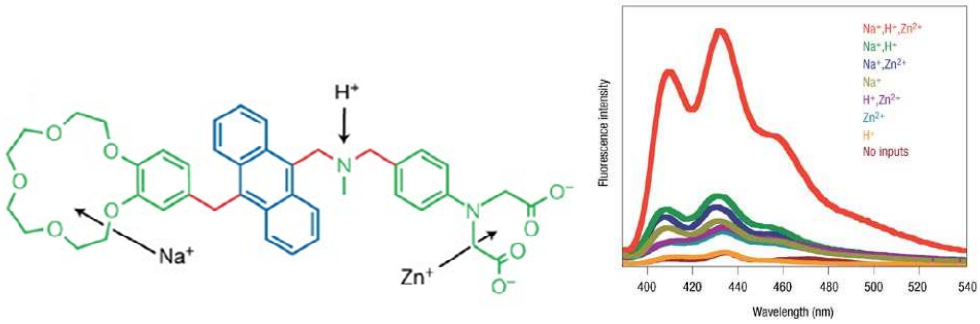

Figure 38 "Lab-on-a-molecule" by de Silva[53]

CHAPTER 3

EXPERIMENTAL RESULTS

3.1. Materials and Methods

All chemicals and reaction solvents are purchased from Sigma-Aldrich and they were used without further purification. Merck Silica Gel 60 (particle size: 0.040-0.063 mm, 230-400 mesh ASTM) was used for column chromatography. Reactions are followed by Merck TLC Silica gel 60 F_{254} thin layer chromatography (TLC).

^{1}H NMR and ^{13}C NMR spectra were recorded on Bruker DPX-400 (operating at 400 MHz for ^{1}H NMR and 100 MHz for ^{13}C NMR). NMR samples were dissolved in $CDCl_3$ with tetramethylsilane as internal standard. All spectra were recorded at 25 ^{o}C and coupling constants (*J* values) were given in Hz. Chemical shifts were expressed in parts per million (ppm). Splitting patterns are designated as s (singlet), d (doublet), t (triplet), q (quartet), m (multiplet), and p (pentet).

Mass spectra were recorded in Agillent Technologies 6530 Accurate-Mass Q-TOF LC/MS Mass spectrometer. Varian absorborption spectrometer was used to obtain absorption spectra. Fluorescence spectra were obtained by using Varian Eclipse spectrofluorometer. All solvent used for spectroscopic measurements selected were spectrophotometric grade. Compounds I[54], II[55], and DPA-BODIPY and Click[56] were synthesized according to literature.

3.2. Synthesis

Synthetic Pathway.

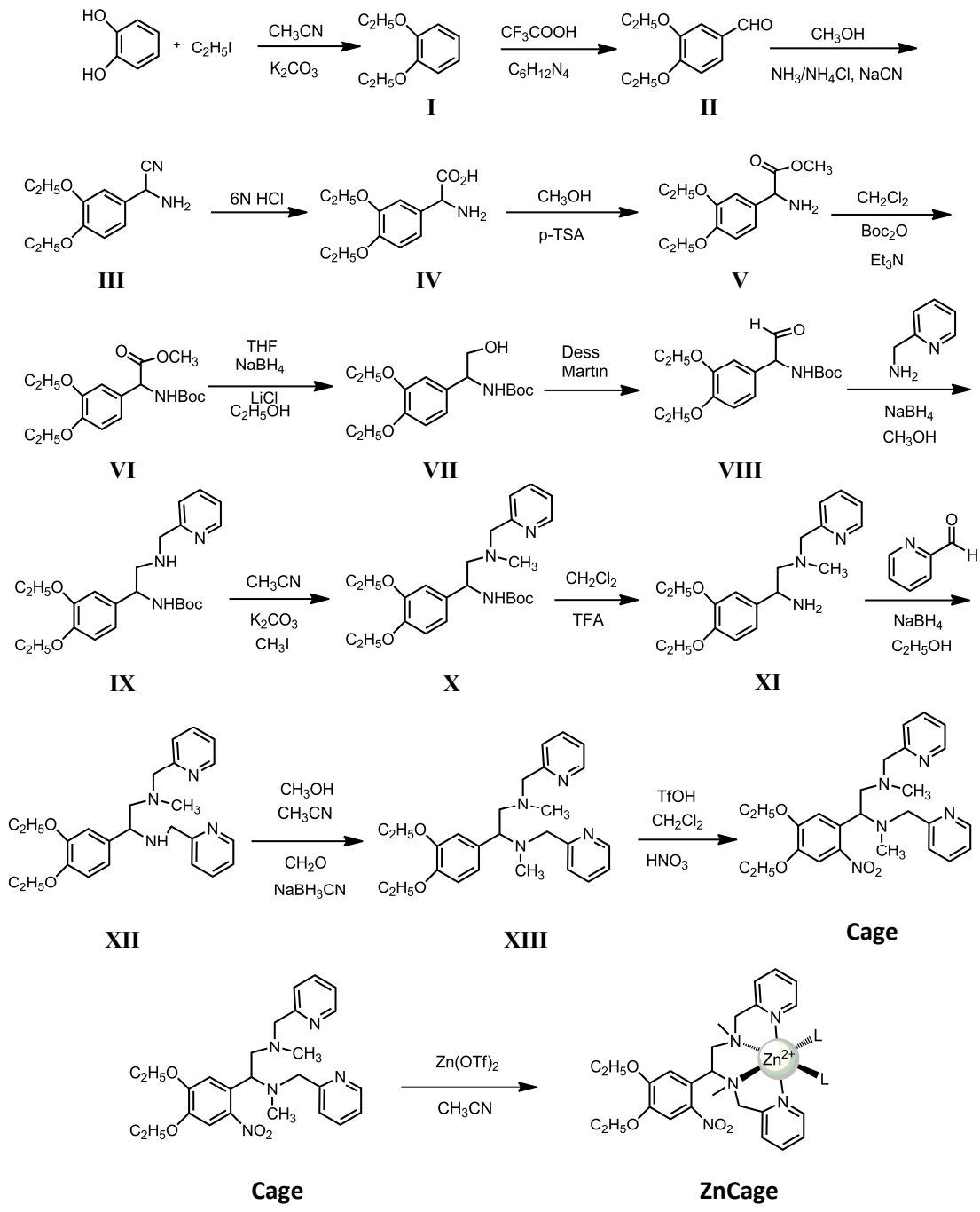

Target Compounds.

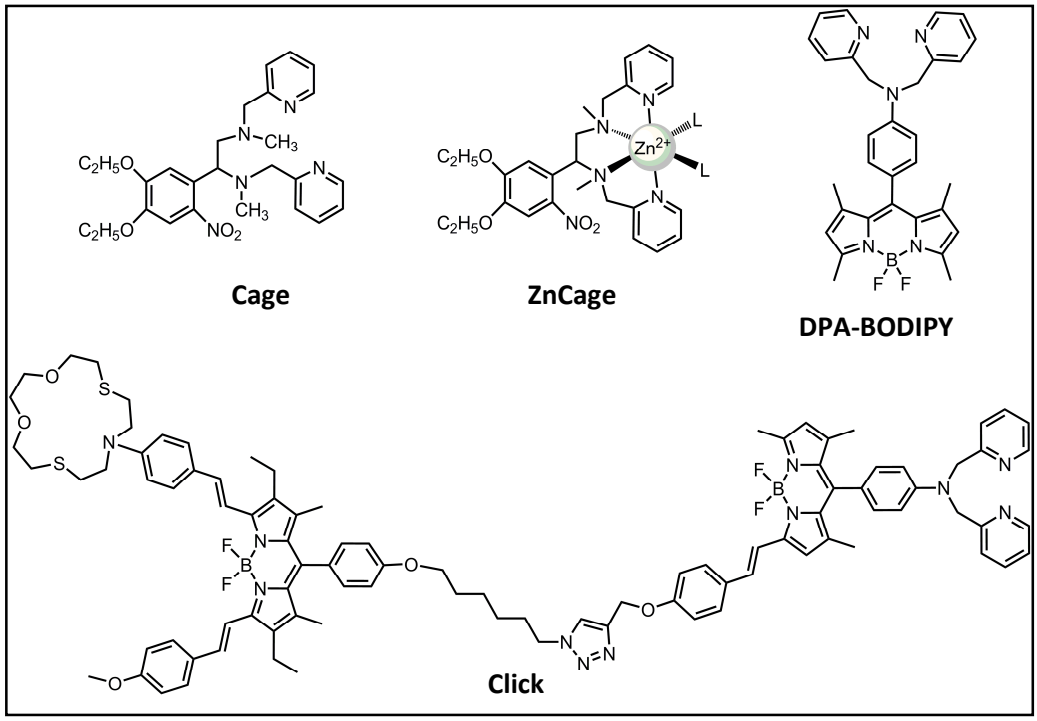

Synthesis of Compound I[54]

Catechol (10 g, 90 mmol) and ethyl iodide (22 mL, 273 mmol) were dissolved in CH_3CN (150 mL) in a 500 mL round-bottomed flask. K_2CO_3 (37.6 g, 273 mmol) and a few crystals of 18-crown-6 were added. The reaction mixture was refluxed for 18 h and followed by TLC silica gel plates using *n*-hexane- ethyl acetate (8:1) as mobile phase. The reaction mixture was filtered and the CH_3CN was evaporated in vacuo. The crude product was purified by silica gel column chromatography using *n*-hexane- ethyl acetate (8:1) as mobile phase. Fraction containing compound I was collected then the solvent was removed under reduced pressure (69.2 mmol, 11.5 g, 76 %).

^{1}H NMR (400 MHz, Chloroform-*d*): δ_H 6.92 (s, 4H), 4.12 (q, J = 7.0 Hz, 4H), 1.47 (t, J = 7.0 Hz, 6H) ppm.

^{13}C NMR (100 MHz, Chloroform-*d*): δ_C 148,89, 121.01, 113.86, 64.56, 14.88 ppm.

Synthesis of Compound II

Compound I (10 g, 60 mmol) were dissolved in trifluoroacetic acid (20 mL) in a 100 mL round-bottomed flask. Hexamethylenetetramine (12.6 g, 90 mmol) was added. The reaction mixture was refluxed for 12 h and followed by TLC silica gel plates using n-hexane- ethyl acetate (5:1) as mobile phase. Then, it was extracted with ethyl acetate and water. Organic layer was dried with Na_2SO_4 and evaporated in vacuo. The crude product was purified by silica gel column chromatography using n-hexane- ethyl acetate (5:1) as mobile phase. Fraction containing compound II was collected then the solvent was removed under reduced pressure (30 mmol, 5.8 g, 50 %).

1H NMR (400 MHz, Chloroform-d): δH 9.83 (s, 1H), 7.44 – 7.21 (m, 2H), 6.98 (d, J = 8.2 Hz, 1H), 4.25 – 4.05 (m, 4H), 1.50 (dt, J = 9.0, 7.0 Hz, 6H) ppm.
13C NMR (100 MHz, Chloroform-d): δC δ 190.53, 154.01, 148.83, 129.73, 126.22, 111.46, 110.47, 64.31, 64.18, 14.44, 14.37 ppm.

Synthesis of Compound III and IV

Compound II (5 g, 25.8 mmol) were dissolved in methanol (15 mL) in a 250 mL round-bottomed flask. Sodium cyanide (1.9 g, 38.6 mmol) and ammonium chloride (2.1 g, 38.6 mmol) in NH_4OH (30 mL, 30%) was added to the reaction mixture in a dropwise manner and the reaction mixture was stirred for 23 h at room temperature. The reaction mixture was filtered and the methanol was evaporated in vacuo. Then, crude product was extracted with ethyl acetate and water. Organic layer was dried with Na_2SO_4 and evaporated in vacuo. Crude product (3) was used in the next step without further purification. Compound III in 6 M HCl (60 mL) was refluxed for 4h. The solution was concentrated in vacuo. Filtration of the resulting yellow suspension gave compound IV as a yellow solid. (4g)

^{1}H NMR (400 MHz, DMSO-d_6): δ_H 8.71 (s,3H), 7.05 (s, 1H), 6.90 (s, 2H),4.87 (s, 1H), 4.00 – 3.85 (m, 4H), 1.23 (q, J = 7.0 Hz, 6H) ppm.

^{13}C NMR (100 MHz, DMSO-d_6): δ_C 170.37, 149.35, 148.57, 125.71, 121.26, 113.67, 113.63, 64.42, 64.30, 55.71, 15.15, 15.12 ppm.

Synthesis of Compound V

Compound IV (4 g, 16.7 mmol) and p-toluenesulfonic acid monohydrate (6.4 g, 33.5 mmol) were dissolved in methanol (50 mL) in 250 mL round-bottomed flask and refluxed for 24 h. The solvent was removed, and the crude product was dissolved in NH4OH (30 mL, 30%) and extracted with CH_2Cl_2. Organic layer was dried with Na2SO4 and evaporated in vacuo. The crude product was purified by silica gel column chromatography using CH2Cl2:CH3OH (100:4) as mobile phase. Fraction containing compound IV was collected then the solvent was removed under reduced pressure (12.3 mmol, 3.1 g, 73 %).

^{1}H NMR (400 MHz, Chloroform-*d*): δ_H 6.85 – 6.70 (m, 3H), 4.44 (s, 1H), 4.01 – 3.89 (m, 4H), 3.60 (s, 3H), 1.85 (b, 2H), 1.34 (td, J = 7.0, 3.2 Hz, 6H) ppm.
^{13}C NMR (100 MHz, Chloroform-*d*): δ_C 174.63, 148.94, 148.59, 132.87, 119.17, 113.48, 112.13, 64.60, 64.58, 58.40, 52.31 ppm.

Synthesis of Compound VI and VII

Compound V (3 g, 11.9 mmol) was dissolved in CH_2Cl_2 (60 mL) in 250 mL round-bottomed flask and triethylamine (1.82 mL, 13 mmol) and di-tert-butyl dicarbonate (2.8 g, 13 mmol) were added. The reaction mixture was stirred for 23 h at room temperature and followed by TLC silica gel plates using CH_2Cl_2:CH_3OH (100:4) as mobile phase. Then, it was extracted sequentially with HCl (1M, 20 mL), sat. $NaHCO_3$ (20 mL) and water (20 mL). Organic layer containing compound VI was dried with Na_2SO_4 and evaporated under reduced pressure. Compound VI was used in the next step without further purification.

Compound VI (4 g, 11.3 mmol) was dissolved in THF (30 mL) in 250 mL round-bottomed flask. After reducing the temperature of the reaction mixture to 0 ^{o}C, $NaBH_4$ (0.86 g, 22.6 mmol), LiCl (0.96 g, 22.6 mmol) and ethanol (20 mL) were

added. The reaction mixture was stirred for 23 h at room temperature and followed by TLC silica gel plates using CH_2Cl_2:CH_3OH (100:4) as mobile phase. The solvent mixture was evaporated in vacuo and the product was extracted with CH_2Cl_2 and water. Organic layer was dried with Na_2SO_4 and evaporated in vacuo. The crude product was purified by silica gel column chromatography using CH_2Cl_2:CH_3OH (100:4) as mobile phase. Fraction containing compound VII was collected then the solvent was removed under reduced pressure (8 mmol, 2.6 g, 70 %).

^{1}H NMR (400 MHz, Chloroform-*d*): δ_H 6.75 – 6.61 (m, 3H), 5.38 (b, 1H), 4.51 (b, 1H), 4.04 – 3.81 (m, 4H), 3.6 (d, J = 5.8 Hz, 2H), 3.28 (t, J = 5.9 Hz, 1H), 1.28 (t, J = 7.0 Hz, 15H) ppm.
^{13}C NMR (100 MHz, Chloroform-*d*): δ_H 156.19, 148.76, 148.07, 132.57, 118.87, 113.66, 112.40, 79.67, 66.29, 64.60, 56.44, 28.31, 14.80 ppm.

Synthesis of Compound VIII

To a 250 mL round-bottomed flask containing argon-degassed CH_2Cl_2 (120 mL) were added Dess-Martin periodinane (4.9 g, 11.5 mmol) and Compound VII (2.5 g, 7.7 mmol). The reaction mixture was stirred for 23 h at room temperature and followed by TLC silica gel plates using CH_2Cl_2:CH_3OH (100:4) as mobile phase. The resulting reaction mixture was quenched by adding solution of saturated sodium thiosulfate. Then, it was extracted with CH_2Cl_2. The crude product was purified by silica gel column chromatography using CH_2Cl_2:CH_3OH (100:4) as mobile phase. Fraction containing compound 8 was collected then the solvent was removed under reduced pressure (7.1 mmol, 2.3 g, 93 %).

^{1}H NMR (400 MHz, Chloroform-*d*): δ_H 9.43 (s, 1H), 6.85 – 6.64 (m, 3H), 5.65 (b, 1H), 5.14 (s, 1H), 4.11 – 3.92 (m, 4H), 1.35 (t, J = 6.8 Hz, 15H) ppm.
^{13}C NMR (100 MHz, Chloroform-*d*): δ_C 195.16, 155.04, 149.40, 149.12, 120.50, 113.76, 112.72, 64.61, 64.54, 64.35, 55.26, 28.25, 14.78, 14.73 ppm.

Synthesis of Compound IX

Compound 8 (2.2 g, 6.8 mmol) and 2-picolylamine (0.9 g, 8.3 mmol) were dissolved in methanol (50 mL) in 100 mL round-bottomed flask and stirred for 6 h at room temperature. After reducing the temperature of the reaction mixture to 0 ^{o}C, $NaBH_4$ (0. 51 g, 13.6 mmol) was added and the resulting mixture was stirred for 18 h at room temperature. The methanol was evaporated in vacuo. Then, crude product was extracted with CH_2Cl_2 and water. Organic layer was dried with Na_2SO_4 and evaporated in vacuo. The crude product was purified by silica gel column chromatography using CH_2Cl_2:CH_3OH (100:6) as mobile phase. Fraction containing compound IX was collected then the solvent was removed under reduced pressure (4.1 mmol, 1.7 g, 60 %).

^{1}H NMR (400 MHz, Chloroform-*d*): δ_H 8.53 (d, *J* = 4.9 Hz, 1H), 7.63 (td, *J* = 7.7, 1.8 Hz, 1H), 7.24 (d, *J* = 7.8 Hz, 1H), 7.16 (ddd, *J* = 7.6, 5.0, 1.2 Hz, 1H), 6.90 – 6.62 (m, 3H), 5.60 (b, 1H), 4.73 (b, 1H), 4.15 (qd, *J* = 7.0, 1.8 Hz, 1H), 4.08 (q, *J* = 4.0 Hz, 4H), 3.88 (d, *J* = 2.4 Hz, 2H), 2.91 (m, 2H), 1.51 – 1.26 (m, 15H) ppm.
^{13}C NMR (100 MHz, Chloroform-*d*): δ_C 159.51, 149.27, 148.82, 147.94, 136.47, 122.20, 121.99, 1202.4, 118.45, 113.67, 112.79, 111.87, 64.63, 64.60, 64.53, 54.83, 54.42, 28.38, 11.88, 14.86 ppm.

MS (TOF - ESI): m/z: Calcd: 415.52582 [M^+], Found: 416.26336 $[M+H]^+$, Δ=-21.5 ppm.

Synthesis of Compound X

Compound IX (1.6 g, 3.9 mmol) and K_2CO_3 (0.8 g, 5.8 mmol) were dissolved in CH3CN (40 mL) in a 100 mL round-bottomed flask. Methyl iodide (0.55 g, 3.9 mmol) was added to the reaction mixture in a dropwise manner. The reaction mixture was stirred for 5 h at room temperature and followed by TLC silica gel plates using CH2Cl2:CH3OH (100:6) as mobile phase. It was filtered and the CH3CN was evaporated in vacuo. The crude product was purified by silica gel column chromatography using CH2Cl2:CH3OH (100:6) as mobile phase. Fraction

containing compound X was collected then the solvent was removed under reduced pressure (2.6 mmol, 1.1 g, 67 %).

^{1}H NMR (400 MHz, Chloroform-*d*): δ_H 8.59 (d, *J* = 2.3 Hz, 1H), 7.66 (td, *J* = 7.7, 1.8 Hz, 1H), 7.32 (d, *J* = 7.9 Hz, 1H), 7.19 (ddd, *J* = 7.5, 4.9, 1.2 Hz, 1H), 6.88 – 6.65 (m, 3H), 5.90 (b, 1H), 4.62 (b, 1H), 4.07 (qd, *J* = 7.0, 1.6 Hz, 4H), 3.80 (d, *J* = 14.2 Hz, 1H), 3.65 (d, *J* = 14.2 Hz, 1H), 2.73 – 2.50 (m, 2H), 2.34 (s, 3H), 1.43 (td, *J* = 7.0, 2.3 Hz, 15H) ppm.

MS (TOF - ESI): m/z: Calcd: 429.26276 [M^+], Found: 430.27953 [M+H]$^+$, Δ=-22.1 ppm.

Synthesis of Compound XI

Trifluoroacetic acid (3 mL) was added to a solution of 10 (1.0 g, 2.3 mmol) in CH_2Cl_2 (30 mL) and stirred at for 23 h at room temperature. After removing the solvent, saturated K_2CO_3 was added to the reaction mixture, and the product was extracted into CH_2Cl_2. Organic layer containing compound XI was dried with Na_2SO_4 and evaporated under reduced pressure. No further purification was required (2.22 mmol, 0.73 g, 95 %).

^{1}H NMR (400 MHz, Chloroform-*d*): δ_H 8.54 (b, 1H), 7.66 (t, *J* = 7.7 Hz, 1H), 7.43 (d, *J* = 7.8 Hz, 1H), 7.17 (t, *J* = 6.2 Hz, 1H), 6.95 (s, 1H), 6.91 – 6.75 (m, 2H), 4.08 (q, *J* = 7.0 Hz, 5H), 3.82 (d, *J* = 14.0 Hz, 1H), 3.68 (d, *J* = 14.2 Hz, 1H), 2.79 – 2.42 (m, 2H), 2.34 (s, 3H), 2.13 (b, 2H), 1.44 (t, *J* = 7.0 Hz, 6H) ppm.

^{13}C NMR (100 MHz, Chloroform-*d*): δ_C δ 159.44, 149.02, 148.82, 147.86, 136.88, 136.44, 122.97, 121.99, 118.93, 113.57, 112.23, 66.47, 64.69, 64.59, 64.24, 53.04, 42.73, 14.89 ppm.

MS (TOF - ESI): m/z: Calcd: 329.21033 [M^+], Found: 330.22473 [M+H]$^+$, Δ=-21.6 ppm.

Synthesis of Compound XII

Compound XI (600 mg, 1.8 mmol) and 2-pyridinecarboxaldehyde (0.2 mL, 2.2 mmol) were dissolved in methanol (50 mL) in 100 mL round-bottomed flask and refluxed for 2 h at room temperature. After reducing the temperature of the reaction mixture to 0 ^{o}C, $NaBH_4$ (140 mg, 3.6 mmol) was added and the resulting mixture was stirred for 18 h at room temperature. The methanol was evaporated in vacuo. Then, crude product was extracted with CH_2Cl_2 and water. Organic layer was dried with Na_2SO_4 and evaporated in vacuo. The crude product was purified by basic alumina column chromatography using CH_2Cl_2:CH_3OH (100:2) as mobile phase. Fraction containing compound XII was collected then the solvent was removed under reduced pressure (1.1 mmol, 460 mg, 60 %).

^{1}H NMR (400 MHz, Chloroform-*d*): δ_H 8.59 – 8.39 (m, 2H), 7.67 (td, *J* = 7.6, 1.8 Hz, 1H), 7.63 – 7.52 (m, 2H), 7.21 – 7.08 (m, 3H), 6.99 (s, 1H), 6.86 – 6.81 (m, 2H), 4.18 – 3.98 (m, 5H), 3.90 – 3.51 (m, 4H), 2.76 (dd, *J* = 12.4, 10.6 Hz, 1H), 2.47 (dd, *J* = 12.4, 3.6 Hz, 1H), 2.25 (s, 3H), 1.44 (td, *J* = 7.0, 4.2 Hz, 6H) ppm.
^{13}C NMR (100 MHz, Chloroform-*d*) δ_C 160.22, 159.64, 149.30, 148.91, 148.79, 147.92, 136.43, 136.12, 134.98, 123.04, 122.50, 121.88, 121.73, 120.06, 113.44, 112.59, 65.65, 64.62, 64.50, 63.98, 59.65, 52.74, 42.56, 14.92, 14.87 ppm.
MS (TOF - ESI): m/z: Calcd: 420.25253 $[M^+]$, Found: 421.26430 $[M+H]^+$, Δ=-10.3 ppm.

Synthesis of Compound XIII

Compound XII (400 mg, 0.95 mmol) was dissolved in CH_3CN/CH_3OH (15/15 mL) in a 100 mL round-bottomed flask. Formaldehyde (37% in water, 3.1 mL), $NaBH_3CN$ (180 mg, 2.9 mmol), AcOH (1.2 mL) were added and the reaction mixture was stirred for 18 h at room temperature. After the solvent was removed, saturated $NaHCO_3$ (10 mL) was added, and the product was extracted into CH_2Cl_2. Organic layer was dried with Na_2SO_4 and evaporated in vacuo. The crude product was purified by basic alumina column chromatography using CH_2Cl_2:CH_3OH (100:4) as mobile phase. Fraction containing compound XIII was collected then the solvent was removed under reduced pressure (0.67 mmol, 290 mg, 70 %).

^{1}H NMR (400 MHz, Chloroform-*d*): δ_H 8.60 – 8.39 (m, 2H), 7.62 (td, *J* = 7.5, 1.9 Hz, 1H), 7.56 – 7.41 (m, 2H), 7.20 (d, *J* = 7.8 Hz, 1H), 7.15 – 7.08 (m, 2H), 6.91 – 6.69 (m, 3H), 4.22 – 3.99 (m, 4H), 3.92 (s, 1H), 3.84 – 3.52 (m, 4H), 3.09 – 2.97 (m, 1H), 2.93 – 2.81 (m, 1H), 2.28 (s, 3H), 2.18 (s, 3H), 1.44 (dt, *J* = 8.6, 7.0 Hz, 6H) ppm.

^{13}C NMR (100 MHz, Chloroform-*d*) δ_C 160.47, 159.75, 148.86, 148.30, 147.88, 136.31, 136.26, 132.31, 123.11, 122.79, 121.79, 121.72, 121.38, 114.45, 112.98, 65.96, 64.62, 64.55, 60.63, 60.31, 55.86, 43.07, 39.01, 14.92, 14.90 ppm.

MS (TOF - ESI): m/z: Calcd: 434.26818 $[M^+]$, Found: 435.27529 $[M+H]^+$, Δ=0.37 ppm.

Synthesis of Cage

Trifluoromethanesulfonic acid (0.26 mL, 2.96 mmol) was dissolved in CH_2Cl_2 (10 mL) and anhydrous HNO_3 acid (0.08 mL, 1.48 mmol) was added, which caused a white, crystalline solid to precipitate from the solution. After reducing the temperature of the reaction mixture to 0 ^{o}C, Compound XIII (160 mg, 0.37 mmol) dissolved in CH_2Cl_2 (2 mL) was added in one portion. The reaction mixture was stirred at to 0 ^{o}C, for 2 h and then quickly poured onto 1 g of crushed ice. A saturated solution of $NaHCO_3$ (10 mL) was added, and the crude reaction mixture was extracted with CH_2Cl_2. Organic layer was dried with Na_2SO_4 and evaporated in vacuo. The crude product was purified by basic alumina column chromatography using CH_2Cl_2:CH_3OH (100:1) as mobile phase. Fraction containing Cage was collected then the solvent was removed under reduced pressure (0.09 mmol, 44 mg, 25 %).

^{1}H NMR (400 MHz, Chloroform-*d*): δ_H 8.61 – 8.33 (m, 2H), 7.62 (td, *J* = 7.7, 1.9 Hz, 1H), 7.51 (td, *J* = 7.7, 1.9 Hz, 1H), 7.40 (s, 1H), 7.34 (d, *J* = 7.8 Hz, 1H), 7.16 – 7.02 (m, 4H), 4.81 (dd, *J* = 8.6, 5.3 Hz, 1H), 4.21 – 4.11 (m, 2H), 4.10 – 3.96 (m, 2H), 3.86 – 3.51 (m, 4H), 2.98 (dd, *J* = 12.7, 5.3 Hz, 1H), 2.80 (dd, *J* = 12.8, 8.5 Hz, 1H), 2.32 (s, 3H), 2.25 (s, 3H), 1.50 (t, *J* = 7.0 Hz, 3H), 1.44 (t, *J* = 7.0 Hz, 3H) ppm.

^{13}C NMR (100 MHz, Chloroform-*d*) δ_C 159.93, 159.30, 151.83, 148.92, 148.67, 146.84, 143.49, 136.39, 136.20, 131.27, 123.14, 122.44, 121.83,11.87, 109.12, 64.90, 64.73, 60.80, 60.08, 59.41, 43.16, 39.61, 29.69, 14.60, 14.56 ppm.

MS (TOF - ESI): m/z: Calcd: 479.25325 $[M^+]$, Found: 480.25847 $[M+H]^+$, Δ=4.25 ppm.

Synthesis of ZnCage

1 mM (0.01 mmol) the stock solution of Compound Cage and Zn(II) triflate (0.01 mmol) ions were stirred for 6 hours. Resultant solution was used without any purification in spectrometric measurements.

CHAPTER 4

EVALUATION

In order to prove molecular logic gates to be an alternative technology to the silicon based computing, more sophisticated molecular logic devices should be implemented rationally by physical integration. Due to input-output heterogeneity between species, designing concatenated molecular logic gates is still an important challenge today.

Physical integration of molecular logic gates has been mentioned recently by Guliyev et al.[56] In this study, a new methodology has been proposed so as to make concatenated systems by using energy transfer as a communication language between fluorophores. This study obviously paves the way for more complicated molecular logic devices.

One alternative solution to the current problem might be in the nature. As we know that there is important information processing, storing and gathering in living systems. One of the significant examples to signal transduction in cells is second messenger systems. Mimicking second messengers to achieve concatenated molecular logic gates might be the covetable inspiration.

Zn^{2+} ion is known today to play an important role in intracellular communication.[9–11] Provided that Zn ions are controlled by the external stimuli, it can be a potential candidate to construct multi-integrated physical molecular logic gates. As we discussed in background chapter, one of the best way to control metal cations is to use photolabile-caged compounds or chelators due to their potential ability to manipulate metal ions spatiotemperally by induced light.[15]

In this study, a new methodology is reported to integrate two distinct physical molecular logic gates by use of photolabile caged Zn^{2+} compounds. To best of our

knowledge, using caged compounds and bridging separate molecular logic gates with metal ions will be the first concepts in molecular logic world. As second part of the study, more sophisticated concatenated molecular logic gates were constructed by using "supermolecule" previously reported by Akkaya laboratory.[25] Figure 39 demonstrates schematic representation of proposed idea. Irradiation of ZnCage Compound with UV light at 360 nm detaches part of the molecule and unleash Zn^{2+} ion. Liberated zinc ion is subsequently captured by dipicolylamine moiety on Click. Zn(II) inhibites the PeT (photoinduced electron transfer) mechanism on the Click Compound so starts excited electron transfer. After that, Hg^{2+} binds thioazo-crown receptor of Click as the last input and leads the fluorophore to making blue-shift so that Click Compound gives fluorescence emission at 660 nm.

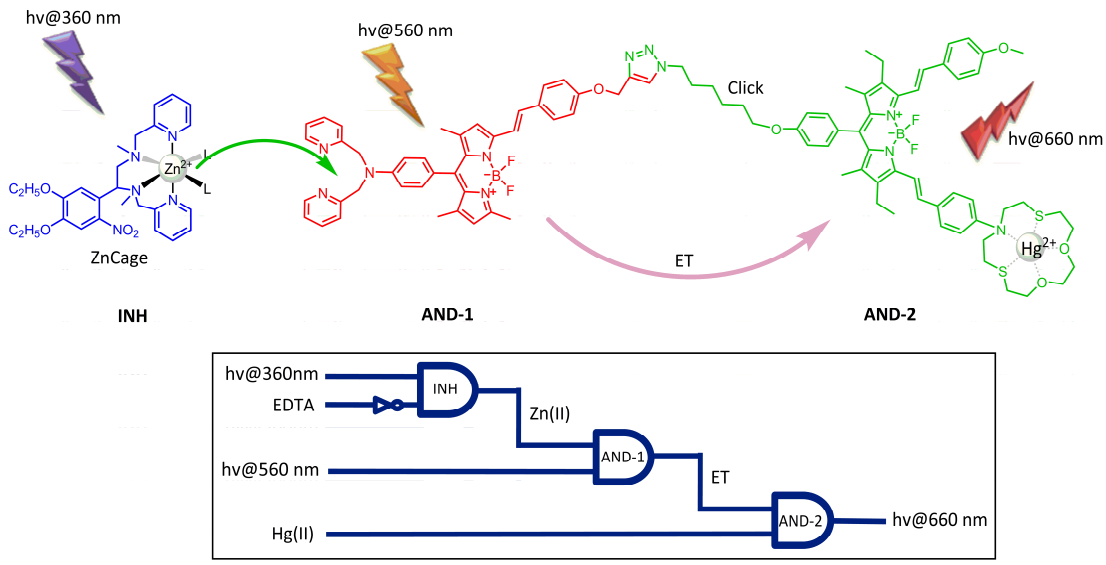

Figure 39 Proposed photochemical process and its logic gate presentation (below)

Photolabile-caged compound with nitrobenzyl group has been studied extensively. There are number of such caged compounds for controlled release of biologically important compounds or metal ions. Recently, Zn^{2+} caged chelators has proposed by Brunette et al as can be seen in Figure 40.[10][11] Zn(ZnCleave-1) molecule was irradiated with UV light in the presence of ZP1B[57] which is emissive when Zn(II) ion binds. Fluorescence spectrum and normalized integrated emission graph say that Zn(ZnCleave-1) compound liberates zinc ion upon UV exposure and this free Zn^{2+} ion is held by ZP1B dye successfully.

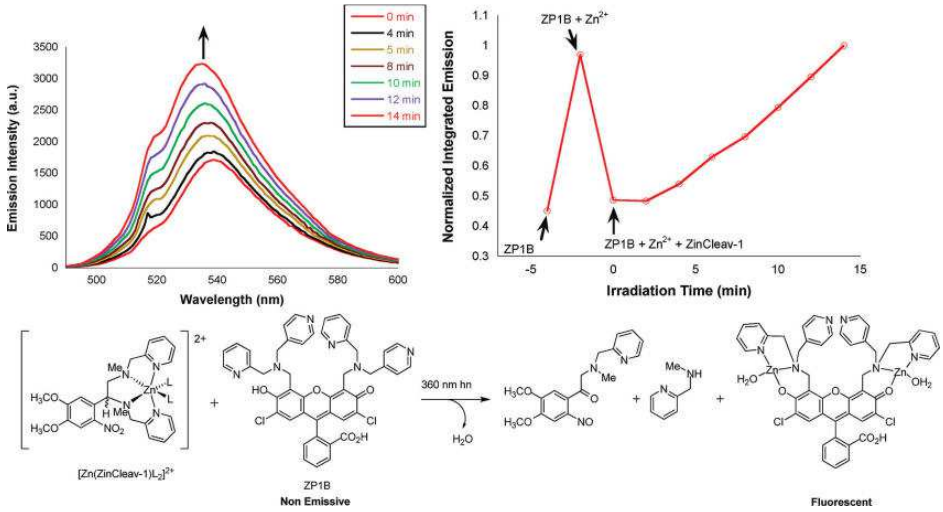

Figure 40 Detaching of ZinCleave-1 and fluorescence emission of ZP1B[10]

Burdette et al has demonstrated that their caged Zn^{2+} compound is capable of releasing Zn(II) ion with light. Using accumulated knowledge of the compound, we have set up ours in order to show Zn transmission from our slightly different Caged Zn Compound (ZnCage) to DPA(dipicolylamine)-BODIPY. In order to obtain ZnCage Compound, 0.01 mmol, 3.6 mg zinc triflate was added to 1 mM (0.01 mmol) the stock solution of Cage Compound in acetonitrile and the reaction mixture stirred for 6 hours to assure that complexation ends up (Figure 41). Free zinc ion was measured by non-fluorescent DPA-BODIPY which becomes emissive when zinc ion binds to it. As it can be seen in the Figure 42-43, addition of DPA-BODIPY to ZnCage solution did not cause any fluorescence enhancement. This mixture was hold at least 6 hours in dark to be sure whether Zn was released by the ZnCage compound. No fluorescence emission was observed from DPA-BODIPY.

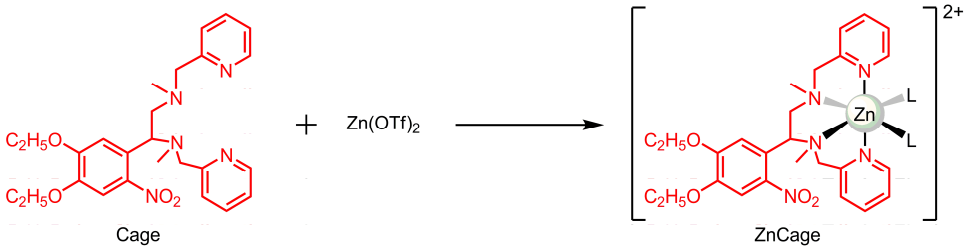

Figure 41 Binding of Zn(II) ion to Cage

In order to irradiate the solution, time-resolved fluorescence spectrometer was employed. 450 watt xenon lamb was arranged 360 nm wavelength**.** Slits widths of

fluorescence spectrometer was fixed at 5-2.5. All spectra were recorded just after excitation.

In order to test ion releasing property of ZnCage and to better understand what concentration of ZnCage and DPA-BODIPY is feasible for next logic operations, we carried out a couple of experiment in which different proportions of Cage and DPA-BODIPY were used. In Figure 42, ZnCage and DPA-BODIPY was taken 5 μM each and the system was exposed to UV light. In every 1.5 min time interval, spectral measurement was recorded. In the experiment, it was observed that initially non-fluorescent DPA-BODIPY got emissive with ongoing photolysis of ZnCage. However, even after full photolysis of ZnCage, emission intensity of DPA-BODIPY was well below from intensity level of purple line showing saturation point of DPA-BODIPY(5 μM) for Zn(II) (5 μM) probably due to the competition for zinc ion between side products and DPA-BODIPY.

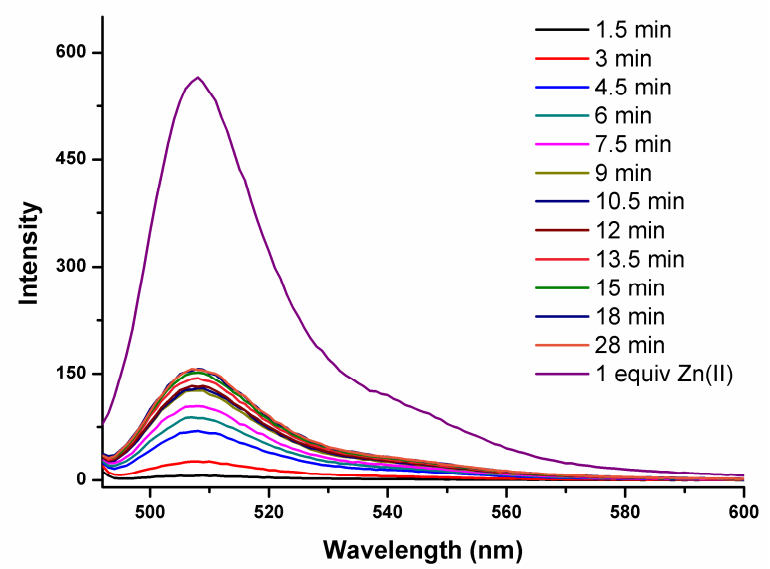

Figure 42 Fluorescence response of compound **DPA-BODIPY** upon (5 μM each) recorded in acetonitrile. Initially compound **DPA-BODIPY** exhibits no fluorescence (quenched due to the active PET process), irradiation of the solution at 360 nm with a 450 W Xe-lamp resulted in the complete photolysis of **ZnCage** which can be followed by the enhanced emission spectrum of compound **DPA-BODIPY**. Purple line represents the maximum emission intensity of **DPA-BODIPY** which was obtained by the addition of 1 equivalent of Zinc(II) triflate cations. (λex=490 nm, slit width=5-2.5).

When ZnCage (10 μM) were added (2:1) equivalency to DPA-BODIPY (5 μM) as in shown in Figure 43, fluorescence enhancement of DPA-BODIPY after UV exposure goes further with respect to (1:1) addition. As it can be estimated, when more amount of ZnCage is cleaved, more Zn(II) ions are released to the media. Concentration equilibrium (2:1) has better resolution and more intense signal in fluorescence spectrum than the solution with proportion (1:1). For that reason, we constructed our INH-AND logic operation in the solution containing ZnCage (10 μM) and DPA-BODIPY (5 μM).

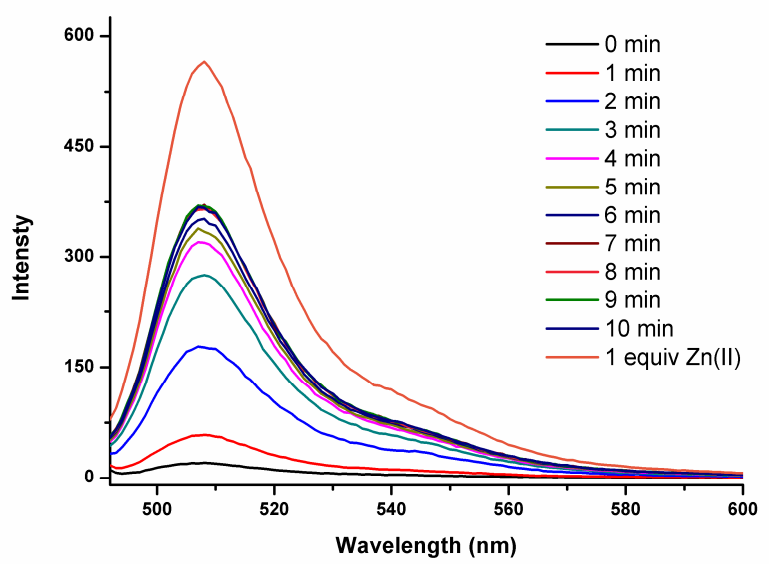

Figure 43 Fluorescence response of compound **DPA-BODIPY** upon uncaging of 2 equivalents of cage compound **ZnCage,** recorded in acetonitrile. Again orange line represents the maximum emission intensity of **DPA-BODIPY** which was obtained by the addition of 1 equivalent of Zinc(II) triflate cations. (λex=490 nm, slit width=5-2.5).

In Figure 44, mechanism of action behind the experiment is depicted. DPA-BODIPY has PeT mechanism due to amine group which contributes electron to the excited state BODIPY core. When ZnCage compound and DPA-BODIPY were mixed, no emission were observed in the experiment. It is because PeT mechanism of unbound electrons of amine group on DPA-BODIPY inhibits its own fluorescence emission. However, when zinc ion binds to dipicolylamine receptor, free electrons on amino group is stabilized by the metal cation so HOMO of the receptor becomes less energetic than HOMO of the fluorophore. This means that receptor part is no more

available to block fluorescence of the BODIPY core. Indeed, that is why we see fluorescence after light exposure.

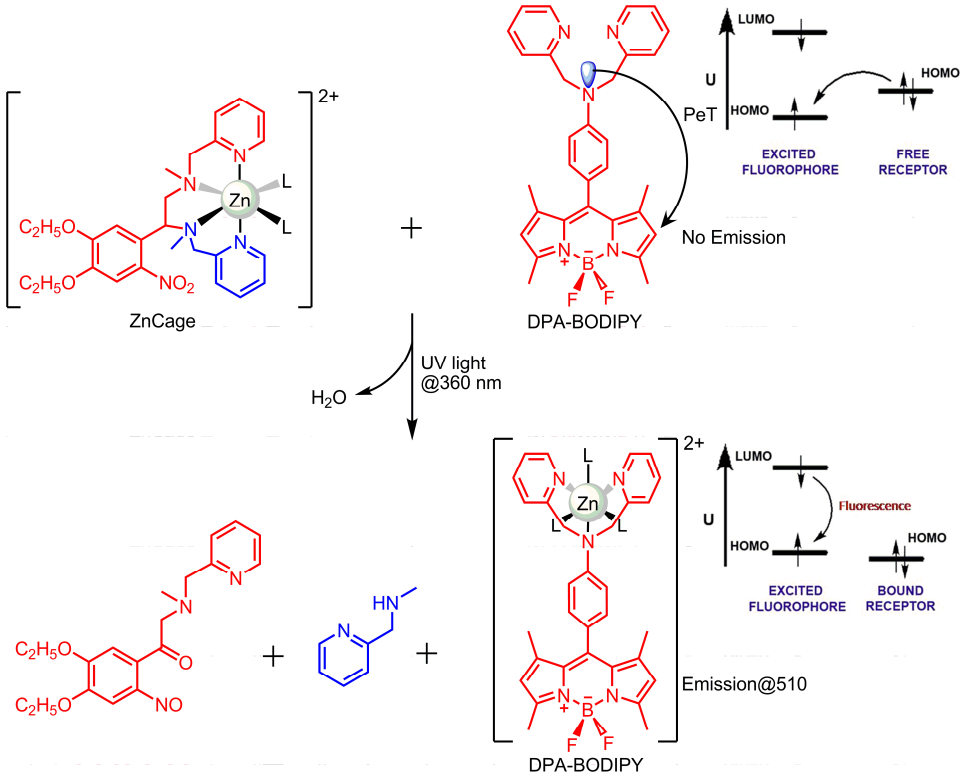

Figure 44 Set of photochemical actions beginning with UV light

What we accomplished by this experiment forms first step of molecular INH gate (ZnCage) and AND gate (DPA-BODIPY). To account for, when first input (360 nm light) was given to the system, we could observe Zn^{2+} by looking at fluorescence signal, 510 nm (output), coming from DPA-BODIPY, at 490 nm (last input). To see logic gate designs, please look at Figure 45.

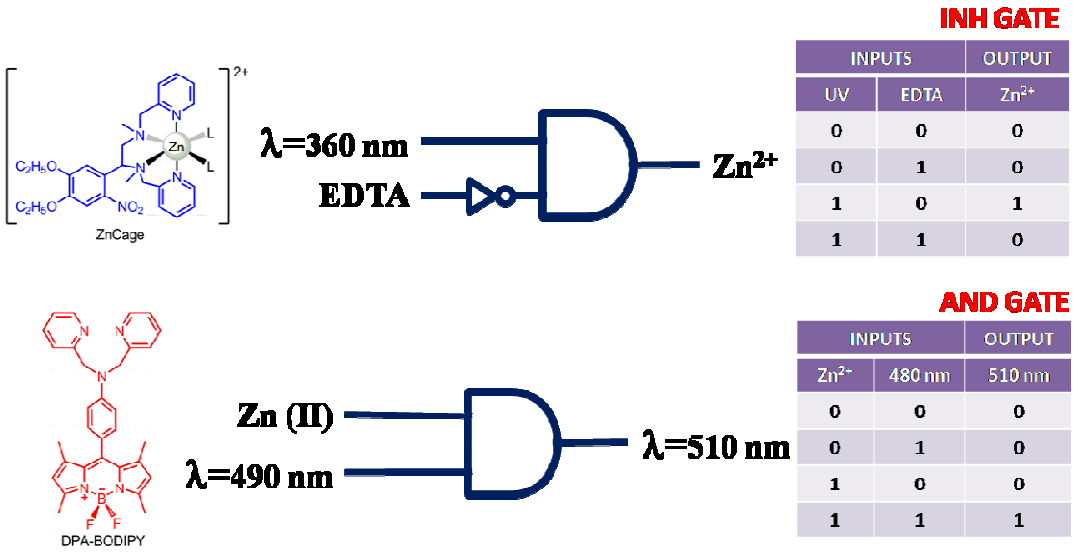

Figure 45 Molecular logic gates based on ZnCage and DPA-BODIPY

For completing INH gate, we still require EDTA to inhibit final output. It can be seen in schematic representation of EDTA inhibition mechanism in Figure 46 that if there is EDTA in the media, it should directly make complex with released zinc ion and prevented it to arrive at DPA-BODIPY. Therefore, final output, 510 nm fluorescence emission, is proposed to not exist.

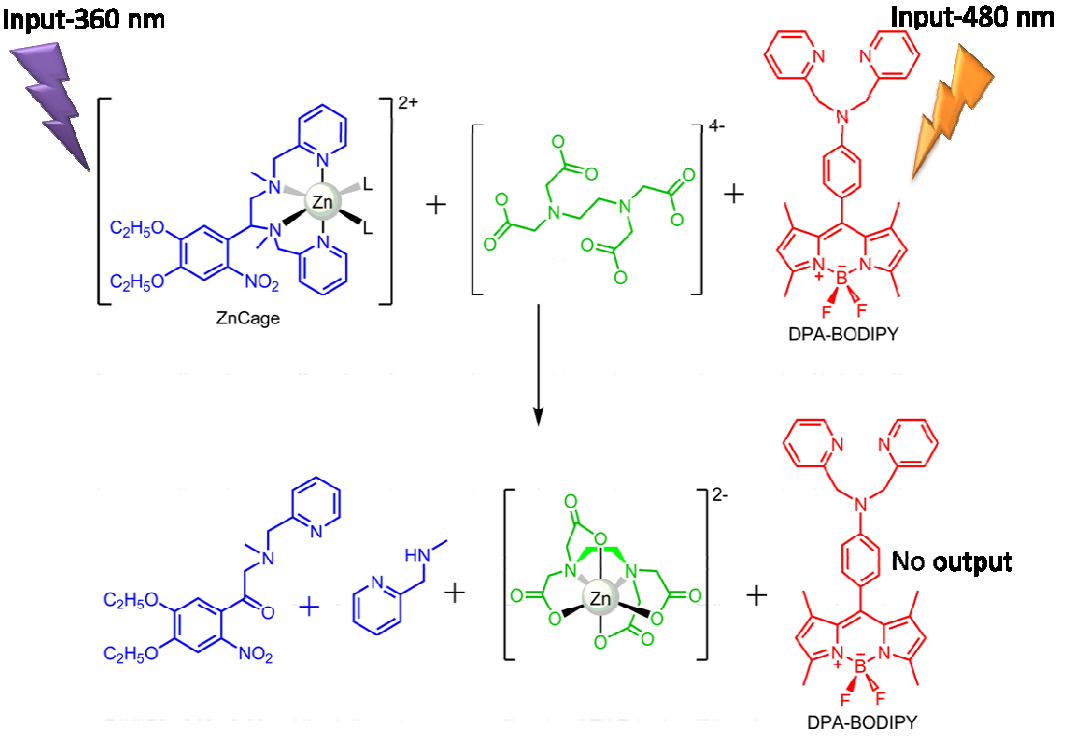

Figure 46 INH gate mechanism, addition of EDTA

To test EDTA (ethylenediaminetetraacetic acetate) effect as an inhibitor, EDTA (2 eq., 10 µM) was added to the solution including ZnCage (2 eq., 10 µM) and DPA-BODIPY(1 eq., 10 µM). Four different series were prepared as (DYE+UV+ZnCage), (DYE+ZnCage), (DYE+ZnCage+EDTA+UV), (DYE+ZnCage+EDTA). As it can be seen in Figure 47, emission spectrum of DPA-BODIPY shows that each series including EDTA has almost no emission. (DYE+ZnCage) group does not show an emission due to lack of external stimuli, UV light. As to why (DYE+UV+ZnCage) case gives emission at 510 nm (output), as it is mentioned above released zinc ions from ZnCage directly go to DPA-BODIPY and abolishes PeT mechanism.

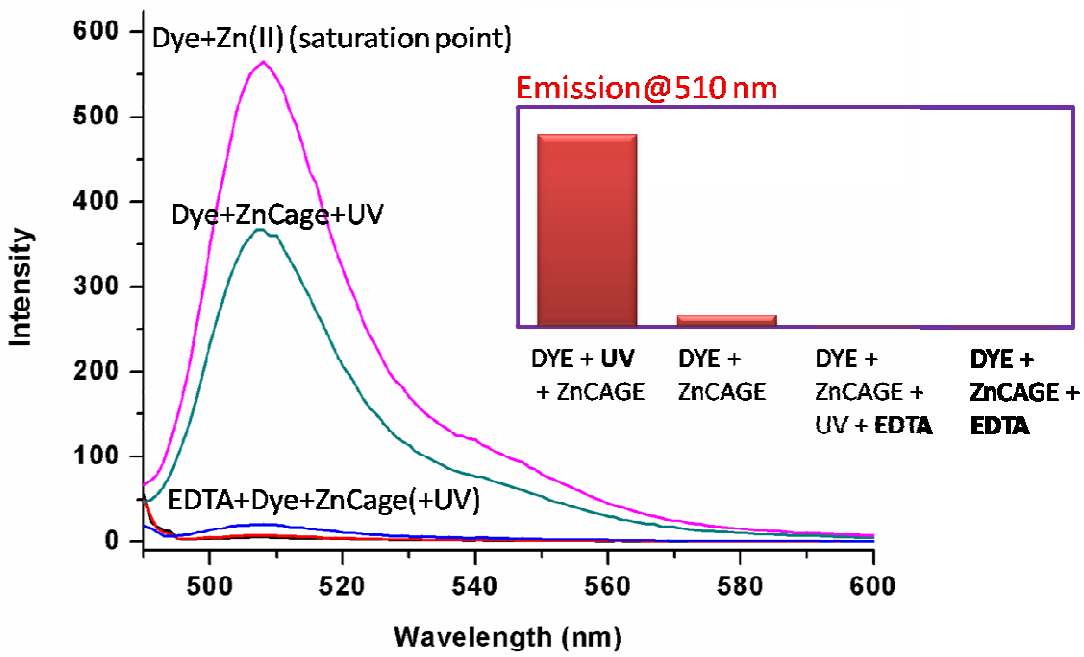

Figure 47 Fluorescence response of **DPA-BODIPY(Dye)** upon uncaging of 2 equivalents of **ZnCage** in the presence of **EDTA** (1 equiv) in acetonitrile solution. (λex=490 nm, slit width=5-2.5).

Physical integration of INH gate and AND gate by bridging them with zinc ion was proved as described above. Rest of the study deals with applying this methodology to more complex molecular logic operations. The supermolecule designed by Akkaya Lab was employed for this purpose. Schematic presentation of the molecule, Click, is given in the Figure 48. [58] Physical concatenation of two logic gates is provided by

energy transfer between two chemically bound fluorophores. Fluorophore containing zinc ion receptor works based on PET mechanism as we discussed above for DPA-BODIPY. When zinc ion binds to the receptor, it blocks PeT and activates energy transfer and fluorescence pathways. However, energy transfer mechanism is more dominant over fluorescence here due to close intermolecular distance between fluorophores. Second fluorophore with a selective mercury ion receptor has an absorbance at about 680 nm. When Hg^{2+} binds receptor cavity absorbance and emission of the fluorophore undergoes blue-shift and final values become 640 and 660 nm respectively. For that reason, output was selected 660 nm as fluorescence emission. To fulfill this AND gate two inputs are required. One is mercury ion, others is energy transfer which is output of the first AND gate. If all inputs are present together, expected signal can be received at 660 nm wavelength as fluorescence emission.

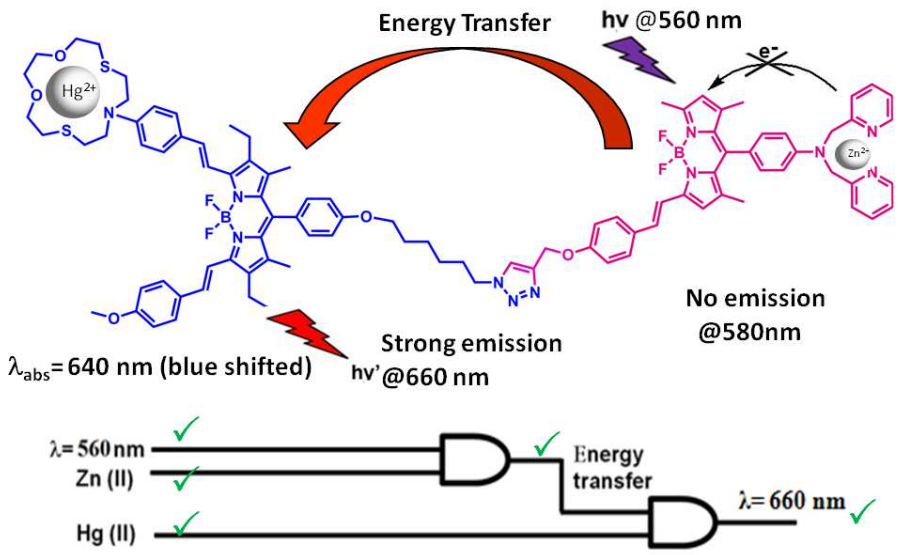

Figure 48 Working principle of Click with two successive AND gate[58]

Control experiment with Click was done in order to understand Hg(II) to bind mercury ion receptor of Click in the presence of ZnCage or Cage by investigating absorbance spectrum of Click. The experiment was recorded in acetonitrile, concentration of species Click, ZnCage and Hg(II) were (3.0 µM, 3.0 µM, 18.0 µM) respectively. As it is shown in Figure 49, absorbance spectrum of Click+ZnCage solution did not change as it was expected. Even UV exposure of ZnCage did not

affect absorbance spectrum of Click. By considering this fact, one can say both UV light and photochemical reaction of ZnCage does not damage on chemical structure of Click. More importantly, it can be understood that free Zn(II) can recognize it is characteristic receptor and does not interfere with Hg(II) receptor. However, Hg(II) addtion to Click+ZnCage mixture with UV light caused a spectral shift to 640 nm. It clearly demostrates that Hg(II) can find the address of thioazo-crown ether in highly complex environment.

When experiment was performed with Cage (without Zn(II)), results were very similar. Like ZnCage, Cage did not show any impact on absorbance spectrum of Click. When Click+Cage was exposed to UV light, Cage probably was broken, however, UV radiation and photochemical reaction of Cage did not lead to a change on Click. Therefore, it can be concluded that Hg(II) can be utilized as an input in our complex molecular logic operations.

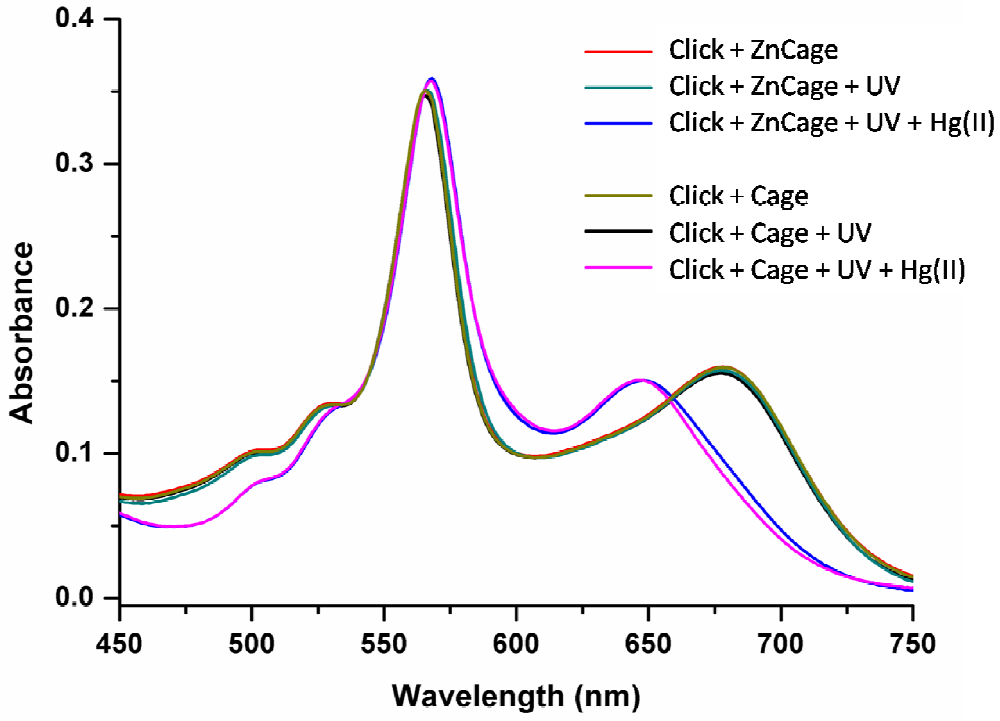

Figure 49 Absorbance spectra of Click (3.0 µM) recorded in acetonitrile, in the presence of ZnCage(or Cage) and Hg(II) cations (3.0 µM, 18.0 µM, respectively).

Last experiment was done so as to see final output from physically integrated INH-AND-AND gates system. Emission spectrum of Click (3.0 μM) in acetonitrile in the presence of ZnCage (3.0 μM) and Hg(II) cations (18.0 μM) were measured.(Figure 50) As it was stated above, output was determined as fluorescence emission of Click at 660 nm. Click+ZnCage, Click+ZnCage+UV, Click+Cage, Click+Cage, Click+Cage+UV solutions could not give a emission at 660 nm. As it was estimated previously, without final input, Hg(II), Click cannot give fluorescence emission at 660 nm because of two reasons. Firstly, energy transfer in between dyad is inefficient since absorption-emission overlapping area is quite narrow to make energy transfer. However, Hg(II) shifts absorption spectrum of acceptor fluorophore to blue side and increases the overlapping area between two fluorophore of Click. Secondly, Hg(II) is essential factor for Click to have emission signal at 660 nm due to blue-shift effect of Hg(II), otherwise the signal would be at longer wavelength. A reasonable question may arise about why Click+Cage+UV+Hg(II) case has a bit more emission signal than others. It is clearly because the fact that even though lack of Zn(II) activates PeT, compound Click still is able to slightly make intermolecular energy transfer, which competes with PeT, to Hg(II) bound fluorophore. For that reason, small amount of emission signal appeared in measurements. In addition, use of excess amount of Hg(II) may lead to weak interaction with dipicolylamine receptor. Weak interaction may have caused photoinduced electron transfer mechanism to be less effective. Although Click+Cage+UV+Hg(II) serie gives small amount of signal, this is not actually a deficit for the system. It is the fact that silicon based logic gates have some interference as well due to noise produced from different reasons such as electricity fluctuations. However, such interferences are eliminated by adding threshold value. Therefore, we also add a threshold value which is slightly above 300 a.u.

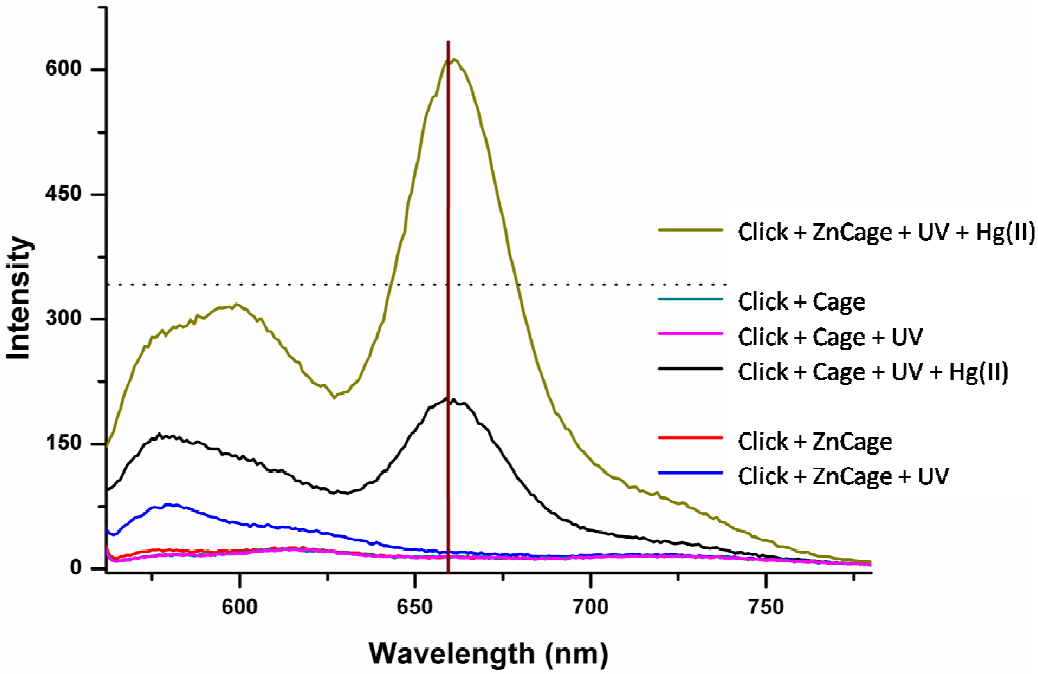

Figure 50 Emission spectra of Click (3.0 μM) in acetonitrile in the presence of ZnCage and Hg(II) cations (3.0 μM, 18.0 μM, respectively). λ_{ex}=560 nm, slit width=5-2.5

Mechanism of working principle of study has been discussed above. However, one can also check Figure 51 to see chain of photochemical events during logic operation. Figure 51 represents photochemical mechanism and corresponding logic gates depended on each situation.

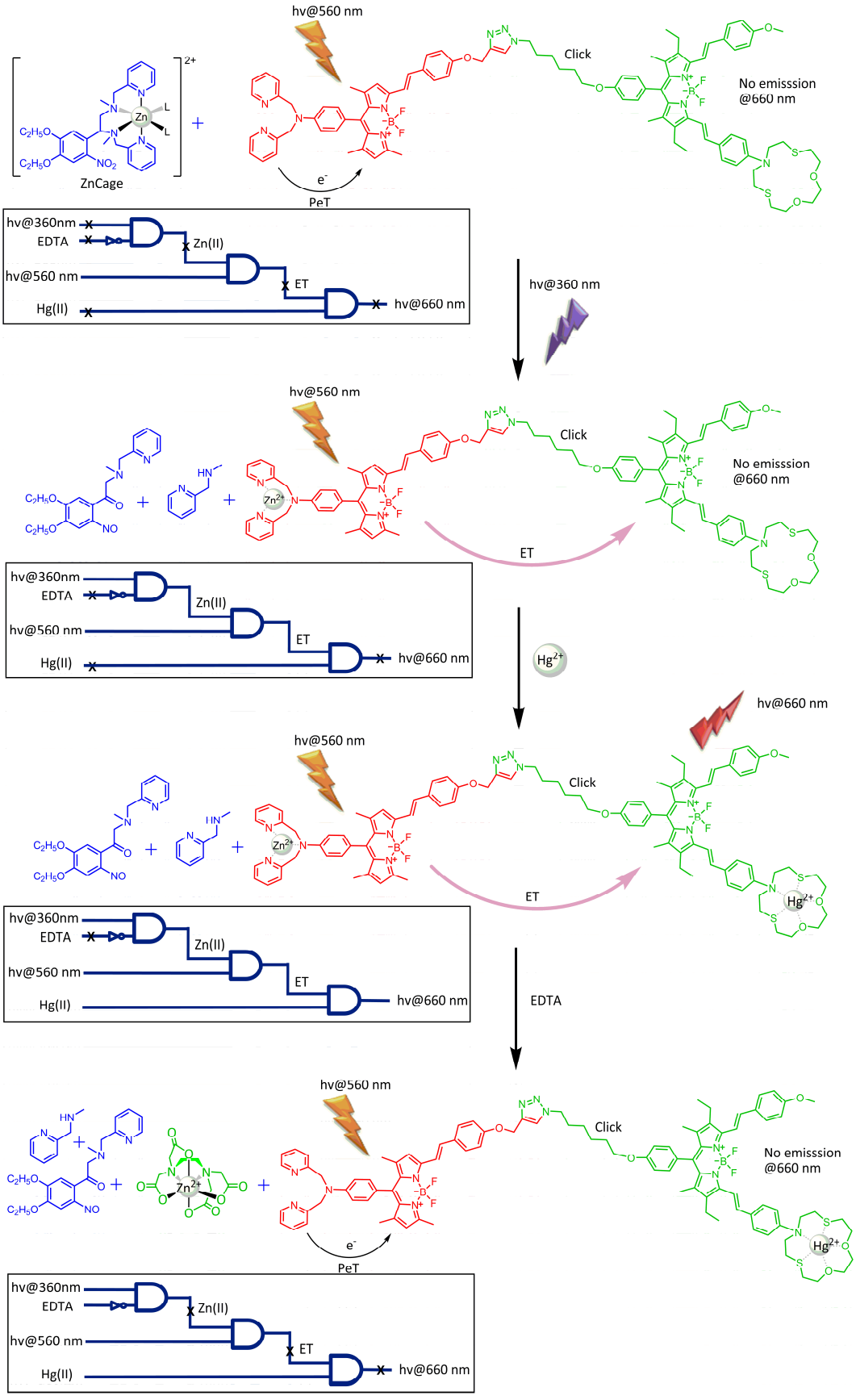

Figure 51 Chain of photochemical events during operation of molecular logic device

CHAPTER 5

CONCLUSION

In this thesis, a novel methodology was proposed for concatenation of two separately operating molecular logic gates through ion signal. For this purpose, we utilized from photolabile caged compounds in order to control Zn(II) ion transfer spatiotemporally. ZnCage, a caged Zn(II) compound, were firstly employed to prove our hypothesis in INH-AND gate system. After having impressive results, we implemented this idea to a more complex molecular logic system by using accumulated knowledge in our laboratory. It was clearly observed that photolabile cage compounds were able to be applied to advanced molecular logic device composed of two coupled AND logic gates.

According to the best of our knowledge, use of photolabile caged compounds and the idea information transfer through biologically important metal ions is the first example in the field of molecular logic phenomenon. In addition, our logic device composed of three separate logic gates can be regarded one of the most complex system in the literature.

Today, concatenation is the biggest barrier in front of molecular logic technology. Therefore, there is significant demand for highly concatenated molecular logic gates. As we have shown in this study, an alternative way to overcome the integration problem of molecular logic gates might be to mimic second messenger systems in nature. Constructing more complex molecular logic devices working with this principle would be quite valuable on this way. If this barrier can be achieved, molecular logic technology will surely have a bright future. We hope that this study contributes to coming of these bright days.

BIBLIOGRAPHY

[1] C. J. Pedersen, “Cyclic Polyethers and Their Complexes with Metal Salts,” no. 157, 1967.

[2] J. Lehn, “SUPRAMOLECULAR CHEMISTRY - SCOPE AND PERSPECTIVES MOLECULES - SUPERMOLECULES -,” 1987.

[3] V. Balzani, A. Credi, F. Raymo, and J. Stoddart, “Artificial Molecular Machines.,” *Angewandte Chemie International Edition*, vol. 39, no. 19, pp. 3348–3391, 2000.

[4] A. P. Desilva, H. Q. N. Gunaratne, and C. P. Mccoy, “A molecular photoionic AND gate based on fluorescent signaling,” *Nature*, vol. 364, no. 6432, pp. 42–44, 1993.

[5] M. Kanellos, “New Life for Moore’s Law,” 2005.

[6] K. Szaciłowski, “Digital information processing in molecular systems.,” *Chemical reviews*, vol. 108, no. 9, pp. 3481–548, Sep. 2008.

[7] E. Katz and V. Privman, “Enzyme-based logic systems for information processing.,” *Chemical Society reviews*, vol. 39, no. 5, pp. 1835–57, May 2010.

[8] S. Silvi, E. C. Constable, C. E. Housecroft, J. E. Beves, E. L. Dunphy, M. Tomasulo, F. M. Raymo, and A. Credi, “All-Optical Integrated Logic Operations Based on Chemical Communication between Molecular Switches,” pp. 178–185, 2009.

[9] S. Yamasaki, K. Sakata-Sogawa, A. Hasegawa, T. Suzuki, K. Kabu, E. Sato, T. Kurosaki, S. Yamashita, M. Tokunaga, K. Nishida, and T. Hirano, “Zinc is a novel intracellular second messenger.,” *The Journal of cell biology*, vol. 177, no. 4, pp. 637–45, May 2007.

[10] H. M. D. Bandara, D. P. Kennedy, E. Akin, C. D. Incarvito, and S. C. Burdette, “Photoinduced release of Zn2+ with ZinCleav-1: a nitrobenzyl-based caged complex.,” *Inorganic chemistry*, vol. 48, no. 17, pp. 8445–55, Sep. 2009.

[11] H. M. D. Bandara, T. P. Walsh, and S. C. Burdette, “A Second-generation photocage for Zn2+ inspired by TPEN: characterization and insight into the uncaging quantum yields of ZinCleav chelators.,” *Chemistry (Weinheim an der Bergstrasse, Germany)*, vol. 17, no. 14, pp. 3932–41, Mar. 2011.

[12] R. a. Colvin, C. P. Fontaine, M. Laskowski, and D. Thomas, “Zn2+ transporters and Zn2+ homeostasis in neurons,” *European Journal of Pharmacology*, vol. 479, no. 1–3, pp. 171–185, Oct. 2003.

[13] E. P. Huang, “Commentary Metal ions and synaptic transmission : Think zinc,” vol. 94, no. December, pp. 13386–13387, 1997.

[14] Y. Zhang, E. Aizenman, D. B. Defranco, and P. A. Rosenberg, “Intracellular Zinc Release , 12-Lipoxygenase Activation and MAPK Dependent Neuronal and Oligodendroglial Death.”

[15] A. M. Gurney, “Flash photolysis of caged compounds,” pp. 389–406.

[16] J. R. Lakowicz, *Principles of Fluorescence Spectroscopy*. New York: Plenum Press, 1999.

[17] R. Guliyev, “RATIONAL DESIGN OF RATIOMETRIC CHEMOSENSOR VIA MODULATION OF ENERGY DONOR EFFICIENCY,” 2008.

[18] X. Peng and D. R. Draney, “Near-IR fluorescent dyes for biological applications,” *Most*, no. May, 2004.

[19] C. Rogers, “Luminescent molecular sensors based on analyte coordination to transition-metal complexes,” *Coordination Chemistry Reviews*, vol. 233–234, pp. 341–350, 2002.

[20] E. M. Nolan and S. J. Lippard, “Tools and tactics for the optical detection of mercuric ion.,” *Chemical reviews*, vol. 108, no. 9, pp. 3443–80, Sep. 2008.

[21] L. Prodi, C. Bargossi, M. Montalti, N. Zaccheroni, N. Su, J. S. Bradshaw, R. M. Izatt, P. B. Savage, and C. G. Ciamician, “An Effective Fluorescent Chemosensor for Mercury Ions,” pp. 6769–6770, 2000.

[22] F. Szurdoki, D. Ren, and D. R. Walt, “A Combinatorial Approach To Discover New Chelators for Optical Metal Ion Sensing metal-binding indicators with diverse optical responses,” vol. 72, no. 21, pp. 5250–5257, 2000.

[23] B. Valeur, *Molecular Fluorescence*, vol. 8, no. 5. Wiley-VCH Verlag GmbH, 2002, p. 399.

[24] N. J. Youn and S.-K. Chang, “Dimethylcyclam based fluoroionophore having Hg2+- and Cd2+-selective signaling behaviors,” *Tetrahedron Letters*, vol. 46, no. 1, pp. 125–129, Jan. 2005.

[25] R. Guliyev, A. Coskun, and E. U. Akkaya, “Design strategies for ratiometric chemosensors: modulation of excitation energy transfer at the energy donor

site.," *Journal of the American Chemical Society*, vol. 131, no. 25, pp. 9007–13, Jul. 2009.

[26] A. Coskun and E. U. Akkaya, "Signal ratio amplification via modulation of resonance energy transfer: proof of principle in an emission ratiometric Hg(II) sensor.," *Journal of the American Chemical Society*, vol. 128, no. 45, pp. 14474–5, Nov. 2006.

[27] A. Coskun, M. D. Yilmaz, and E. U. Akkaya, "Boratriazaindacene as an NIR-Emitting Chemosensor for Hg (II)," no. II, pp. 385–387, 2007.

[28] S. Atilgan, T. Ozdemir, and E. U. Akkaya, "A sensitive and selective ratiometric near IR fluorescent probe for zinc ions based on the distyryl-bodipy fluorophore.," *Organic letters*, vol. 10, no. 18, pp. 4065–7, Sep. 2008.

[29] T. Yogo, Y. Urano, Y. Ishitsuka, F. Maniwa, and T. Nagano, "Highly efficient and photostable photosensitizer based on BODIPY chromophore.," *Journal of the American Chemical Society*, vol. 127, no. 35, pp. 12162–3, Sep. 2005.

[30] Y. Cakmak, S. Kolemen, S. Duman, Y. Dede, Y. Dolen, B. Kilic, Z. Kostereli, L. T. Yildirim, A. L. Dogan, D. Guc, and E. U. Akkaya, "Designing excited states: theory-guided access to efficient photosensitizers for photodynamic action.," *Angewandte Chemie International Edition*, vol. 50, no. 50, pp. 11937–41, 2011.

[31] S. Ozlem and E. U. Akkaya, "Thinking outside the silicon box: molecular and logic as an additional layer of selectivity in singlet oxygen generation for photodynamic therapy.," *Journal of the American Chemical Society*, vol. 131, no. 1, pp. 48–9, Jan. 2009.

[32] A. Burghart, L. H. Thoresen, J. Chen, K. Burgess, F. Bergström, and L. B.-Å. Johansson, "Energy transfer cassettes based on BODIPY® dyes," *Chemical Communications*, no. 22, pp. 2203–2204, 2000.

[33] S. Kawahara, T. Uchimaru, and S. Murata, "Sequential multistep energy transfer: enhancement of efficiency of long-range fluorescence resonance energy transfer," *Chemical Communications*, vol. 1, no. 6, pp. 563–564, 1999.

[34] S. C. Hung, R. a Mathies, and a N. Glazer, "Optimization of spectroscopic and electrophoretic properties of energy transfer primers.," *Analytical biochemistry*, vol. 252, no. 1, pp. 78–88, Oct. 1997.

[35] L. G. Lee, S. L. Spurgeon, C. R. Heiner, S. C. Benson, B. B. Rosenblum, S. M. Menchen, R. J. Graham, a Constantinescu, K. G. Upadhya, and J. M. Cassel, "New energy transfer dyes for DNA sequencing.," *Nucleic acids research*, vol. 25, no. 14, pp. 2816–22, Jul. 1997.

[36] C.-W. Wan, A. Burghart, J. Chen, F. Bergström, L. B. Johansson, M. F. Wolford, T. G. Kim, M. R. Topp, R. M. Hochstrasser, and K. Burgess, "Anthracene-BODIPY cassettes: syntheses and energy transfer.," *Chemistry (Weinheim an der Bergstrasse, Germany)*, vol. 9, no. 18, pp. 4430–41, Sep. 2003.

[37] S. Kolemen, O. A. Bozdemir, Y. Cakmak, G. Barin, S. Erten-Ela, M. Marszalek, J.-H. Yum, S. M. Zakeeruddin, M. K. Nazeeruddin, M. Grätzel, and E. U. Akkaya, "Optimization of distyryl-Bodipy chromophores for efficient panchromatic sensitization in dye sensitized solar cells," *Chemical Science*, vol. 2, no. 5, p. 949, 2011.

[38] J. R. Lakowicz, *Principles of Fluorescence Spectroscopy*, 2nd ed. Kluwer Academic / Plenum Publishers, 1999, pp. 374–443.

[39] Graceway Pharmaceticuls, "CALCIUM DISODIUM VERSENATE (edetate calcium disodium) injection," *Daily Med*. [Online]. Available: http://dailymed.nlm.nih.gov/dailymed/lookup.cfm?setid=e71cc7d9-4093-4a5c-aeda-06b54a354499.

[40] G. C. R. Ellis-davies, "Caged compounds : photorelease technology for control of cellular chemistry and physiology," vol. 4, no. 8, pp. 619–628, 2007.

[41] J. E. T. Corrie, *Photoremovable Protecting Groups Used for the Caging of Biomolecules*, vol. 1999. 1999, pp. 1–94.

[42] R. P. Haugland, *The Molecular Probes® Handbook—A Guide to Fluorescent Probes and Labeling Technologies*, 11th ed. Life Technologies, 2010.

[43] P. Klán, T. Šolomek, C. G. Bochet, A. Blanc, R. Givens, M. Rubina, V. Popik, A. Kostikov, and J. Wirz, "Photoremovable protecting groups in chemistry and biology: reaction mechanisms and efficacy.," *Chemical reviews*, vol. 113, no. 1, pp. 119–91, Jan. 2013.

[44] G. . Moore, "Cramming More Components Onto Integrated Circuits," *IEEE*, vol. 86, pp. 82–85, 1998.

[45] S. Uchiyama, G. D. McClean, K. Iwai, and a P. de Silva, "Membrane media create small nanospaces for molecular computation.," *Journal of the American Chemical Society*, vol. 127, no. 25, pp. 8920–1, Jun. 2005.

[46] J. Andréasson and U. Pischel, "Smart molecules at work--mimicking advanced logic operations.," *Chemical Society reviews*, vol. 39, no. 1, pp. 174–88, Jan. 2010.

[47] M. de Sousa, M. Kluciar, S. Abad, M. a Miranda, B. de Castro, and U. Pischel, "An inhibit (INH) molecular logic gate based on 1,8-naphthalimide-sensitised europium luminescence.," *Photochemical & photobiological sciences :*

Official journal of the European Photochemistry Association and the European Society for Photobiology, vol. 3, no. 7, pp. 639–42, Jul. 2004.

[48] A. P. de Silva, N. Gunaratne, and G. Maguire, "'Off–on' fluorescent sensors for physiological levels of magnesium ions based on photoinduced electron transfer (PET), which also behave as photoionic OR logic gates," *Journal of the Chemical Society, Chemical Communications*, no. 1213–1214, 1994.

[49] A. P. De Silva and N. D. Mcclenaghan, "Proof-of-Principle of Molecular-Scale Arithmetic," no. 23, pp. 3965–3966, 2000.

[50] O. A. Bozdemir, R. Guliyev, O. Buyukcakir, S. Selcuk, S. Kolemen, G. Gulseren, T. Nalbantoglu, H. Boyaci, and E. U. Akkaya, "Selective manipulation of ICT and PET Processes in styryl-Bodipy derivatives: applications in molecular logic and fluorescence sensing of metal ions.," *Journal of the American Chemical Society*, vol. 132, no. 23, pp. 8029–36, Jun. 2010.

[51] S. J. Langford and T. Yann, "Molecular logic: a half-subtractor based on tetraphenylporphyrin.," *Journal of the American Chemical Society*, vol. 125, no. 37, pp. 11198–9, Sep. 2003.

[52] N. Wise, "Interview: Molecular logic," *Chemical Technology*, 2009.

[53] A. P. de Silva and S. Uchiyama, "Molecular logic and computing," *Nature Nanotecnology*, vol. 2, no. 7, p. 410, 2007.

[54] P. . Paduraru, R. T. W. Popoff, N. R., R. Gries, G. G., and P. E., "Synthesis of Substituted Alkoxy Benzene Minilibraries, for the Discovery of New Insect Olfaction or Gustation Inhibitors," *Journal of Combinatorial Chemistry*, vol. 10, no. 1, pp. 123–134, 2008.

[55] T. Cardinaels, J. Ramaekers, P. Nockemann, K. Driesen, K. Van Hecke, L. Van Meervelt, S. Lei, S. De Feyter, D. Guillon, B. Donnio, and K. Binnemans, "Imidazo [4 , 5-f] -1 , 10-phenanthrolines : Versatile Ligands for the Design of Metallomesogens," no. 4, pp. 3755–3768, 2008.

[56] R. Guliyev, S. Ozturk, Z. Kostereli, and E. U. Akkaya, "From Virtual to Physical : Integration of Chemical Logic," pp. 9826–9831, 2011.

[57] B. A. Wong, S. Friedle, and S. J. Lippard, "Subtle Modification of 2 , 2-Dipicolylamine Lowers the Affinity and Improves the Turn-On of Zn (II) -Selective Fluorescent Sensors," no. Ii, pp. 7009–7011, 2009.

[58] R. Guliyev, "DESIGN STRATEGIES FOR CHEMOSENSORS AND THEIR APPLICATIONS IN MOLECULAR SCALE LOGIC GATES," 2013.

APPENDIX A: NMR SPECTRA

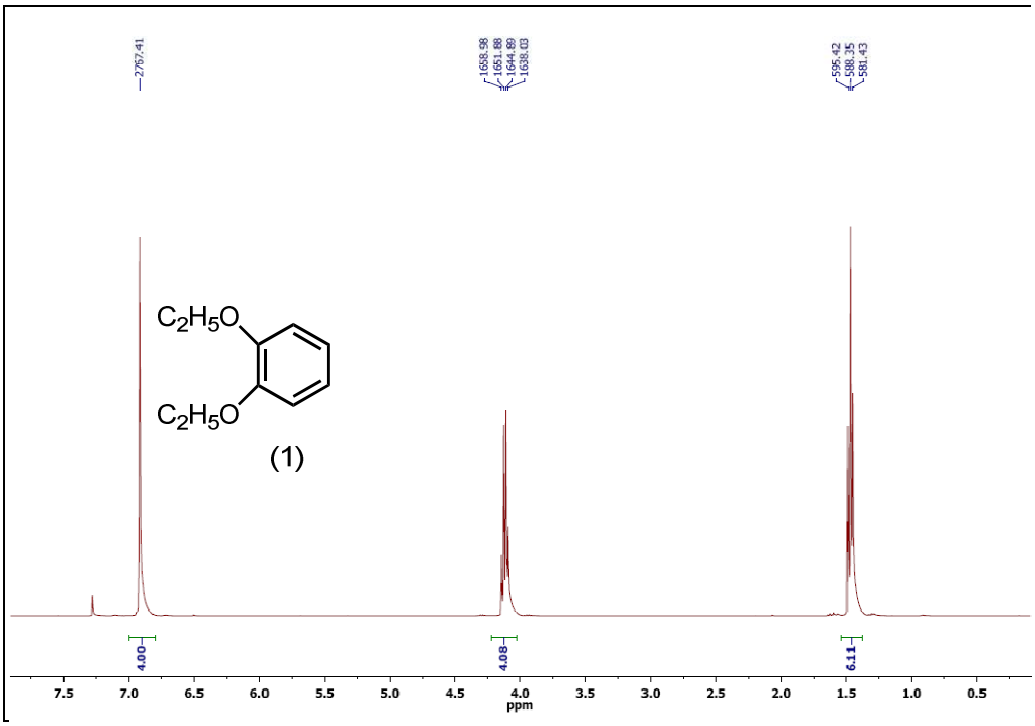

Figure 52 ^{1}H NMR spectrum of compound I (400 MHz, $CDCl_3$)

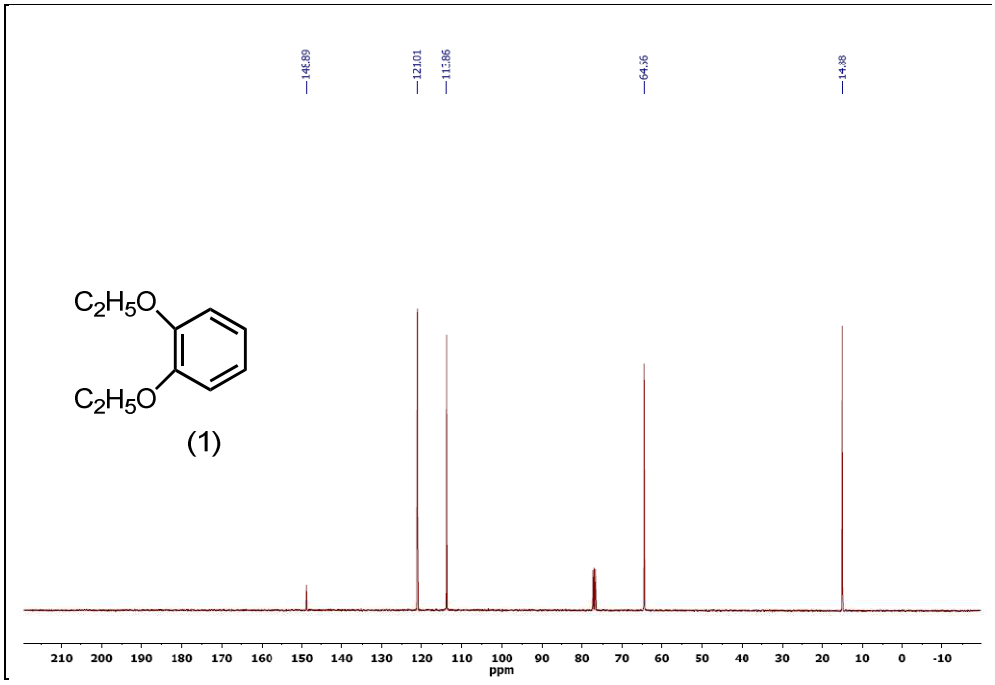

Figure 53 ^{13}C NMR spectrum of compound I (100 MHz, $CDCl_3$)

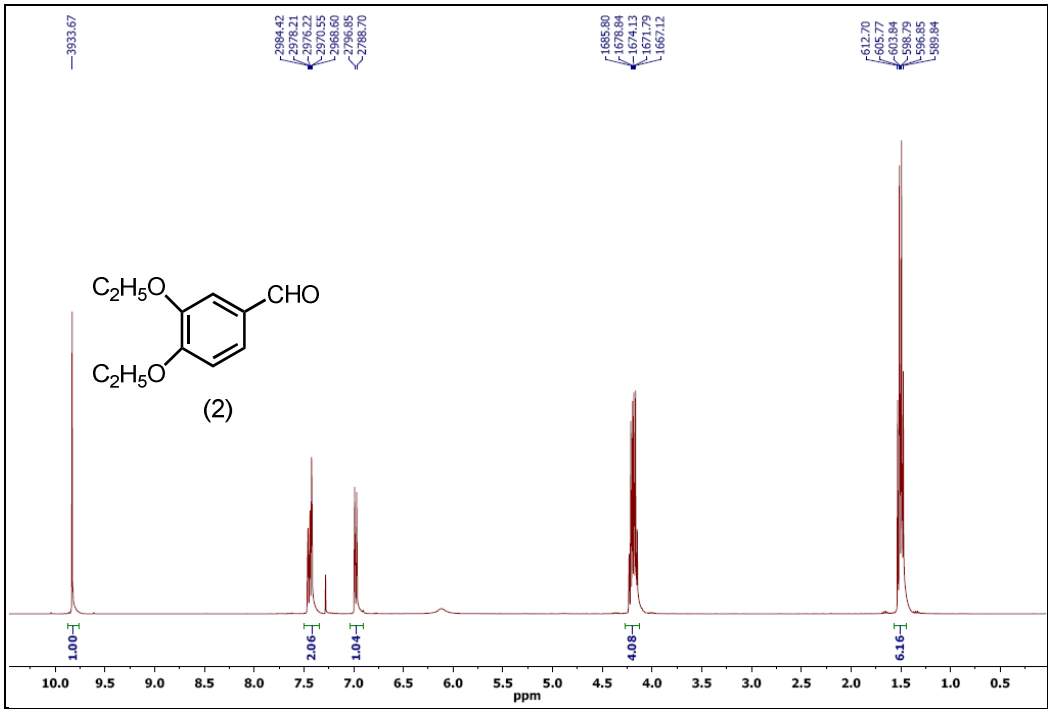

Figure 54 ^{1}H NMR spectrum of compound II (400 MHz, $CDCl_3$)

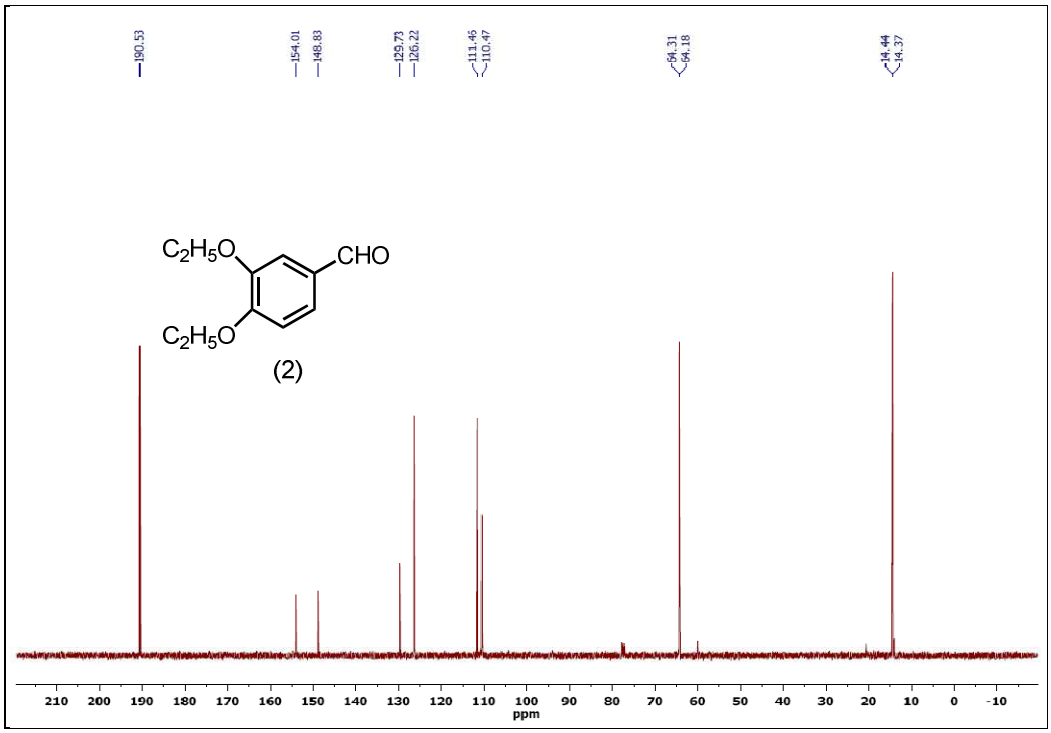

Figure 55 ^{13}C NMR spectrum of compound II (100 MHz, $CDCl_3$)

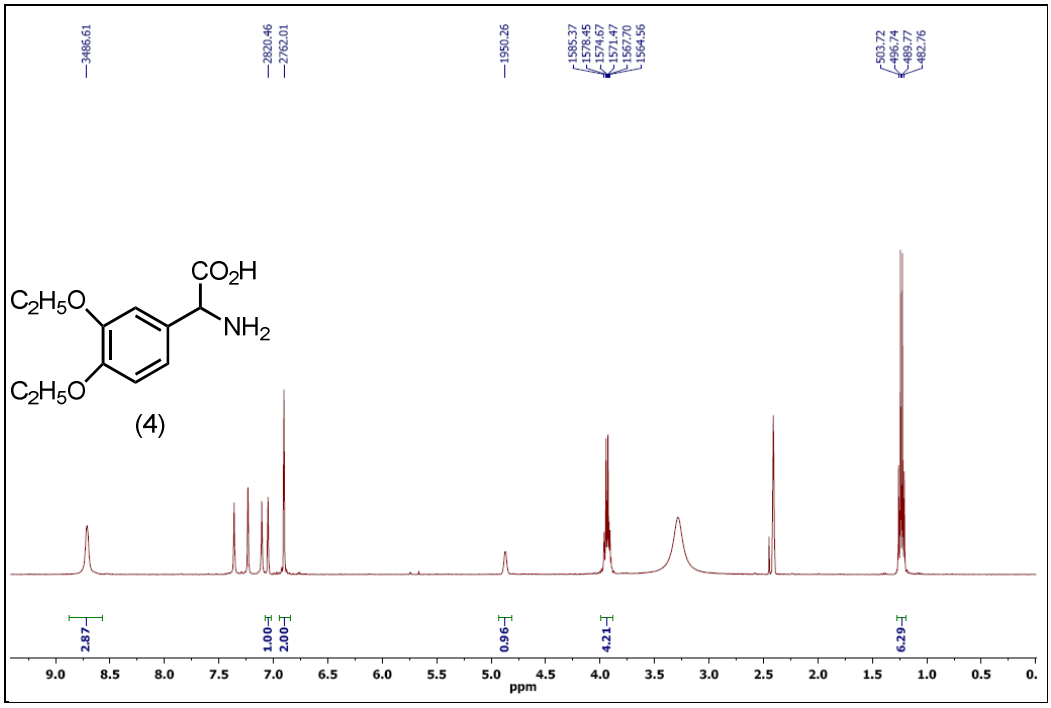

Figure 56 ^{1}H NMR spectrum of compound IV (400 MHz, $CDCl_3$)

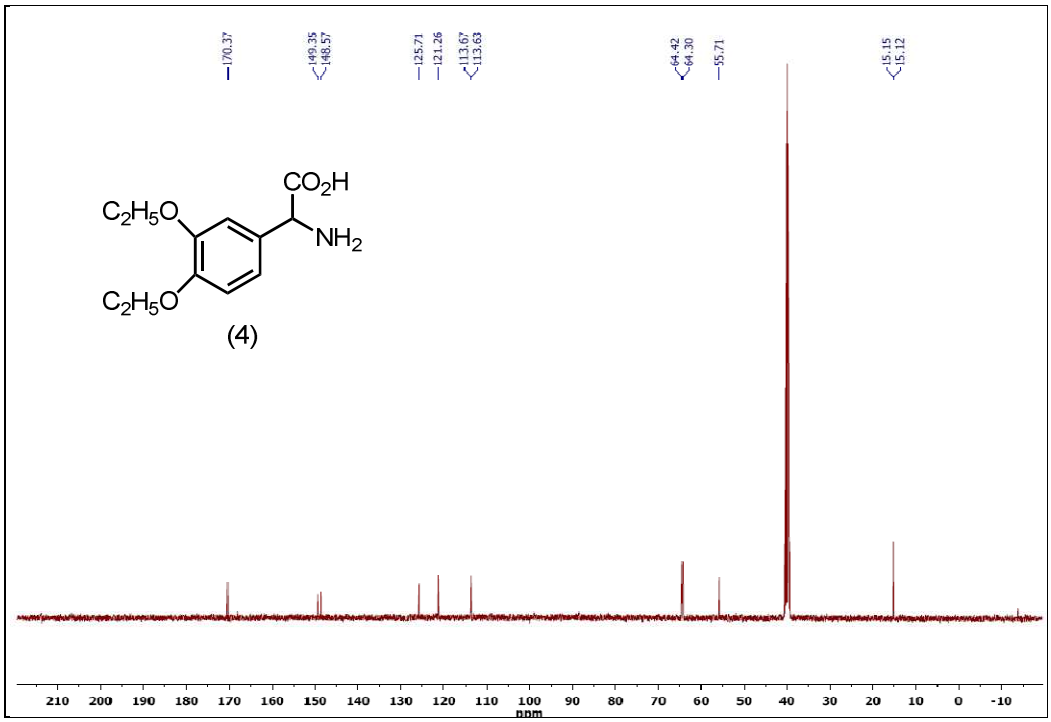

Figure 57 ^{13}C NMR spectrum of compound IV (100 MHz, $CDCl_3$)

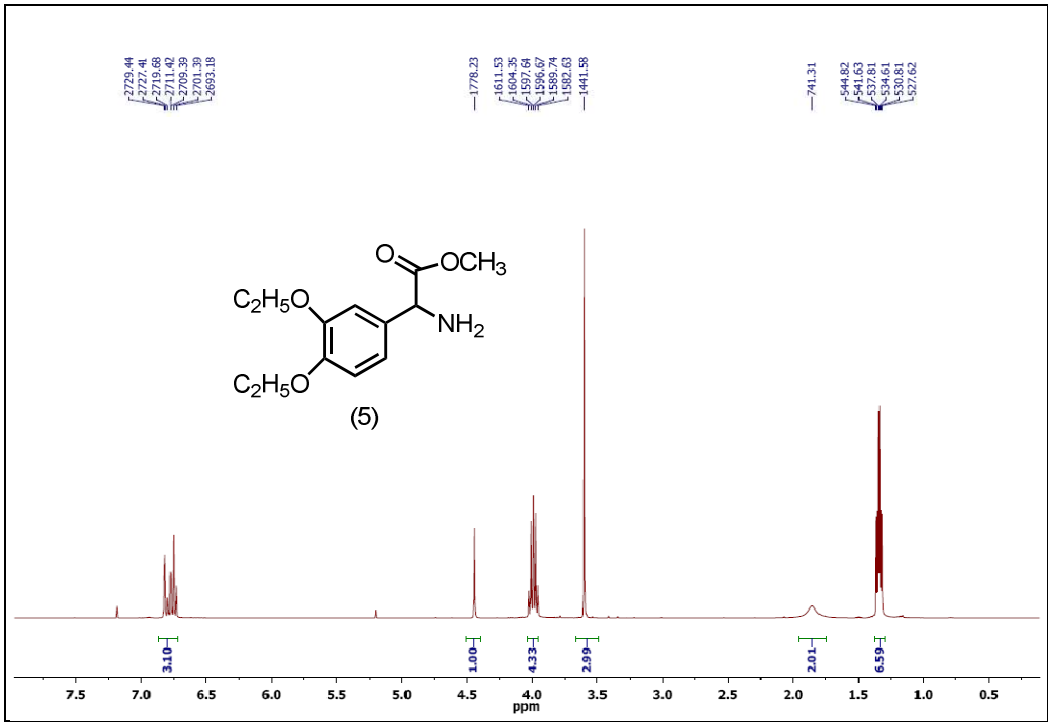

Figure 58 ^{1}H NMR spectrum of compound V (400 MHz, $CDCl_3$)

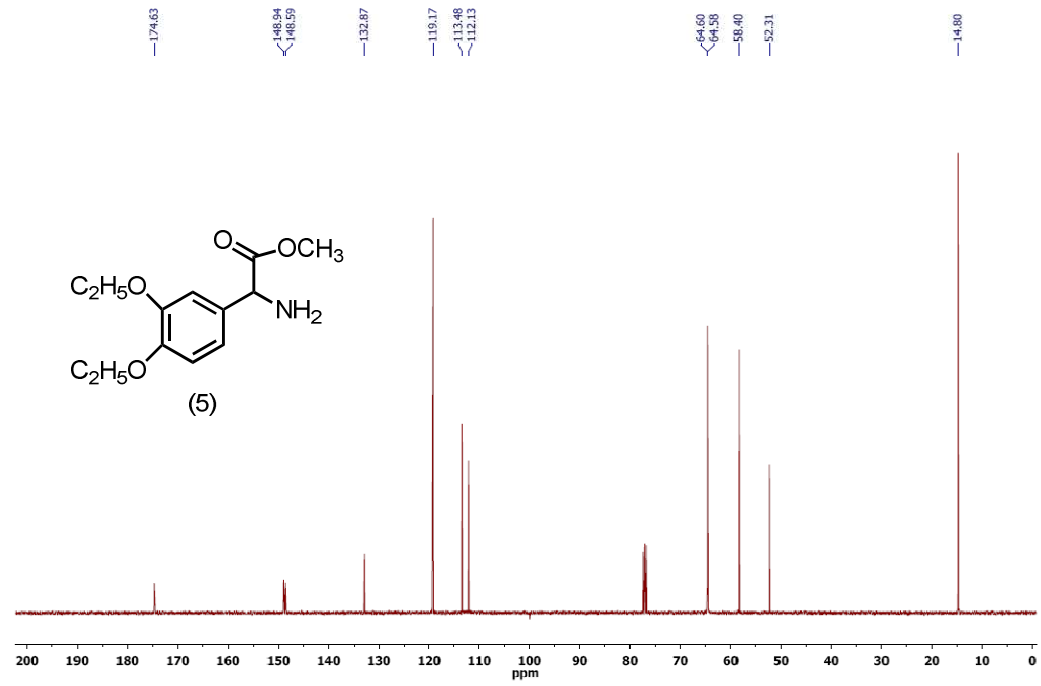

Figure 59 ^{13}C NMR spectrum of compound V (100 MHz, $CDCl_3$)

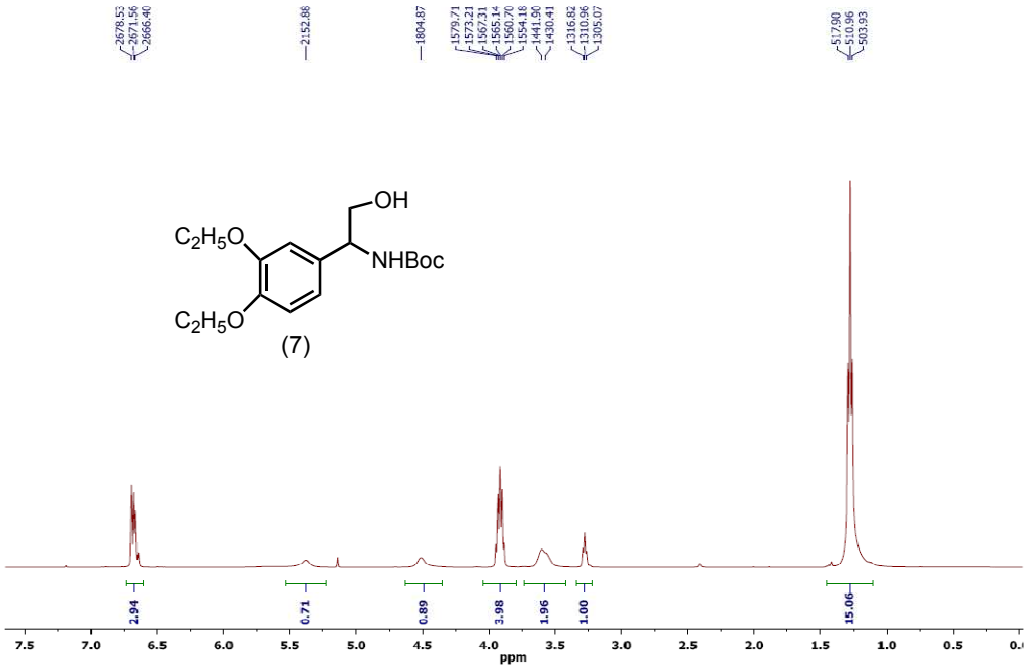

Figure 60 ^{1}H NMR spectrum of compound VII (400 MHz, $CDCl_3$)

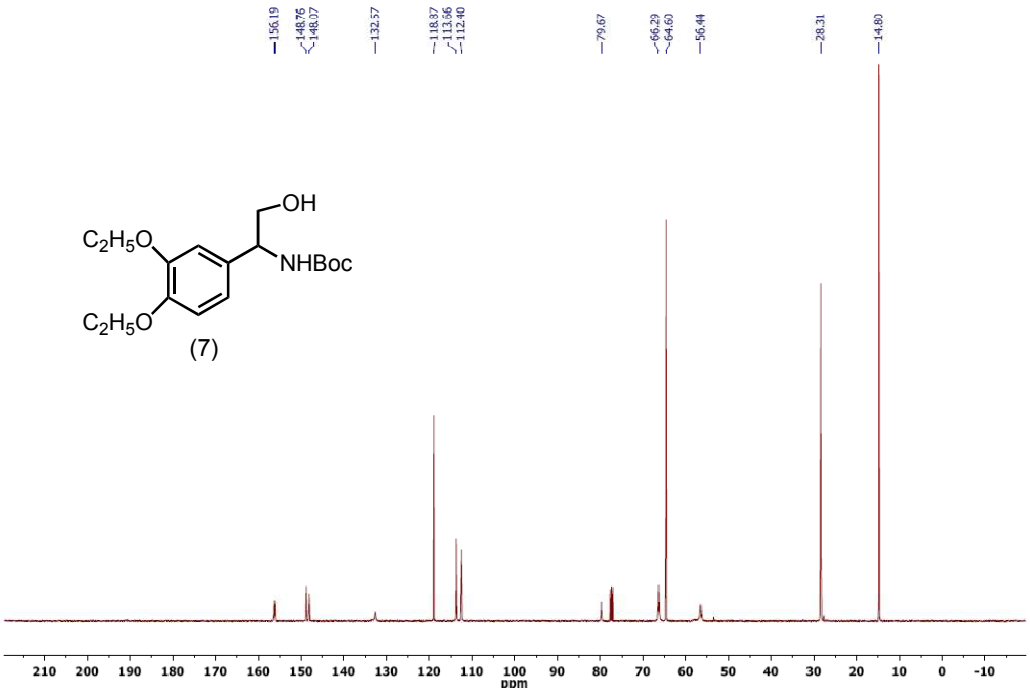

Figure 61 ^{13}C NMR spectrum of compound VII (100 MHz, $CDCl_3$)

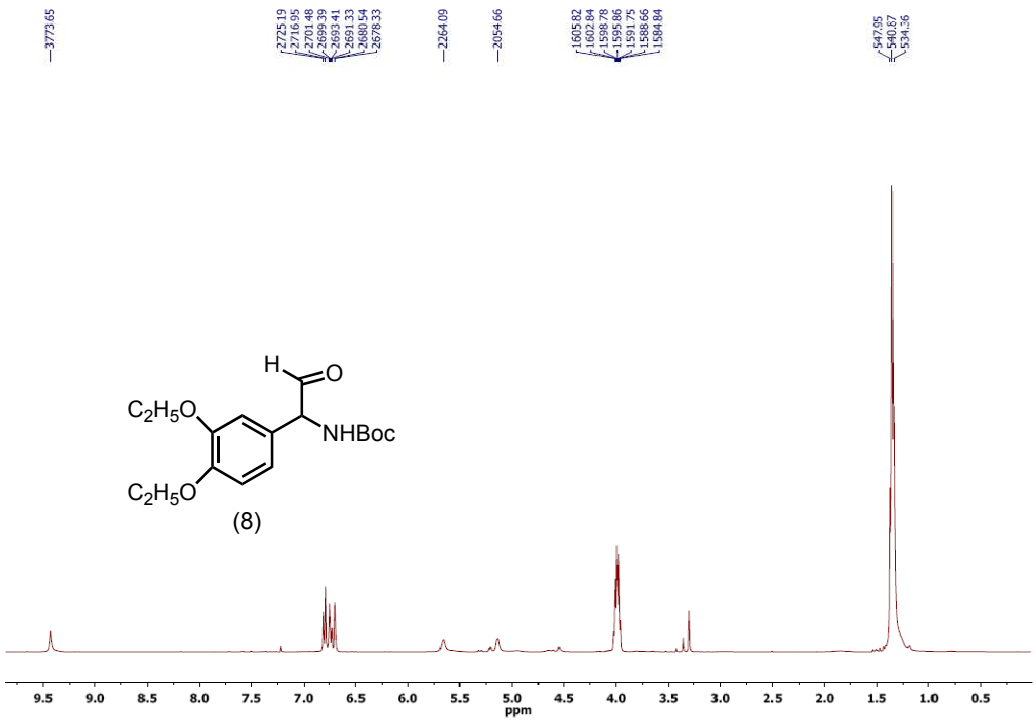

Figure 62 ^{1}H NMR spectrum of compound 8 (400 MHz, $CDCl_3$)

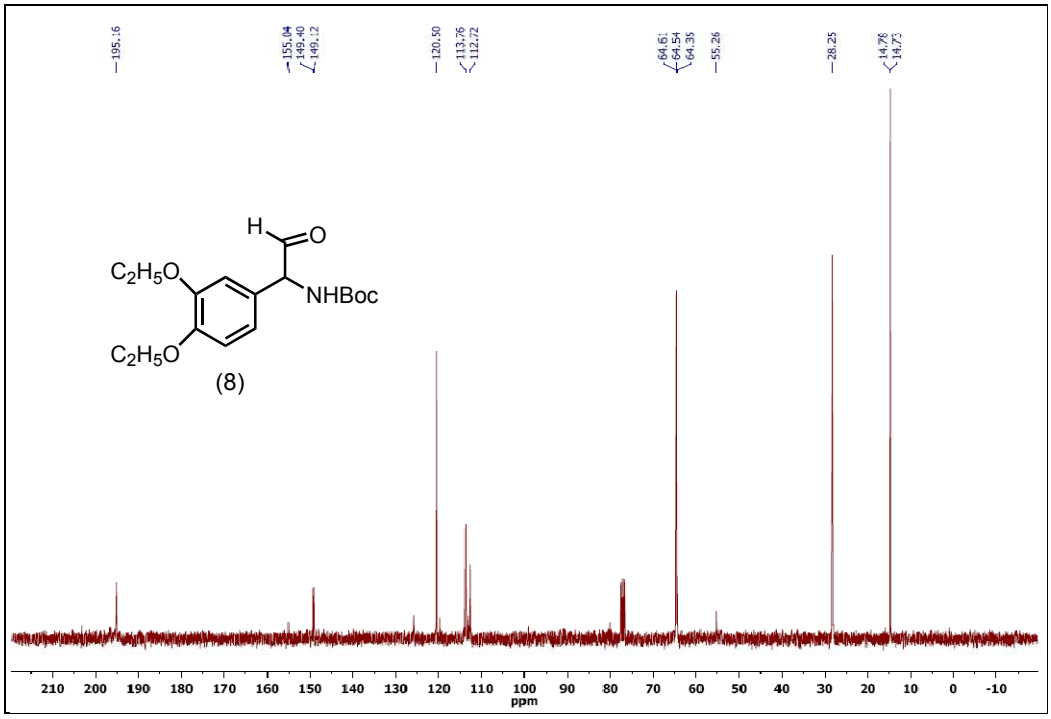

Figure 63^{13}C NMR spectrum of compound 8 (100 MHz, $CDCl_3$)

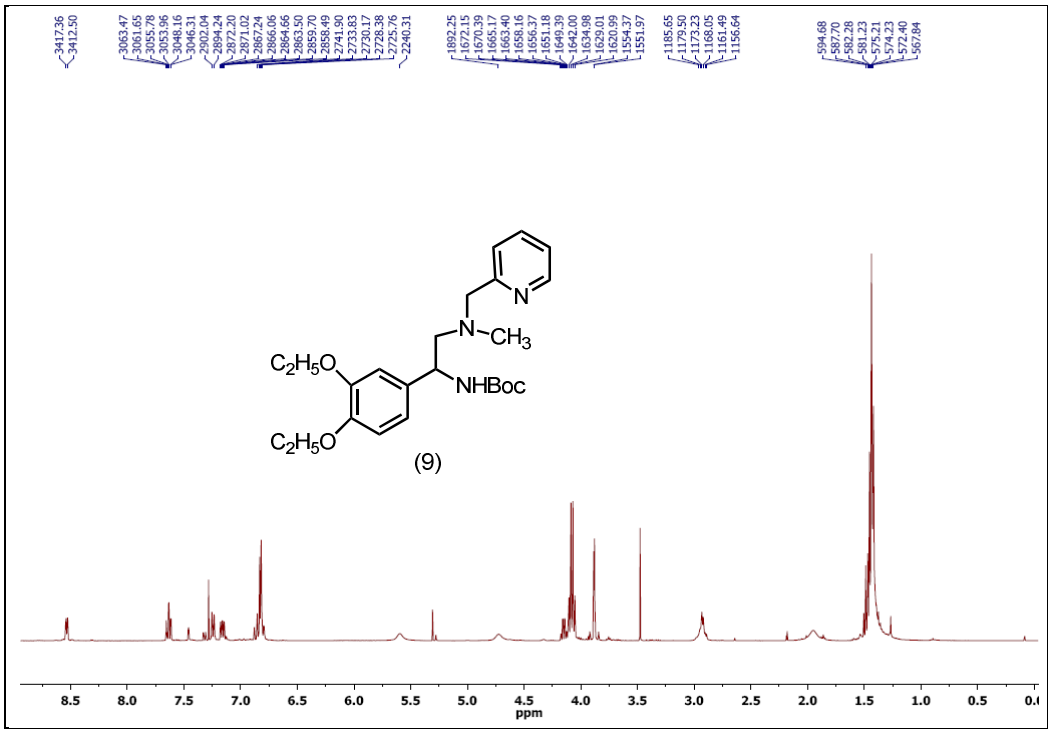

Figure 64 ^{1}H NMR spectrum of compound IX (400 MHz, $CDCl_3$)

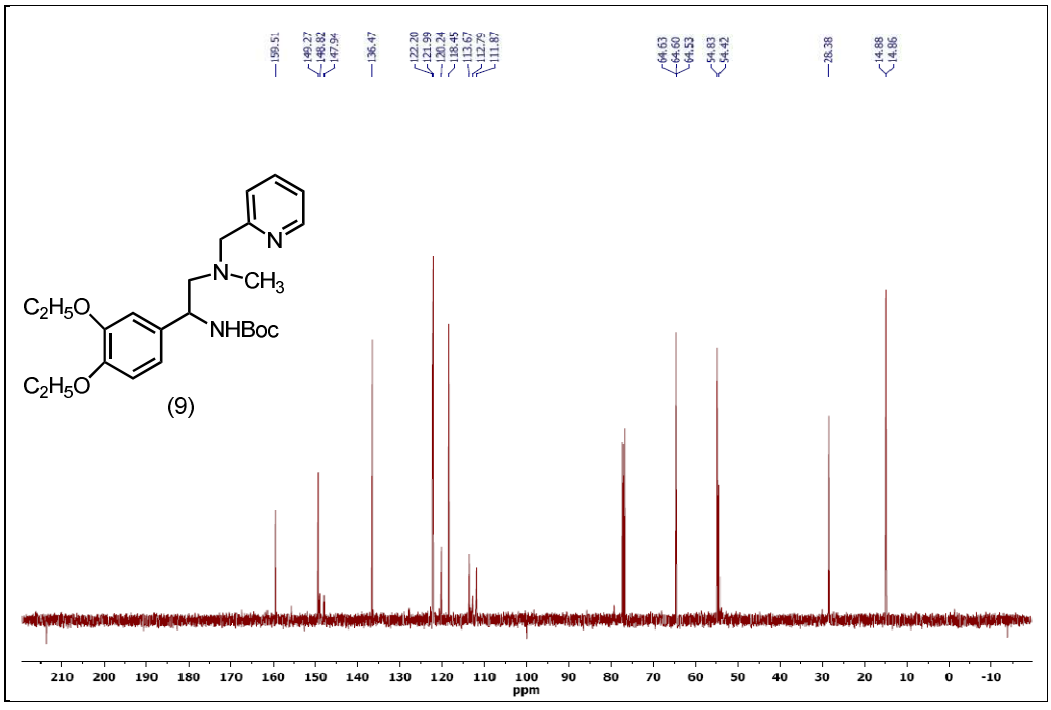

Figure 65 ^{13}C NMR spectrum of compound IX (100 MHz, $CDCl_3$)

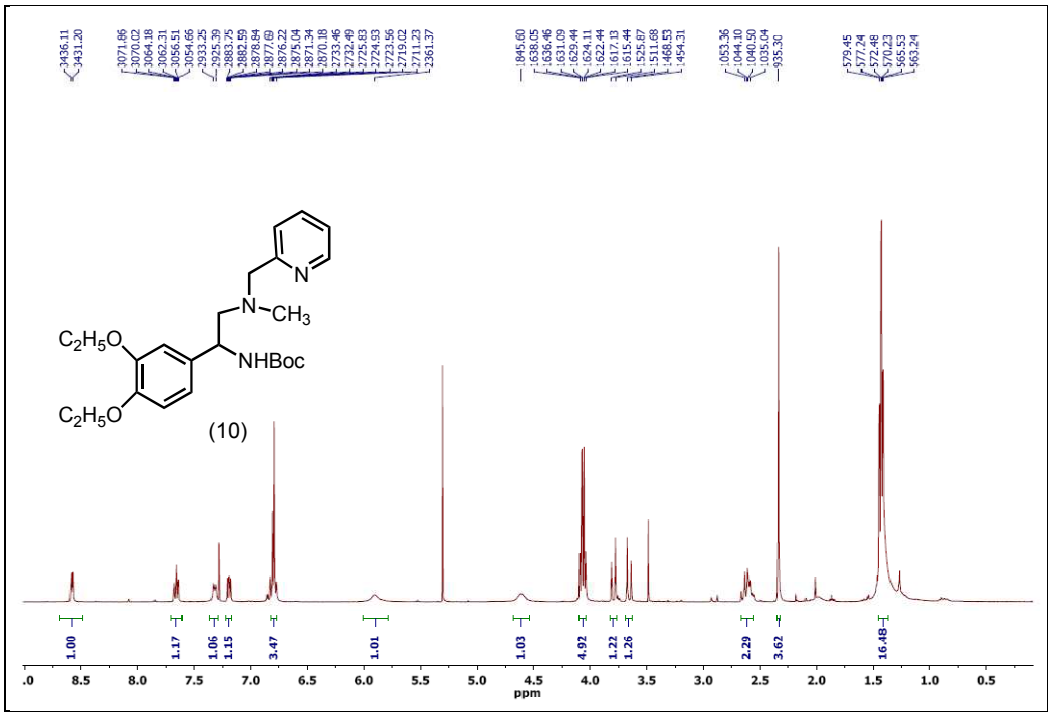

Figure 66 ^{1}H NMR spectrum of compound X (400 MHz, $CDCl_3$)

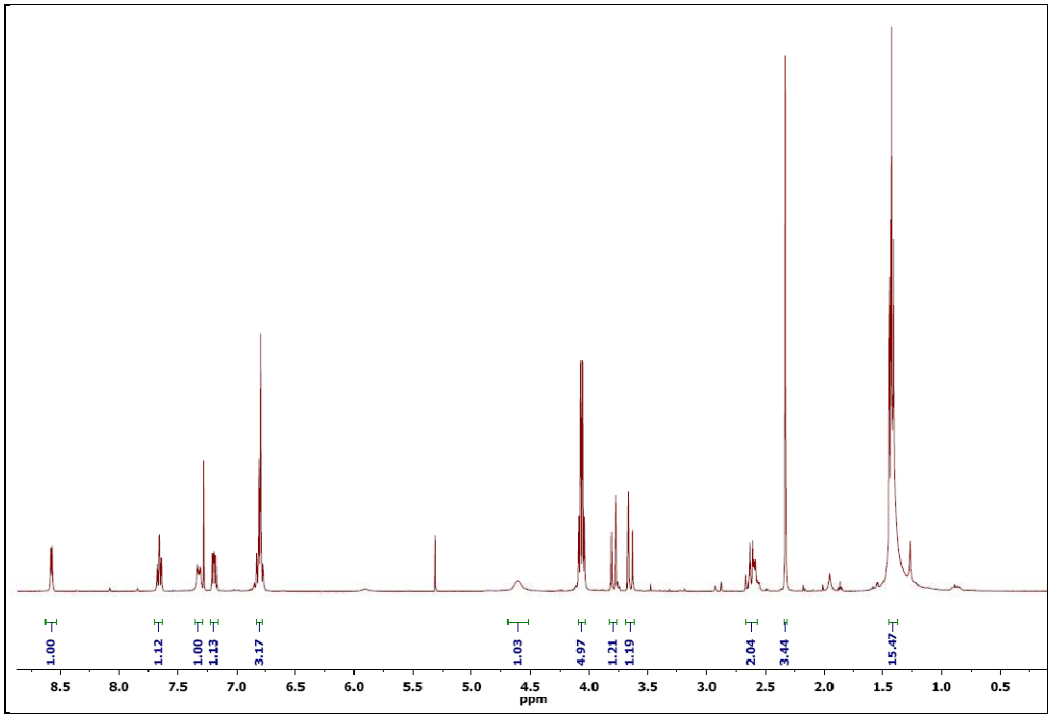

Figure 67 ^{1}H NMR spectrum of compound X (400 MHz, $CDCl_3$)

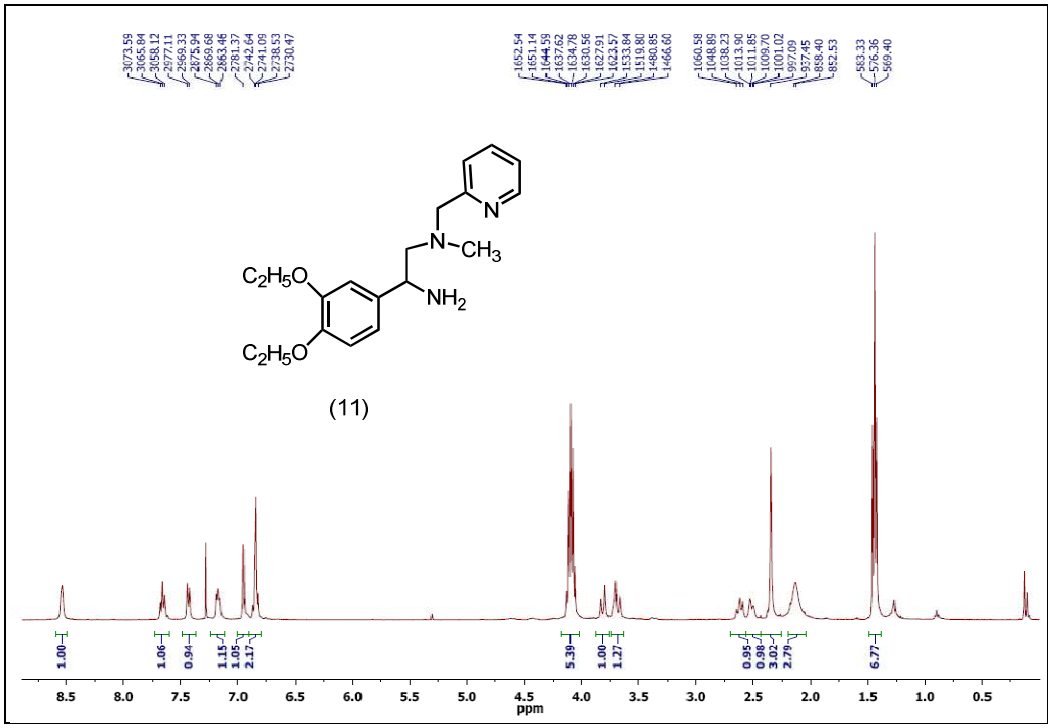

Figure 68 ^{1}H NMR spectrum of compound XI (400 MHz, $CDCl_3$)

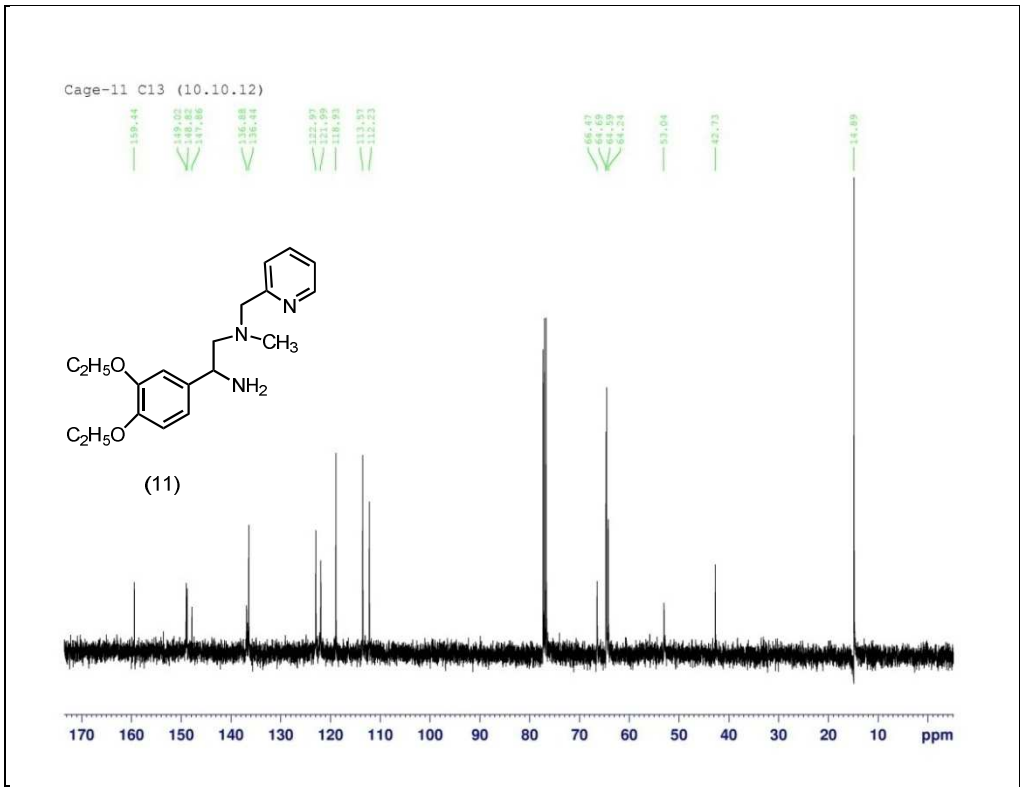

Figure 69 ^{13}C NMR spectrum of compound XI (100 MHz, $CDCl_3$)

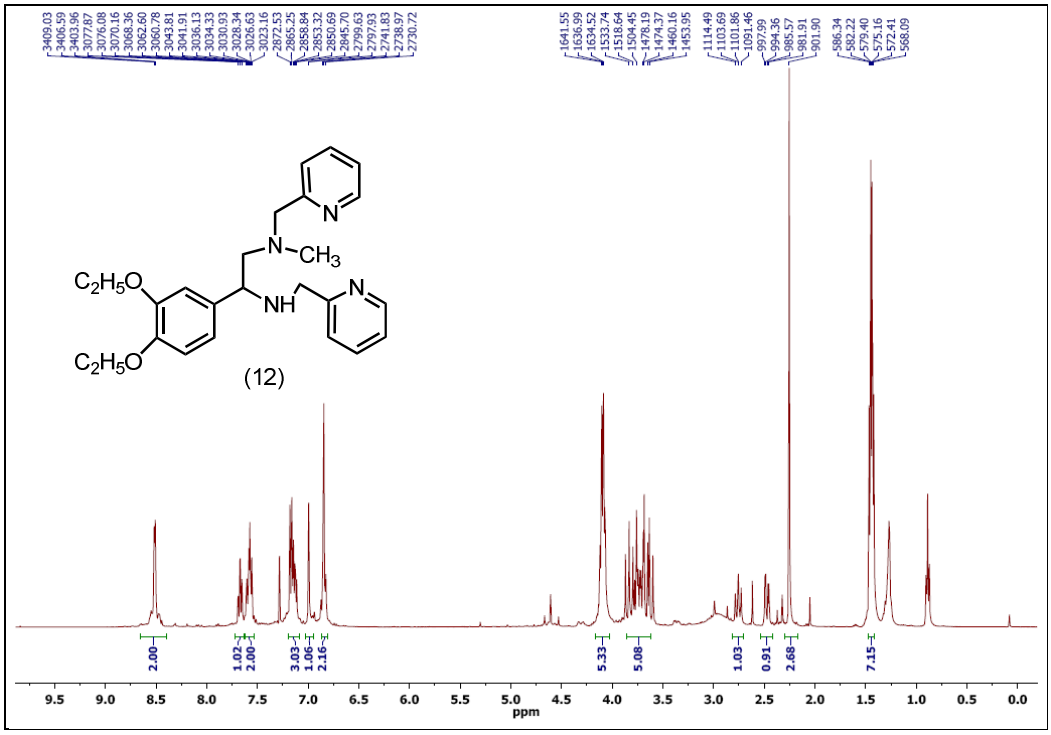

Figure 70 ^{1}H NMR spectrum of compound XII (400 MHz, $CDCl_3$)

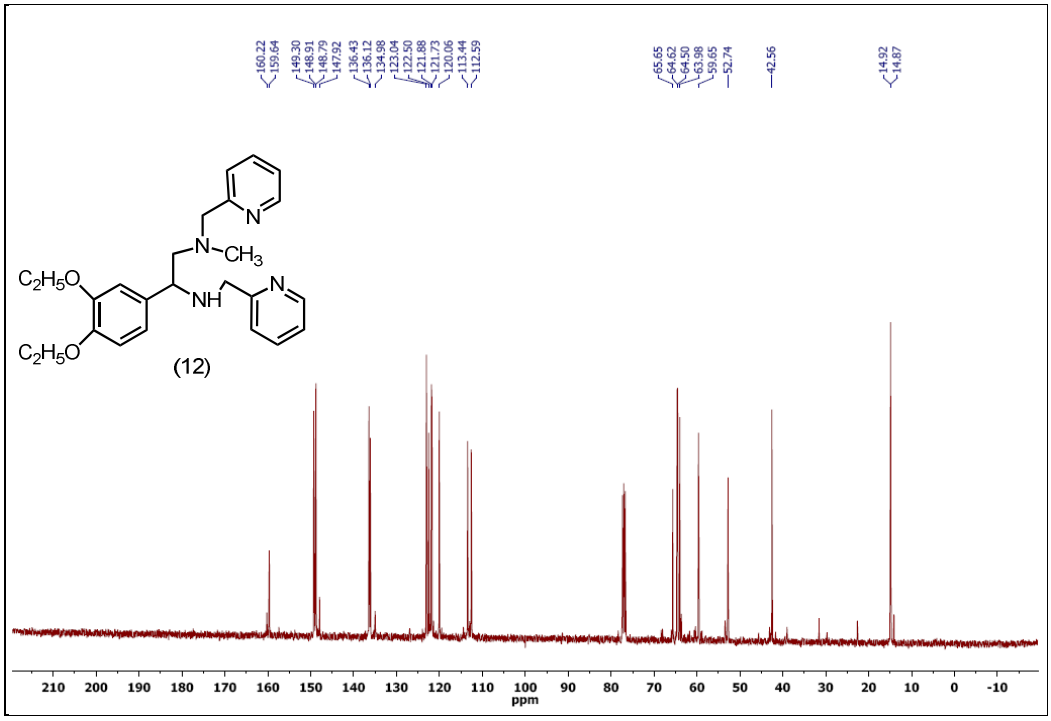

Figure 71 ^{13}C NMR spectrum of compound XII (100 MHz, $CDCl_3$)

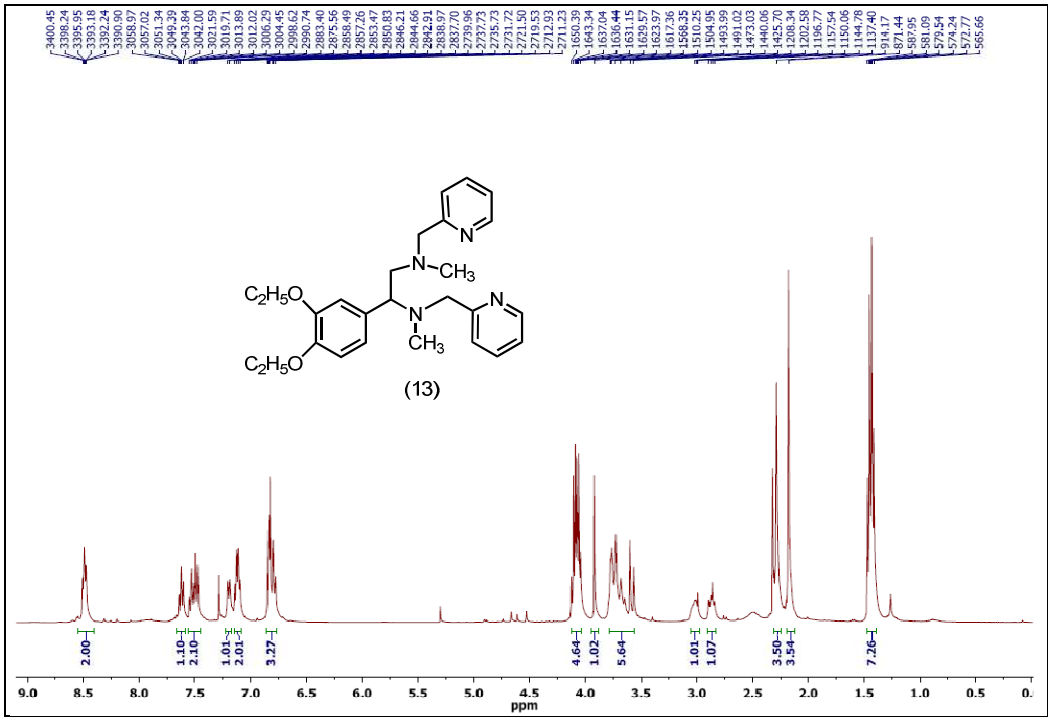

Figure 72 ^{1}H NMR spectrum of compound XIII (400 MHz, $CDCl_3$)

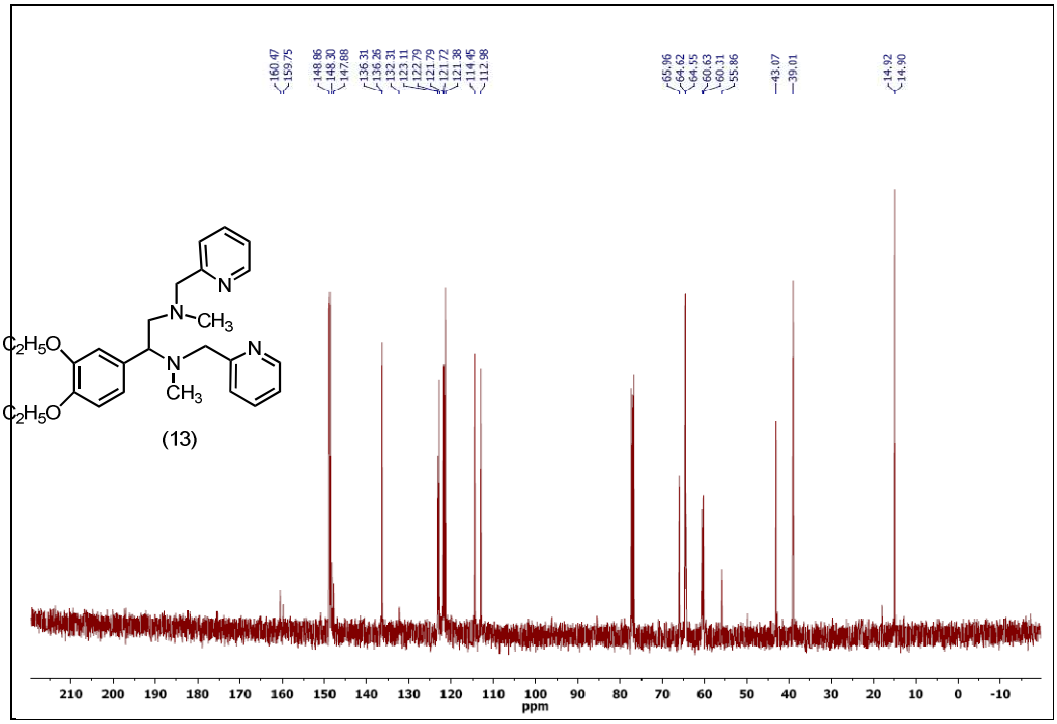

Figure 73 ^{13}C NMR spectrum of compound XIII (100 MHz, $CDCl_3$)

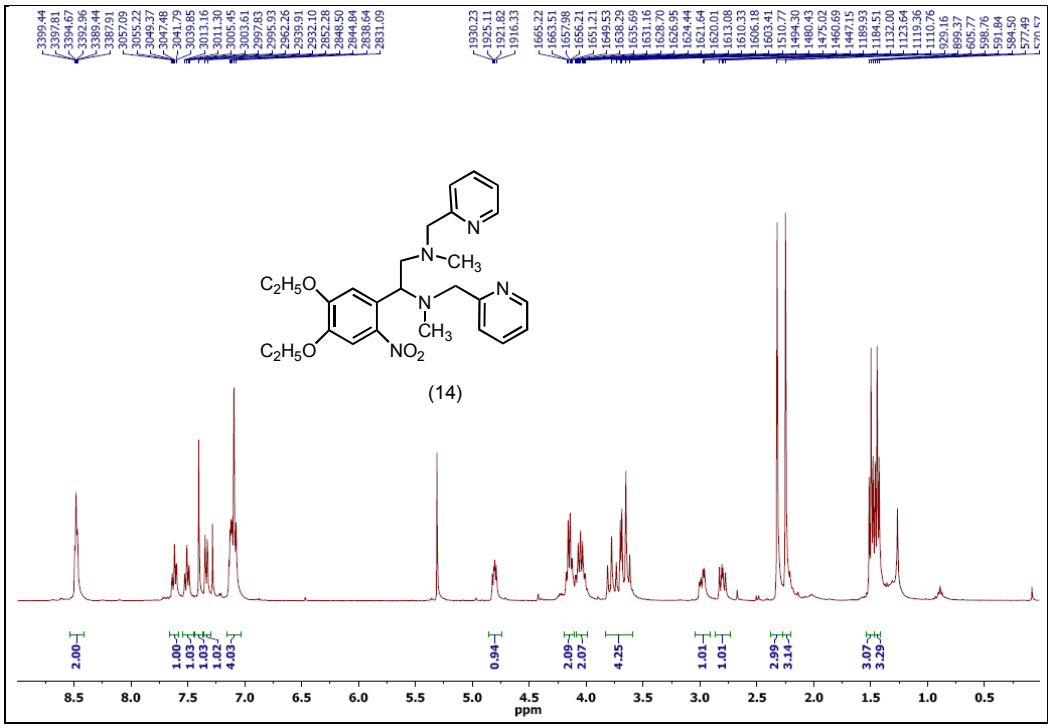

Figure 74 ^{1}H NMR spectrum of Cage (400 MHz, $CDCl_3$)

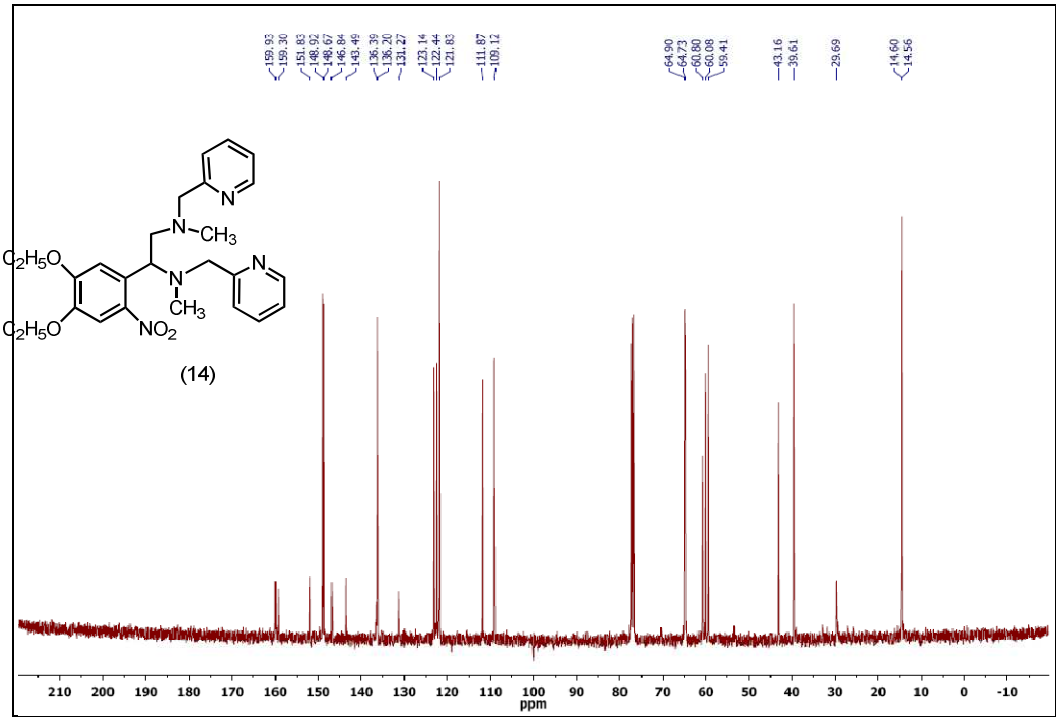

Figure 75 ^{13}C NMR spectrum of Cage (100 MHz, $CDCl_3$)

APPENDIX B: MASS SPECTRA

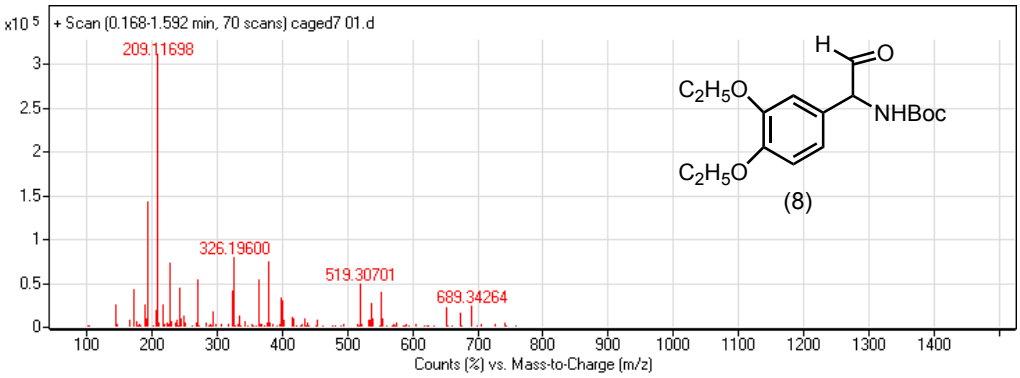

Figure 76 Mass spectrum of compound 8

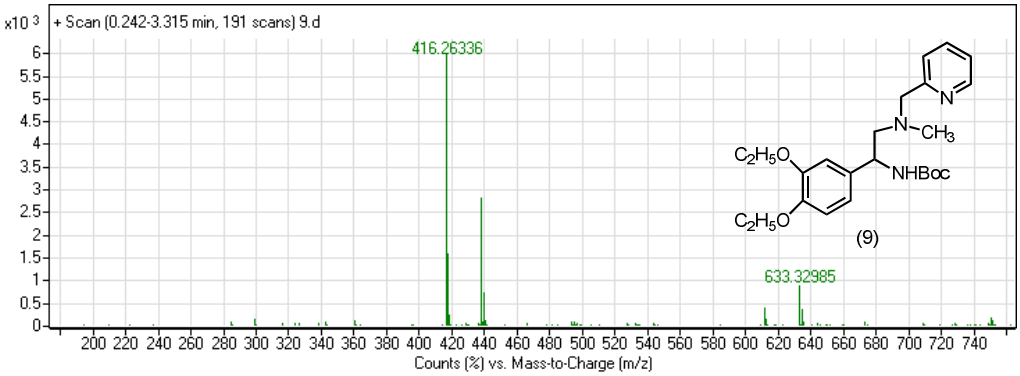

Figure 77 Mass spectrum of compound IX

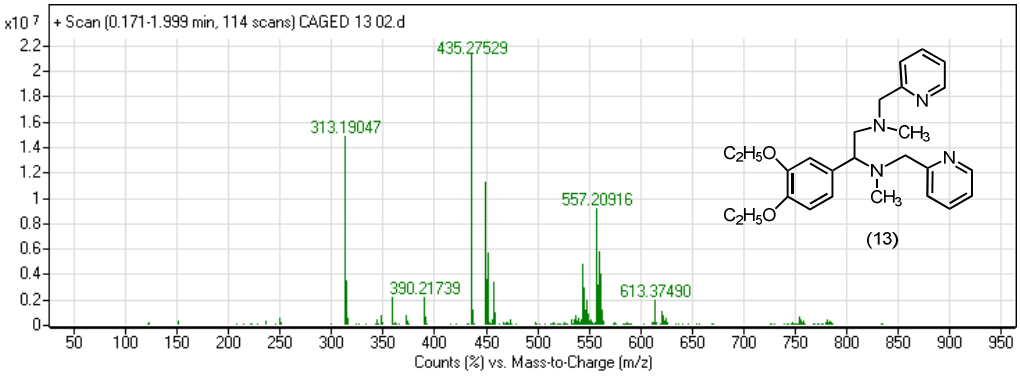

Figure 78 Mass spectrum of compound XIII

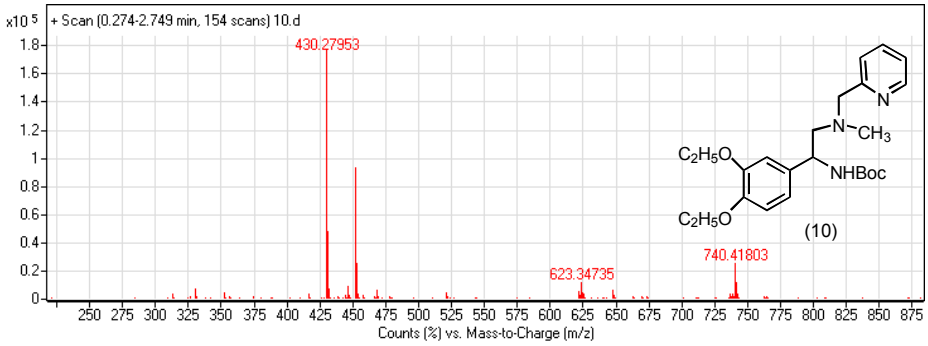

Figure 79 Mass spectrum of compound X

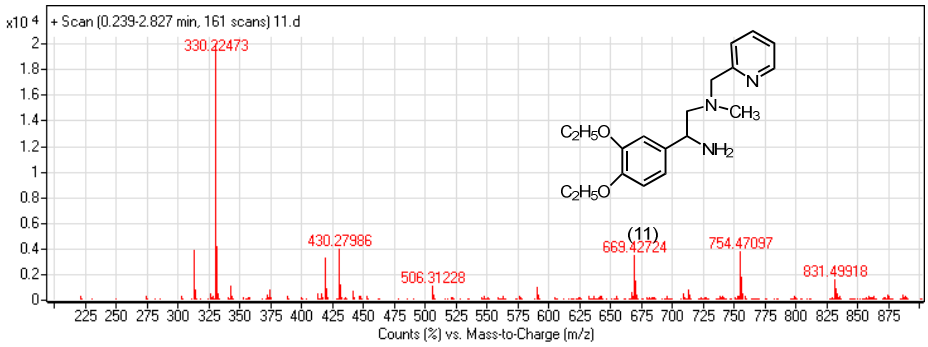

Figure 80 Mass spectrum of compound XI

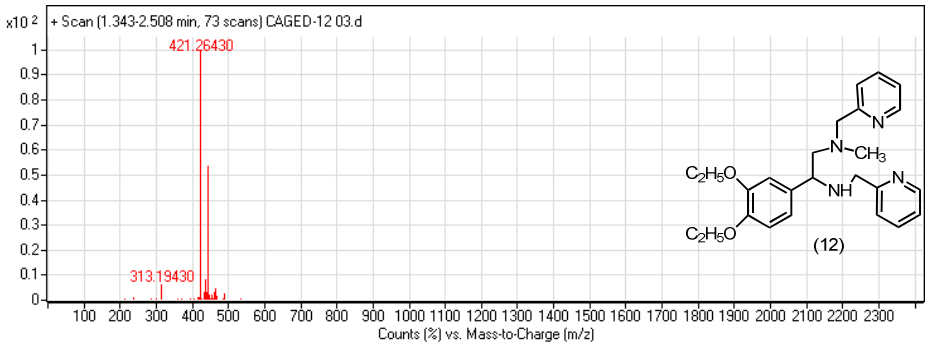

Figure 81 Mass spectrum of compound XII

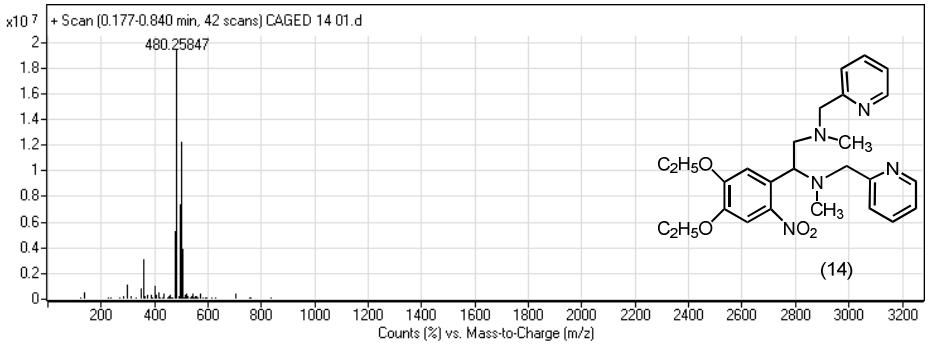

Figure 82 Mass spectrum of Cage